UNIVERSITY OF OKLAHOMA

GRADUATE COLLEGE

THE ECOLOGICAL AND DEVELOPMENTAL DIMENSIONS OF A POST-EXTINCTION RADIATION IN ORDOVICIAN–SILURIAN CRINOIDS (SUPERORDER FLEXIBILIA)

A THESIS

SUBMITTED TO THE GRADUATE FACULTY

in partial fulfillment of the requirements for the degree of

MASTER OF SCIENCE

By KIERA D. CROWLEY

Norman, Oklahoma

2026

THE ECOLOGICAL AND DEVELOPMENTAL DIMENSIONS OF A POST-EXTINCTION RADIATION IN ORDOVICIAN–SILURIAN CRINOIDS (SUPERORDER FLEXIBILIA)

A THESIS APPROVED FOR THE

SCHOOL OF GEOSCIENCES

BY THE COMMITTEE CONSISTING OF

Dr. David F. Wright, Chair

Dr. Selina R. Cole

Dr. Katharine A. Marske

ABSTRACT

The origin and early evolution of a major crinoid clade, Superorder Flexibilia, remains enigmatic despite over a century of work by paleontologists. Our uncertainty regarding the time and place of origination for members of the clade hinders our ability to characterize the ways in which the group was impacted by (and responded to) the Late Ordovician mass extinction (LOME). The LOME was the first of the five largest episodes of abrupt diversity decline recorded in the past half billion years, and fundamentally altered the morphological and ecological trajectories of major organismal groups including flexible crinoids. Analyzing the species-level response of this group — taxonomically, morphologically, and ecologically — during its radiation in the aftermath of the LOME provides a novel case study for interpreting the processes shaping macroevolutionary dynamics during an interval of significant environmental and biotic change.

Phylogenetic and biogeographic analyses of Late Ordovician through early Silurian flexible crinoids place the origin of the superorder in central Laurentia within the peak of the Great Ordovician Biodiversification Event, ~458 Ma. Contrary to previous findings, the inferred evolutionary relationships between early members of the clade suggest that (1) flexible crinoids did not arise from a hypothesized ancestral taxon in the genus *Cupulocrinus*, but are rather a closely related sister lineage to that group, and (2) the status of nominal orders within Flexibilia are indeed monophyletic for early taxa, not paraphyletic as recovered in previous analyses. Paleobiogeographic patterns document the broader dispersal of euflexibles compared to cupulocrinid flexibles, and highlight the parallel taxonomic radiations occurring across separate paleocontinents for several higher-order flexible subclades. Macroevolutionary models fit to the phylogenetic inference of Ordovician through middle Silurian (Wenlock) flexible species suggest that diversification trajectories for three morphological traits directly related to crinoid ecology

and development likely experienced a shift in tempo and/or mode during the LOME. But this response was not uniform across all traits, and the general increase in flexible body size, accomplished via post-extinction ecological release, appears mechanistically different than the expansion in calyx complexity accomplished by a post-LOME increase in evolutionary rate. Additionally, the relative filtration fan area of the clade remained largely constrained across the study interval, indicating that at least one aspect of flexible crinoid morphology pertaining to feeding ecology was less significant in driving the ecomorphological radiation of the clade in the aftermath of the LOME. The varying responses of these diversification trajectories points to the differing processes driving evolution in Flexibilia and provides a unique opportunity to explore the process-based biological underpinnings of observed macroevolutionary patterns.

TABLE OF CONTENTS

Introduction

The Late Ordovician mass extinction (LOME), the first of the five largest episodes of abrupt, catastrophic diversity decline observed in the Phanerozoic marine fossil record, represents an interval of significant and long-lasting restructuring of the marine biota in response to geologically rapid environmental change (Ausich and Deline, 2012; Marshall, 2023). Triggered by glaciation and severe sea level drop that proved catastrophic for the majority of marine species (Harper, 2024), the biological impacts of the LOME are expressed in multiple, quasi-independent macroevolutionary currencies: taxonomic diversity, morphologic disparity, and functional ecology (Jablonski, 2022). Despite extensive work focused on elucidating the effects of the LOME on various aspects of paleocommunities (Bapst et al., 2012; Ausich and Deline, 2012; Darroch and Wagner, 2015; etc.), there remains much yet to be done within a temporally constrained phylogenetic framework in order to gain deeper insight into mechanisms driving mass extinction selectivity and subsequent faunal rebound among surviving clades (Jablonski and Edie, 2025). Specifically, the use of tip-dated fossil phylogenies along with paleontologically-motivated phylogenetic comparative methods permits novel modeling approaches for investigating the tempo and mode of diversification in these macroevolutionary currencies spanning mass extinction events (Slater, 2013; Wright, 2017a; Soul and Wright, 2021).

Crinoids provide an ideal study system for evaluating morphological trait evolution (Foote, 1999; Wright, 2017b), and they preserve a rich fossil record of skeletal elements which indicate their feeding ecology and functional morphology (Cole et al., 2019). The LOME caused major shifts in the taxonomic richness and ecologic abundance of crinoid higher taxa, and the transition from the Ordovician to the Silurian witnessed a significant reorganization of crinoid

communities such that while most major crinoid clades were present on both sides of the O–S, the dominance of various clades pre- and post-extinction varied substantially (Ausich et al., 1994). For example, the species-rich cladid genus *Cupulocrinus* went extinct at the LOME, but its hypothesized closest relatives, members of the major lineage Superorder Flexibilia, survived and radiated considerably in the Silurian (Brower, 2001; Wright, 2017a; Wright and Toom, 2017). However, no species-level phylogenetic framework for *Cupulocrinus* and early Paleozoic flexibles yet exists, which hinders our understanding of the evolutionary origin and post-extinction diversification of this major crinoid clade in the aftermath of the LOME.

In Chapter I, I construct a species-level, time-calibrated phylogenetic tree of Ordovician–early Silurian (Llandovery) cupulocrinid and early flexible taxa using Bayesian tip-dated phylogenetic methods incorporating the fossilized birth–death (FBD) process. Comprehensive sampling of flexible species and the inclusion of temporal stratigraphic information in the estimation of phylogenetic relationships (1) allows for the explicit testing of likely ancestry for Superorder Flexibilia and (2) provides the most temporally constrained estimates yet for the origination of Flexibilia and the divergences of its major subclades. I use the paleobiogeographic distributions of species in the phylogeny to infer likely locations of origin for unsampled ancestral nodes in the tree, and document the spatial patterns of taxonomic diversification within Flexibilia, noting the possible biogeographic implications for extinction selectivity among flexible subclades.

In Chapter II, I expand upon that phylogenetic framework, and generate a phylogeny for all flexible species from the Late Ordovician through the middle Silurian (Wenlock). Using that broader set of focal taxa, I employ comparative methods to fit multiple process-based macroevolutionary models of trait diversification in order to test alternative hypotheses involving

shifts in evolutionary tempo and/or mode across the LOME. Trait diversification is evaluated for three morphological traits directly related to crinoid feeding and development: body size, relative filtration fan area, and calyx complexity. By assessing the support for each process-based model, and considering the biological significance of differential responses in phenotypic trajectories among the tested ecological and developmental traits, we gain a more nuanced understanding of the manner in which biotic and abiotic drivers impacted the early evolutionary history of Superorder Flexibilia.

Chapters I and II are formatted as standalone entities, and represent the two publications which will result from this thesis work. Chapter I is intended for submission to the *Journal of Paleontology* in spring 2026. Its systematic revision of early flexible taxa and description of a new specimen from recent fieldwork on Anticosti Island (Québec) align well with the scope and strengths of that journal. Chapter II is styled in a shorter form, and is intended for submission in summer 2026. It expands upon the phylogenetic framework of my first chapter and refers to some of the findings from that analysis within; in those instances, I have used in-text citations of "Crowley and Wright, (in prep.)" to emulate the format required at time of journal submission. I have combined the references sections for both chapters into one combined unit at the end of this document in order to eliminate the occupation of space by largely redundant reference lists. Additionally, associated data files for both chapters are appended to the end of this thesis, rather than housed in their relevant chapter sections.

Chapter I: On the origin and evolution of Superorder Flexibilia (Echinodermata): a Bayesian tip-dated phylogenetic assessment of Ordovician–Silurian flexible crinoids

Abstract.—The crinoid Superorder Flexibilia originated in the late Middle Ordovician and, following the Late Ordovician mass extinction (LOME), radiated to comprise one of the major constituents in Paleozoic crinoid communities. For over a century, the canonical origin of the flexibles has largely been posited to be direct descendance from the paraphyletic cladid genus *Cupulocrinus*, which went extinct during the LOME. However, this hypothesis has yet to be tested within a comprehensive, species-level phylogenetic framework, especially one that capitalizes on the novel temporal and biogeographic context provided by the ten new species of flexibles that have been discovered in the past two decades alone.

Here, we conduct a Bayesian tip-dated phylogenetic analysis utilizing the fossilized birth–death process to investigate evolutionary relationships among 38 cupulocrinid and flexible crinoid species spanning the Ordovician to the middle Silurian. Results suggest that flexibles are sister to, but not direct descendants of, the genus *Cupulocrinus*, and that both lineages arose in the latest Darriwilian or earliest Sandbian (~458 Ma) during the Great Ordovician Biodiversification Event. The two orders within Flexibilia, Sagenocrinida and Taxocrinida, are recovered as monophyletic among early taxa, as are several flexible families within the study interval. Phylogenetic biogeographic analyses reveal the probable geographic point of origin for Flexibilia to be central Laurentia. By the middle of the Katian (~448 Ma) flexibles had dispersed throughout Laurentia and into the neighboring

paleocontinent of Baltica, demonstrating a widespread taxonomic and geographic radiation that was underway well before the onset of the LOME. These findings provide a spatiotemporally constrained understanding of the origin and early evolution of Superorder Flexibilia, and highlight the swift geographic spread and taxonomic diversification of this major crinoid clade during an important interval of faunal turnover in crinoid communities between the Ordovician and the Silurian.

Non-technical summary.—Crinoids, a major group of marine animals related to starfish and sea urchins, have been inhabiting Earth for nearly half a billion years. They have survived each of the "Big Five" mass extinctions that have occurred during that time, including the first such event: the Late Ordovician mass extinction (LOME) approximately 443 million years ago. One of the major goals of paleontological research is to use the fossil record to better understand the patterns and processes of extinction and rebound during major episodes of environmental change. Here, we conduct a case study using a major group of crinoids, the "flexibles," in order to investigate the timing and magnitude of extinction faced by a major marine animal group at the LOME. We answer the questions of when, where, and from whom flexible species originated, and characterize their diversification in post-extinction communities. By identifying the evolutionary relationships between species and constraining the age and location of origination events, our analyses provide new information on the extent to which the LOME impacted this clade and reveal the ways in which flexibles radiated in the aftermath.

Introduction

The Late Ordovician mass extinction (LOME), the first of the five largest episodes of abrupt, catastrophic diversity decline observed in the Phanerozoic marine fossil record, represents an interval of significant and long-lasting restructuring of the marine biota in response to geologically rapid environmental change (Ausich and Deline, 2012; Marshall, 2023). Triggered by glaciation and severe sea level drop that proved fatal for some 40% of marine genera and 80% of marine species (Harper, 2024), crinoids likewise faced biological upheaval during the LOME: the transition from the Ordovician to the Silurian witnessed a significant reorganization in the taxonomic richness and ecological abundance of crinoid higher taxa (Ausich et al., 1994). While most major crinoid clades spanned the O–S, the dominance of various clades pre- and post-extinction varied substantially. Analogous to the broadly recognized historical turnovers in global biota termed the Phanerozoic "evolutionary faunas" (Sepkoski, 1981), the O–S transition marked the fall of the Early Paleozoic crinoid evolutionary fauna (CEF) and the rise of the Middle Paleozoic CEF, with, among others, its dominant constituent of flexible crinoids (Ausich and Deline, 2012; Wright and Toom, 2017; Cole and Wright, 2022; Cole et al., 2025).

Flexible crinoids are rare in Ordovician and lower Silurian strata, and their evolutionary origin remains enigmatic. The rise in taxonomic richness, disparity, and abundance of flexibles after the LOME largely coincides with the start of their better-documented fossil record, from the middle Silurian until the clade's ultimate demise at the end-Permian mass extinction (Springer, 1920; Wright and Toom, 2017). However, in recent decades, nearly ten new flexible taxa have been described from latest Ordovician (Hirnantian) and earliest Silurian (Llandovery) rocks, shedding new light on the taxonomic

richness and geographic distribution of the clade nearer its point of origin (Eckert and Brett, 2001; Ausich and Copper, 2010; Wright and Toom, 2017; Cole et al., 2025).

Here, we conduct a Bayesian tip-dated phylogenetic analysis to test the hypothesis of *Cupulocrinus* ancestry for the Flexibilia and to estimate the most likely evolutionary relationships among early members of the clade. We use this phylogenetic framework to reconstruct the most probable biogeographic history of early flexibles and to characterize their place of origin and subsequent directions of dispersal both preceding and following the global environmental shifts associated with the LOME. We use a comprehensive species-level analysis of Ordovician through middle Silurian flexible taxa to best constrain the estimation of origination times and biogeographic affinities in the early history of the group. This study provides a fundamental framework from which to investigate the macroevolutionary response of flexibles leading up to the extinction pressures of the LOME and during their subsequent Silurian radiation as they rose to dominance in the Middle Paleozoic CEF. More broadly, this work serves as a high-resolution case study — in a major crinoid clade — for contextualizing the dynamics of faunal turnover during one of the largest mass extinction events in the last half billion years.

Taxonomic history of the Flexibilia

The Flexibilia comprise a taxonomically and morphologically distinct clade of crinoids ranging from the late Middle Ordovician to the end-Permian. Flexibles are characterized by the possession of a dicyclic cup with three infrabasal plates, a loosely sutured calyx with plating joined by short ligament fibers, and uniserial and non-pinnulate arms that often curl

inwards upon death (Fig. 1) (Springer, 1920; Moore and Laudon, 1943; Moore, 1978). Interradial and interbrachial plating also typifies many genera, as does the presence of a patelloid process on the brachial midline (Moore, 1978). The most extensive treatment to date of flexible crinoid morphology, systematics, and inferred interrelationships remains the seminal monograph of Frank Springer, *The Crinoidea Flexibilia* (1920). Springer's work documented all then-known flexibles and postulated an origin of the group from the genus *Cupulocrinus* d'Orbigny, 1850, based on the co-occurrence and morphological similarity of that genus to the oldest known flexible at the time, *Protaxocrinus* Springer, 1906; both taxa shared a medial column of plates in the anal sac and the brachial patelloid process diagnostic for many members of Flexibilia. Morphological assessment of the infrabasals in the two lineages also suggested a close relationship: aberrations in the infrabasal circlet of hundreds of *Cupulocrinus* specimens indicated an underlying developmental lability in disparate populations whereby ~3.4% percent of specimens exhibited an anomalous number of infrabasals compared to the typical *Cupulocrinus* number of five (Peter, 2019). Indeed, over half of the observed aberrations involved ankylosis (fusion) of a pair of the infrabasal plates, which is the process hypothesized to have occurred twice in flexibles in order to generate their invariant morphology of three unequal infrabasal plates. Peter (2019) did not identify any species of *Cupulocrinus* to be more variable than others, nor draw conclusions regarding specific cupulocrinid ancestry for the flexibles. But the propensity for cupulocrinids to vary in their infrabasal number in a manner similar to that diagnostic for flexibles was another line of evidence consistent with their being an ancestor, or a close relative of the ancestor, to Flexibilia (Peter, 2019).

Authors in the decades following Springer's report largely maintained his model of ancestry via a paraphyletic *Cupulocrinus,* including in early cladistic analyses of flexible evolution (Moore and Laudon, 1943; Moore, 1978; Brower, 2001). More recently, Bayesian tip-dating phylogenetic approaches have been applied to the analysis of early flexible evolution as a means of quantifying the probability of Springer's hypothesis. The first such test, conducted at the genus level between *Cupulocrinus* and five early flexible taxa as part of a larger study on the higher systematics of Paleozoic crinoids, explicitly evaluated a model for the ancestor-descendant relationship between *Cupulocrinus* and Flexibilia and recovered a posterior probability of 0.99 (Wright, 2017a). Although this result indicated that *Cupulocrinus* was likely paraphyletic, the genus-level resolution of the study did not allow for the examination of which exact cupulocrinid species was the most probable ancestor to the rest of the flexibles.

Yet the recovery of *Cupulocrinus* as sister to flexible genera in the phylogeny, as well as the strong support (99% probability) for it representing an ancestral morphotaxon to the flexibles, led the authors to remove *Cupulocrinus* from the Cladida and place it within the Flexibilia in a new stem-defined definition of the clade that united the inferred ancestor with all of its descendants (Wright, 2017a; Wright et al., 2017). We follow the classification of Flexibilia as defined by Wright et al. (2017) herein, and consider *Cupulocrinus* species to be placed within Superorder Flexibilia, which together comprise the sister clade to the Eucladida. However, we acknowledge the necessity of distinguishing between taxa that have historically been assigned to the clade (i.e., Flexibilia *sensu* Moore (1978)) separately from those species of *Cupulocrinus* which are now also, technically, "flexibles" *sensu* Wright et al. (2017). Going forward, we propose the term Euflexibilia to refer to those taxa that

possess three infrabasal plates and that have historically been designated as flexible crinoids (i.e., non-*Cupulocrinus* flexibles).

The most recent phylogenetic treatments of early flexibles have maintained usage of character matrices designed to capture genus-level variations in morphology (Wright and Toom, 2017; Cole et al., 2025). The inclusion of newly described euflexible genera, most notably, from outside the paleocontinent of Laurentia, has begun to alter previous notions regarding the tempo of evolution in Superorder Flexibilia, as it has become clear that multiple euflexible lineages were evolving in disparate locations well before the end of the Ordovician. The probability of direct *Cupulocrinus* ancestry to Euflexibilia decreases with this broader taxonomic sampling (0.21 to 0.84, depending on *Cupulocrinus* paraphyletic status; Wright and Toom, 2017), but requires a species-level morphological framework for more definitive assessment. Such an analysis, which makes full use of the morphological data, stratigraphic durations, and biogeographic distributions of all *Cupulocrinus* and euflexible species, is undertaken here in order to best characterize the nature of the origin and evolution of Superorder Flexibilia.

Materials and methods

Taxon selection.—Thirteen species of *Cupulocrinus* and twenty-five species of euflexibles were included in the phylogenetic analysis. This entailed nearly complete coverage of all recognized Ordovician species in these two lineages, including an undescribed specimen, Sagenocrinid sp., from the Katian of Anticosti Island, Québec. Silurian coverage entailed, minimally, complete genus-level representation of flexibles up to the Wenlock stage. For

non-monotypic flexible genera, additional Silurian species were added to inform divergence time estimates and biogeographic analysis such that species representing the type genus, earliest occurrence, and/or first occurrence of a genus in a particular geographic region were also included. In practice, this meant that all but six flexible species known from the study interval were incorporated; the omissions comprised a few members of the speciose genera *Protaxocrinus* and *Clidochirus* Angelin, 1878, that were otherwise well-sampled in the phylogeny and for which the benefits of their inclusion was not deemed to outweigh the loss of analytical resolution granted by increasing the ratio of the number of taxa analyzed compared to the overall number of character traits coded in the morphological matrix. Three Late Ordovician species of the eucladid genus *Dendrocrinus* Hall, 1852, were also coded and set as the outgroup in the analysis according to their proximal phylogenetic placement outside of Superorder Flexibilia as recently defined by Wright et al. (2017).

Characters and coding.—A total of 60 characters were coded for traits relating to crown and proximal column morphology in the 41 taxa analyzed. The character matrix generated is an expanded version of the one used by Cole et al. (2025) in the most recent phylogenetic analysis of flexible crinoids, modified to capture species-level variation among a larger set of focal taxa. We supplemented the Cole et al. (2025) matrix with additional characters related to the size and location of the posterior plates, which have previously been used to capture differences in cladid crinoid morphology (Wright et al., 2017), as well as characters from Brower's (2001) analysis that characterize the variation in size, number, and arrangement of interradial and interbrachial plates. The added focus on morphology of the posterior and lateral interrays aligns with those features primarily used to assign taxa among

the two euflexible orders, Sagenocrinida and Taxocrinida. The type species for these orders occur outside of our study interval, and exhibit representative morphologies that are most distinct in later Paleozoic euflexibles and less obvious among early members of the clade. We aim to evaluate the monophyly of these orders in Ordovician and early Silurian representatives, which is something that has previously been called into question (Moore and Laudon, 1943; Moore, 1978; Wright and Toom, 2017; Cole et al., 2025). Additionally, based on recent work using aspect ratios of the calyx to distinguish between species of *Cupulocrinus* and *Protaxocrinus* (Ausich and Copper, 2010), three new ratio-based traits were added to capture these relative size differences: the height of the infrabasal circlet compared to the height of the cup; the length of the arms compared to the height of the cup; and the width to height ratio of the first primibrachials. Length measurements were made for all these dimensions, and the continuous distribution of ratios was discretized into character states by looking for natural breaks in the clustering of ratios; breaks largely aligned with the interquartile ranges for the spread of values in all taxa, and character states were assigned accordingly.

Polymorphic traits were relatively rare among flexible taxa but were coded as such where relevant to capture the multistate calyx ornamentation patterns of a few species. The default treatment of character states was unordered; however, three characters were treated as ordered: number of infrabasal plates, presence of interradials, and presence of interbrachials. Ordering in the number of infrabasals was justified given the developmental lability exhibited in some *Cupulocrinus* populations, whereby a small fraction of individuals possess a total number of infrabasals (four) which is intermediary between the typical *Cupulocrinus* number (five) and the number in the euflexibles (three). Such aberrations in

the infrabasal circlet likely indicate an underlying pathway for reduction in plate number from five to four to three, and we order the character states based on that assumption (Peter, 2019). Similarly, some of the earliest flexibles express variability in their possession of interradial and interbrachial plates; some species may overwhelmingly be lacking in both, but occasionally have individuals that possess one or a few small, irregular plates in some or multiple of their interradial and interbrachial regions. We hypothesize that it is more likely for a lineage which has sometimes exhibited interradial/interbrachial plating to give rise to a descendant with similar morphology rather than for such a species to arise from an ancestor that has uniformly lacked any such interradial/interbrachial plating. The coded character matrix and a description of all character states are included in Appendix I.

Phylogenetic analysis.—Evolutionary relationships were assessed via Bayesian inference incorporating the fossilized birth–death (FBD) process (Heath et al., 2014), which is a tip-dating approach that jointly estimates a phylogeny and divergence times among lineages with explicit incorporation of fossil sampling and diversification dynamics (Wright, 2017a; Wright et al., 2021; Mulvey et al., 2025). The FBD process thus allows for inclusion of the temporal information of fossil stratigraphic data alongside morphological character data to better constrain the estimation of divergence times in inferred phylogenies (Wright, 2017a; Wright and Warnock, 2022). We used the sampled ancestor implementation of the FBD process (Gavryushkina et al., 2014) to set a prior distribution on branch durations, and placed broad priors on FBD parameters as in recent flexible phylogenetic analyses (Wright and Toom, 2017; Cole et al., 2025). The morphological character evolution model was set to the variable rates Mk model of Lewis (2001) with a ‘relaxed-clock’ inverse gamma prior

distribution that accounted for heterogeneity in rates of character evolution across the tree, and a standard gamma distribution modeling rate variation among characters (Ronquist et al., 2012; Heath and Moore, 2014; Wright and Hopkins, 2025). Species of *Dendrocrinus* were used as an outgroup in the analysis. Age calibrations on the stratigraphic ranges of included taxa were based on the 2024 International Chronostratigraphic Chart (Cohen et al., 2025) and regional stage correlation in Goldman et al. (2020). The posterior distribution was estimated using Markov chain Monte Carlo (MCMC) simulation in MrBayes v3.2.7 (Ronquist et al., 2012). Two MCMC runs with two chains were run for 20 million generations, reaching an average deviation of split frequencies < 0.01. Chains were sampled every 10,000 generations, and the first 20% of samples were discarded as burn-in. Convergence was diagnosed through inspection in Tracer 1.7.2 (Rambaut et al., 2018) and visual assessment of chain mixing efficiency (Nascimento et al., 2017). Node support was evaluated by examining their posterior probability, which is calculated as the frequency with which clades are recovered across trees in the posterior distribution.

To quantify age estimates for the origination of Flexibilia and its two major subclades, *Cupulocrinus* and Euflexibilia, node ages from the tree outputs of the FBD analysis were calculated for both the maximum clade credibility (MCC) tree as well as the subset of trees from the posterior (n = 1480, 92.44% of trees) that recovered a reciprocally monophyletic relationship between the two flexible lineages. Assessing the concordance of age estimates between the point estimate for phylogeny (MCC tree) versus a distribution of phylogenies helps to evaluate the robustness of age estimates to uncertainties in tree topology across the posterior distribution (Soul and Wright, 2021).

Biogeographic analysis.—To infer the probable geographic origin and evolution of Flexibilia, we estimated ancestral biogeographic states on the MCC tree using a discrete-state Markov model (Pagel, 1999; Revell and Harmon, 2022). Ancestral biogeographic states were inferred using the R package *corHMM* (Beaulieu et al., 2022), which allows multistate tip input and estimates marginal likelihoods for each state at each node.

We assigned species to geographic basins defined by physical and environmental barriers within paleocontinents (e.g., Appalachian Foreland Basin and Cincinnati Basin within Laurentia) as well as between adjacent paleocontinents (e.g., Avalonia, Baltica) (Lam et al., 2018; Stigall, 2023; Vilela-Andrade and Stigall, 2025). Fossil occurrences were compiled from the primary literature and assigned to paleogeographic regions based on their paleocontinental location at latest Ordovician time. A total of eight regions were occupied by Late Ordovician and early-middle Silurian flexibles: Avalonia (A), for occurrences in the United Kingdom and southern Ireland; Baltica (B), for occurrences in Sweden and Estonia; and six regions within Laurentia, including Scoto-Appalachia (O), for occurrences in southern Scotland; eastern Canada (E), for occurrences in eastern Québec (including Anticosti Island); the Appalachian Foreland Basin (F), for occurrences in New York, southern Ontario, and southwestern Québec; the Cincinnati Basin (C), for occurrences in Ohio and northern Kentucky; the Upper Mississippi River Valley (U), for occurrences in Minnesota, Wisconsin, Iowa, Illinois, and Missouri; and the Southern Appalachian Basin (S), for occurrences in Tennessee. Taxon regional assignments are provided in Appendix II.

Repositories and institutional abbreviations.—Specimens were examined from the Field Museum of Natural History (UC); the Geological Survey of Canada (GSC); the Department

of Geology at Tallinn University of Technology, Estonia (GIT); the Fossil Invertebrates collections at the American Museum of Natural History (AMNH); and the Buffalo Museum of Science (BMS). An undescribed sagenocrinid specimen included in this study is reposited in the Invertebrate Paleontology collections at the Sam Noble Oklahoma Museum of Natural History (OU), Oklahoma, USA, under catalog number OU 238400.

Results

Phylogenetic results.—The MCC tree from the Bayesian FBD analysis recovers vanishingly little support for the hypothesis of direct *Cupulocrinus* ancestry for Euflexibilia (Fig. 2). The earliest divergence within the ingroup shows very high posterior probability (PP) for a reciprocally monophyletic relationship between *Cupulocrinus* and Euflexibilia (PP = 0.95 and 0.93, respectively). Indeed, across the posterior distribution of trees, over 92% (n = 1480) of the sampled phylogenies support a topology with monophyletic cupulocrinid and euflexible clades. In a random subset (20%) of the posterior phylogenies which did *not* support a reciprocally monophyletic relationship between the two flexible subgroups (n = 121), none recovered a paraphyletic *Cupulocrinus*, but rather sampled topologies with uncertainty in placement for *Paerticrinus* and species of *Protaxocrinus*. The cumulative posterior probability that known species of *Cupulocrinus* are sampled ancestors within the phylogenetic analysis is < 0.01. Thus, Springer's model was not supported in the MCC tree, nor was it an area of tree space frequently explored during the Bayesian analysis.

Within Euflexibilia, the first major bifurcation largely demarcates taxa that have nominally been assigned to the order Taxocrinida from those that have been assigned to

Sagenocrinida. This contrasts with previous Bayesian analyses for early flexibles, which recovered a paraphyletic 'Taxocrinida' (Wright, 2017a; Wright and Toom, 2017; Cole et al., 2025). Genera previously assigned to Taxocrinida include *Ladacrinus*, *Paerticrinus*, and *Protaxocrinus*. Excluding the placement of *Ladacrinus*, the MCC topology reflects a reciprocally monophyletic relationship between the two orders. The strongly supported (PP = 0.86) relationship between *Ladacrinus* and the sagenocrinid genus *Hormocrinus*, both of which share characters of posterior and lateral interray plating different from the other euflexible clades, indicates that the former is more accurately placed within Sagenocrinida, making the two orders monophyletic within our study interval.

In addition to the well-supported basal split within Flexibilia, several clades at the family and genus level received posterior probabilities greater than 0.5. This included a monophyletic Icthyocrinidae family (including genera *Clidochirus*, *Prolixocrinus*, and *Icthyocrinus*) at probabilities ranging from 0.71–0.98; a monophyletic Homalocrinidae family (including genera *Tintinnabulicrinus*, *Cryptanisocrinus*, and *Homalocrinus*) at probabilities ranging from 0.95–1; a monophyletic Sagenocrinitidae family (including *Scapanocrinus* and an unnamed form from Anticosti Island, Québec) at a probability of 0.94; and strong support (PP = 0.58–0.81) for the grouping of all species of *Protaxocrinus* except for *P. girvanensis*, which had support < 0.5.

The family Anisocrinidae, including genera *Anisocrinus*, *Kyphosocrinus*, and *Anticosticrinus*, is recovered as paraphyletic and ancestral to the Sagenocrinitidae, though with node support less than 0.5. The genus *Proanisocrinus*, which has historically been a member of Anisocrinidae, is not recovered as closely related to other members of the family, however its placement elsewhere is relatively uncertain (PP = 0.22). The genus

Cryptanisocrinus, also historically considered a member of the Anisocrinidae, is instead strongly supported (PP = 1) as a member of the Homalocrinidae.

Clade origination dating results.—The posterior distribution of node ages for the origin of Flexibilia and its two major subclades, *Cupulocrinus* and Euflexibilia, is depicted in Fig. 3. The mean origination age for Flexibilia across the posterior distribution is 463.6 Ma (Darriwilian), which is similar to the value on the MCC tree (463.2 Ma). This is within the range of origination estimates (458.9 to 468.2 Ma) from previous studies with differing interpretations for the phylogenetic position of *Cupulocrinus* (Wright and Toom, 2017; Cole et al., 2025). The recovered Sandbian origin of *Cupulocrinus* is nearly identical to that found in Cole et al. (2025), with an average of 458.1 Ma across the posterior distribution and 457.7 Ma on the MCC. The euflexibles have an average origination of 458.4 Ma (latest Darriwilian), and 456.5 Ma (Katian) on the MCC tree. This is 6 to 8 million years younger than the most recent estimate (Cole et al., 2025), but in line with the estimate of Wright and Toom (2017).

A conservative estimate for the time required to assemble the euflexible bodyplan from an ancestral cladid morphology is calculated by subtracting the mean age of origination for Euflexibilia from the mean age of origination for all Flexibilia. Across the posterior distribution, this value is 5.1 myr. The MCC tree infers a slightly longer assembly time for the euflexible bauplan, at 6.7 myr.

Biogeographic results.—The common ancestor of all Flexibilia is reconstructed to have occupied the Upper Mississippi River Valley of Laurentia, as are the ancestors of the *Cupulocrinus* and euflexible clades (Fig. 4). After an early Sandbian origin, the cupulocrinids dispersed throughout Laurentia during the Katian and, by the end of the Hirnantian, occupied all Laurentian basins except for the Southern Appalachian basin. Most species of *Cupulocrinus* remained within the Upper Mississippi River Valley, Cincinnati Basin, and Appalachian Foreland Basin for the duration of the clade's history. It was not until the middle-late Katian, roughly 449 Ma, when they dispersed out of central Laurentia, leading to the origination of new species of *Cupulocrinus* in the distal Laurentian areas of Eastern Canada and Scoto-Appalachia. At the time that *Cupulocrinus* went extinct during the LOME, the clade had not dispersed outside Laurentia.

The inferred Sandbian origin of Euflexibilia was more quickly followed by dispersal to distal Laurentian areas and neighboring paleocontinents. By the middle of the Katian, roughly 450.5 Ma, the homalocrinids had originated in Baltica and the anisocrinids had arisen in Eastern Canada (Anticosti Island). The remaining sagenocrinid euflexibles largely stayed contained to the Upper Mississippi River Valley of Laurentia until the Silurian, although at least one icthyocrinid species is known from Eastern Canada in the early Hirnantian. The taxocrinid euflexibles are reconstructed to have most likely arisen in the Appalachian Foreland Basin of Laurentia during the early Katian, and by the latest Ordovician they occupied distal Laurentian basins in Eastern Canada and Scoto-Appalachia. They are not found in Baltica until Silurian time.

Discussion

Flexible origins.—We applied a Bayesian tip-dated phylogenetic framework to species-level morphological data that explicitly incorporated probabilistic assessment of ancestor-descendant relationships in early flexibles. Contrary to long-held belief, the origin of Euflexibilia via direct descendance from a paraphyletic *Cupulocrinus* is not supported. Rather, the two lineages appear to be separate monophyletic groups within Superorder Flexibilia, and both arose in latest Darriwilian or early Sandbian time. The estimated origination of the most recent common ancestor of both *Cupulocrinus* and Euflexibilia (i.e., the most recent common ancestor of Flexibilia), arose in central Laurentia in the early-middle Darriwilian. This places the origin of Flexibilia within the initial phase of a globally significant interval of biotic and abiotic change known as the Great Ordovician Biodiversification Event (GOBE) (Webby et al., 2004; Stigall et al., 2019, 2020, 2026). The GOBE is a period of elevated origination rates which resulted from increased oceanographic cooling, oxygenation, and sea level rise that altered circulation patterns, enhanced primary productivity, and drove biotic diversification worldwide (Stigall et al., 2019). A vast array of marine organisms, including crinoids, exhibited enhanced diversification at higher taxonomic levels as part of the GOBE (Wright and Toom, 2017; Cole, 2018). The origin of Superorder Flexibilia fits within this pattern. Subsequent origins in the Sandbian of *Cupulocrinus*, Euflexibilia, and the euflexible orders Taxocrinida and Sagenocrinida are likewise manifestations of the Ordovician Radiations within the peak of the GOBE.

Evolutionary patterns and paleobiogeography.—Our tip-dated phylogenetic analysis indicates that the time required to assemble the euflexible bodyplan from the most recent common ancestor of all Flexibilia is roughly 5–7 myr. Additionally, the earliest known fossils of euflexible crinoids are not found until 5–7 myr after their inferred divergence. Flexibles are rare in early Paleozoic assemblages, especially prior to the O–S turnover in crinoid evolutionary faunas when the post-LOME diversification of flexibles increased their richness and abundance within crinoid communities. However, despite this rarity, estimates of species-level sampling probabilities for flexibles are actually higher than estimates for other Paleozoic crinoid genera (Wright and Toom, 2017). Instead, part of the explanation for their unsampled early evolution lies not with preservational biases but with the skewed paleogeographic distribution of historical sampling and worker effort. The Ordovician rocks of central Laurentia are well known, and the species contained therein were the ones available to Springer (1920) when he was first building a hypothesis for the likely ancestry of the Euflexibilia. Taxocrinids have the most diverse fossil record of all euflexibles in the Late Ordovician of central Laurentia; that Springer would draw conclusions based on the morphological similarities between co-occurring *Cupulocrinus* and *Protaxocrinus* genera is not surprising. What Springer did not know, and what has become profoundly clear with increased sampling of late Ordovician and early Silurian localities outside central Laurentia, is that 'derived' sagenocrinid lineages coexisted alongside taxocrinids and plesiomorphic sagenocrinids during the Katian. Over half of the sagenocrinid species in our phylogeny are from recently described faunas of Anticosti Island, Québec, and deposits from the paleocontinents of Baltica and Avalonia. These taxa demonstrate that at the time *Protaxocrinus* was diversifying in the Appalachian Foreland Basin of Laurentia,

contemporaneous diversification was underway for the anisocrinids in eastern Canada and the homalocrinids in Baltica. Knowledge of parallel radiations within Euflexibilia — by middle Katian time — highlights how fundamentally the description of new species from under-sampled paleogeographic regions can alter our perception of the tempo of evolution in the clade. Continued field work and taxonomic assessment of crinoid faunas from this time interval, focusing on under-sampled paleogeographic regions, may shorten the gap between the estimated origination of Euflexibilia and its sampled occurrences in the fossil record. Such work is essential to contextualize the spatial dynamics of early flexible evolution, and draw meaningful connections between dispersal and speciation events within Flexibilia and the environmental factors that may have facilitated them.

Based on our present understanding of the diversity and biogeography of early flexible taxa, there are interesting similarities and differences among major flexible clades in the timing and implications of dispersal events inferred in our biogeographic reconstruction. Global tectonic processes led to eustatic sea level rise that culminated in the early Katian, and high sea levels alongside modeled ocean surface circulation routes facilitated larval dispersal among Laurentia, Baltica, and Avalonia for brachiopods, trilobites, and other marine benthos (Lam et al., 2018; Stigall et al., 2019). The Katian expansion of *Cupulocrinus* and *Protaxocrinus* into distal regions of Laurentia, and the Sandbian dispersal of sagenocrinid euflexibles as far as Baltica (Wright and Toom, 2017), are consistent with the timing of dispersals in other taxa, although opposite directionality (i.e., dispersal from Baltica/Avalonia into Laurentia, rather than vice versa) was more common in several other benthic marine clades (Lam et al., 2018). What is noteworthy in a macroevolutionary sense is that the euflexibles, which had a wider geographic distribution leading up to the LOME,

survived the extinction while their sister lineage, the cupulocrinid flexibles, did not. Whether this was merely the random result of stochastic extinction, or because cupulocrinids faced heightened extinction selectivity in their narrower range, is an interesting avenue of future research. The rise of flexibles as a major constituent of the Middle Paleozoic CEF documents only the rise of Euflexibilia, and investigating the ecological differences between the two major groups of flexibles, as well as comparing them to other groups of Ordovician–Silurian crinoids, will help to elucidate the biotic mechanisms contributing to differential survival and faunal turnover across the LOME.

Systematic paleontology

Classification and terminology.—The higher classification of crinoids used here follows Ausich et al. (2015) and Wright et al. (2017). Morphologic terminology follows Ubaghs (1978), Wright (2015), and Ausich et al. (2020). Conventions for open nomenclatural assignment follow Bengtson (1988).

Class Crinoidea Miller, 1821

Subclass Pentacrinoidea Jaekel, 1918

Infraclass Inadunata Wachsmuth and Springer, 1885

Parvclass Cladida Moore and Laudon, 1943

Superorder Flexibilia Zittel, 1895

Remarks.—Our phylogenetic analysis largely supports the monophyly of euflexible orders and families within our study interval. Taxocrinida, one major branch of Euflexibilia, consists of the genera *Paerticrinus* and *Protaxocrinus*. The genus *Ladacrinus*, while previously considered a taxocrinid, is instead strongly supported as a close relative of the sagenocrinid *Hormocrinus*. Unlike all other taxocrinids, the radianal and anal X plates in the posterior interray of *Ladacrinus* are not in contact with one another, and this, together with the number and relative size of its interradial plates, more closely allies this genus within the Sagenocrinida.

The family Icthyocrinidae is recovered within our study interval as a strongly supported Laurentian clade that originated in the middle Katian of the Upper Mississippi River Valley. Early members of the family belong to the genus *Clidochirus*, which Eckert and Brett (2001) noted was a genus in need of revision to correct a series of emended diagnoses that rendered it of little taxonomic value. Such revision is beyond the scope of this project, however the recovered substructure within the species of *Clidochirus* included in our phylogeny points to the accuracy of their hypothesis. Regardless, the family is monophyletic, with Ordovician species of *Clidochirus* giving way to the Silurian genera *Prolixocrinus* and *Icthyocrinus.*

The early evolution of the family Homalocrinidae comprises a monophyletic lineage of Baltic and Avalonian taxa that arose in the middle Katian. *Tintinnabulicrinus*, described from Baltic sediments in Estonia, is the earliest known member of the family and the only known Ordovician representative. In the Silurian, *Cryptanisocrinus* and *Homalocrinus* are known from Baltic and Avalonian strata. *Cryptanisocrinus* has most recently been included

in the family Anisocrinidae, although at the time it was described, Donovan et al. (1992) noted that the triangular appearance of the species' basal plates due to basal invagination of the calyx was much more reminiscent of the morphology of *Homalocrinus*. Our phylogeny supports the close relationship between these two genera. Similarly, the biogeographic occurrence of *Cryptanisocrinus* outside of Laurentia is consistent with its placement within the Homalocrinidae, as opposed to the otherwise Laurentian-bound family of Anisocrinidae.

Family Cupulocrinidae Moore and Laudon, 1943

Genus *Cupulocrinus* d'Orbigny, 1850

Type species.—Scyphocrinus heterocostalis Hall, 1847, by subsequent designation.

Other species.—Cupulocrinus angustatus (Meek and Worthen, 1870); *C. canaliculatus* Brower and Veinus, 1978; *C. crossmani* Brower, 1992; *C. heterobrachialis* Ramsbottom, 1961; *C. humilis* (Billings, 1857); *C. jewetti* (Billings, 1859); *C. kentuckiensis* Springer, 1911; *C. latibrachiatus* (Billings, 1857); *C. levorsoni* Kolata, 1986; *C. molanderi* Kolata, 1975; *C. plattevillensis* Kolata, 1975; *C. polydactylus* (Shumard, 1858).

Occurrence.—Late Ordovician (Sandbian–Katian) from Canada (Québec, Ontario), the United States (Minnesota, Wisconsin, Iowa, Illinois, Missouri, Ohio, Kentucky, New York), and the United Kingdom (Scotland).

Remarks.—We feel it is warranted to reiterate a few taxonomic notes pertaining to other putative species of this genus given that — perhaps due to the obscure location of some of these notes in the literature — several names continue to linger in recent studies on early flexibles yet we omit them from consideration in our analysis.

The first example is *Cupulocrinus minimus* Springer, 1911, from the Katian Waynesville Limestone of Ohio. As Brower (2002) noted, this is merely the common historical designation for juveniles of *C. polydactylus*; the frequent co-occurrence of the two forms and the presence of a continuous growth sequence between them supports the idea that *C. minimus* is a junior synonym of *C. polydactylus*. Another example is *C. sepulchrum* Ramsbottom, 1961, from the Katian Gaerfawr Group of the United Kingdom. We concur with Brower (1992) that the morphology of the arms and the anal sac in this specimen differs from that typical of *Cupulocrinus* and much more closely resembles that of the genus *Dendrocrinus* (and we used that assignment as an outgroup taxon in our phylogenetic analysis). Additional to the morphological differences, the geographic occurrence of this species on the paleocontinent of Avalonia falls outside the otherwise Laurentian-bound geographic range of *Cupulocrinus*.

Similarly, the species *C. austrogracilis* Jell, 1999, from the Devonian of Australia, falls well outside the understood spatial and temporal range of the genus; Brower (2001)

pointed to the unusual anal sac of this specimen in addition to its lengthy separation in space and time from other members of *Cupulocrinus* as evidence that the generic assignment was in error. Even Jell (1999) expressed some hesitancy in his placement but ultimately decided in favor given the affinity of his species with *C. drummuckensis* Kolata, 1975 (=*C. gracilis* Ramsbottom, 1961) However, Brower (1992) had in fact moved that species out of the genus *Cupulocrinus* and tentatively into his new genus, *Praecupulocrinus*. Thus, while the "true" generic placement of Jell's species is unknown to us, we feel certain it is not a species of *Cupulocrinus*.

Lastly, both Brower (1992) and Wright et al. (2019) correctly noted that *Dendrocrinus erraticus* Miller, 1881, from the Cincinnatian of Ohio, is in fact a specimen of *Cupulocrinus*. Neither report had Miller's type specimen on hand and simply left the assignment at *C. erraticus*. After locating Miller's specimen in the collections of the Field Museum, we have identified it as a specimen of *C. polydactylus* (see Figs. 1.1, 1.2).

Clade Euflexibilia Crowley and Wright, new clade

Definition.—The Euflexibilia is stem-defined as the most inclusive clade containing *Taxocrinus macrodactylus* (Phillips, 1841) but not *Cupulocrinus heterocostalis* (Hall, 1847).

Remarks.—Euflexible crinoids are strongly supported (posterior probability = 0.93) as a monophyletic group in our phylogenetic analysis, and are sister to the flexible clade

containing species of *Cupulocrinus*. The morphology of euflexibles relative to other crinoid clades has most recently been summarized in Wright et al. (2017) in the definition for Flexibilia Zittel, 1895; the same apomorphies described therein and used in previous studies (Springer, 1920; Moore and Laudon, 1943; Moore, 1978) to describe the Superorder are applicable to the Euflexibilia: typical lowermost circlet comprised of three (rather than five) infrabasal plates, with one smaller azygous plate in the C ray (except for the derived *Forbesiocrinus*); universally uniserial arms that lack pinnules and often curl inwards upon death; posterior plate arrangements similar to other cladids but which are sometimes absent in more derived euflexibles; possession of interradial/interbrachial plating in many species, in contrast to other cladids; and a stem that is nearly always transversely circular (Springer, 1920; Wright et al., 2017). Euflexibles arose in the Middle/Late Ordovician and range through the Permian.

Order Sagenocrinida Springer, 1913

Superfamily Sagenocrinitacea Roemer, 1854

Family Homalocrinidae Angelin, 1878

Genus *Cryptanisocrinus* Donovan et al., 1992

Type species.—Cryptanisocrinus kilbridensis Donovan et al., 1992, by monotypy.

Remarks.—This genus is moved to the Homalocrinidae based on its recovered phylogenetic relationship with other members of the family. The morphology of *Cryptanisocrinus* is within the range of that diagnostic for homalocrinids. This species is the earliest representative of the family from Avalonia (Silurian: Telychian).

Family Sagenocrinitidae Roemer, 1854

Sagenocrinid sp.

Figs. 1.10, 1.11

Description.—Calyx preserved from approximately the middle secundibrachials to tips of the strongly incurved arms. Crown medium (maximum width 30 mm; preserved height 20 mm). Cup bowl-shaped, wider than high. Plate sutures flush with plate surfaces; rugose pitting ornamenting interray plates, interbrachials, and fixed brachials, and single median spine present in fixed secundibrachials and proximal tertibrachials. Nature of the infrabasal, basal, and radial circlets, the primibrachials, the posterior plating, and the tegmen, column, and holdfast unknown.

Interrays wide, composed of numerous irregularly shaped but roughly pentagonal and hexagonal plates that decrease in size distally from the base of the crown, extending to the level of the tertibrachials. Brachials fixed through the tertibrachials; intersecundibrachials also pentagonal/hexagonal, decreasing in size distally, forming a single row of plates until about the secundibrachitaxis, where they begin to form smaller, laterally

adjacent rows of plates. A few very small, irregular intertertibrachials are present in most rays.

Free arm openings 20, four per ray. Arms branching isotomously at least 4 times, with branching points roughly symmetric on either side of each ray axis and the inner branch of the half-ray splitting lower than the outer branch; all bifurcations give rise to arms of equal size. Patelloid processes visible on secundibrachials and above. Arms curve inwards at about the level of the quartibrachials.

Remarks.—Notwithstanding the incomplete preservation of this specimen, particularly of the infrabasal and posterior plating that is typically used to diagnose members of Flexibilia, we place it within that Superorder on the following grounds: 1) uniserial, non-pinnulate arms are one of the chief diagnostic characters of flexible crinoids, as is the commonality for distal portions of those arms to curl inward (Springer, 1920; Moore and Laudon, 1943); and 2) the seeming presence of a patelloid process in this specimen (see Fig. 1.11) affiliates it with most members of *Cupulocrinus* and several other early flexible species in the genera *Protaxocrinus* and *Clidochirus*, and is not a feature known to occur in other groups of crinoids (Brower, 2001). Our assignment of this new form to Sagenocrinitidae specifically pertains to the numerous interradial and interbrachial plates of the species, comparable in abundance within this time interval only to *Scapanocrinus muricatus* Eckert and Brett, 2001, from the Telychian Wolcott Limestone of New York. While we currently refrain from making generic and specific diagnosis on the basis of this single incomplete specimen, we nonetheless emphasize the novelty of this form and its unique combination of characters as the first Ordovician representative of Sagenocrinitidae and the oldest member of its family,

pushing back the known origin of Sagenocrinitidae by at least 7 myr. This specimen joins the growing number of examples from recent decades where the description of new flexible crinoid taxa from outside the continental United States has greatly enhanced our understanding of the paleogeographic distribution and tempo of evolution in Euflexibilia leading up to and following the Late Ordovician mass extinction.

Occurrence.—The only known specimen, OU 238400, is from the Vauréal Formation (Late Ordovician: Katian) at Carleton Point, Anticosti Island, Québec (49.72809° N, 62.93836° W).

Acknowledgments

We thank Paul Mayer and Bill Simpson (Field Museum of Natural History) and Tiffany Adrain (Paleontology Repository at the University of Iowa) for assistance with curated specimens. Melanie Hopkins, Selina Cole, Gabriel Soto, and Jake Spicer are thanked for assistance during fieldwork resulting in the collection of OU 238400. This research was supported in part by NSF EAR #2346400 to D.F.W., and through funding to K.D.C. from the N. Gary Lane Student Research Grant (Paleontological Society), the Bob & Jay Gilson Educational Fellowship (Oklahoma Geological Foundation), and the School of Geosciences at the University of Oklahoma. The specimen described in this study was collected and accessioned with permission of the Ministère de l'Environnement et de la Lutte contre les changements climatiques, de la Faune et des Parcs under permit no. 7912-09-01-0000403, ref. 402486935.

Figures

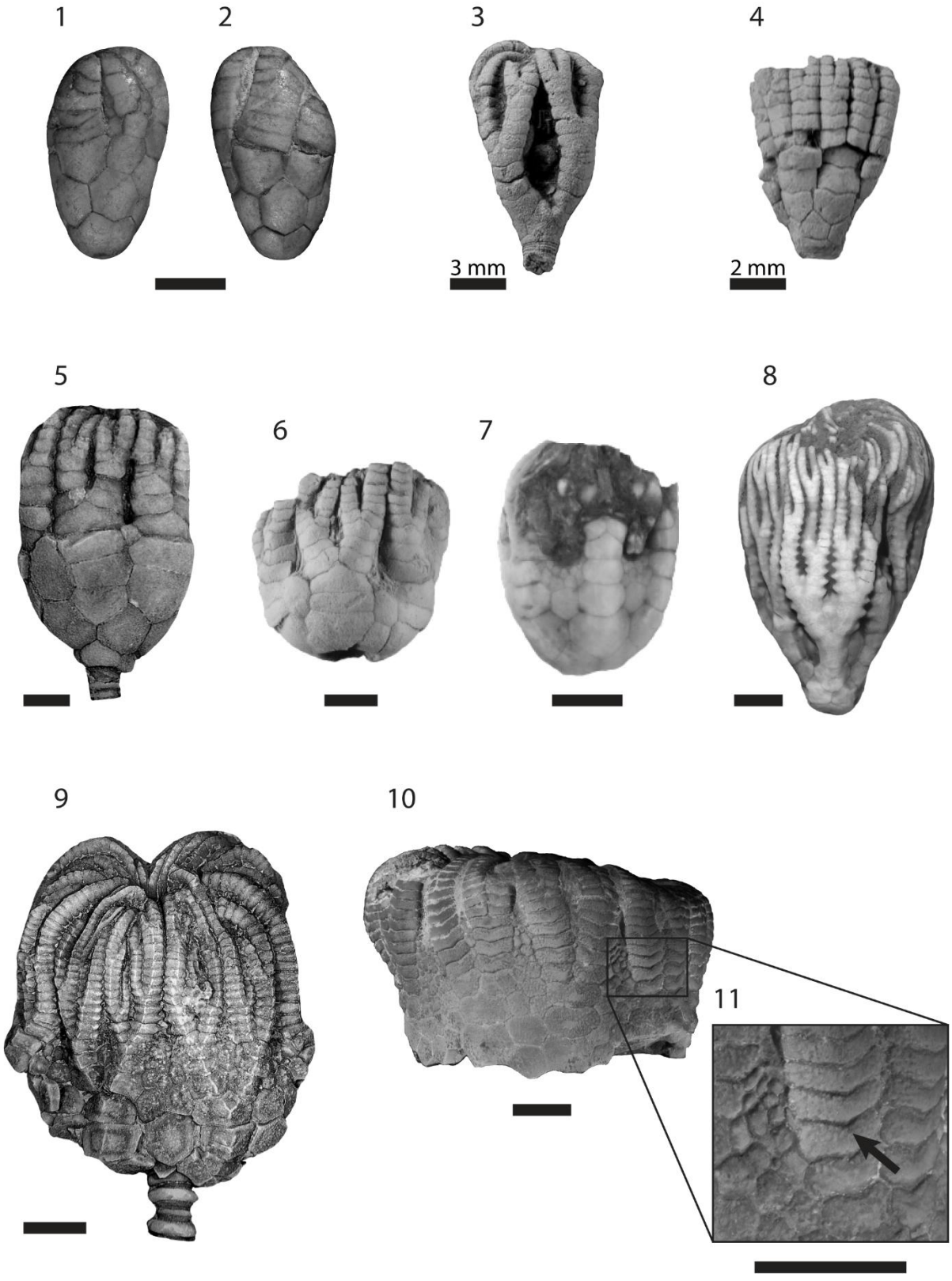

Figure 1. Representative diversity of Ordovician and lower Silurian flexible crinoids. **(1–2)** *Cupulocrinus polydactylus* (Shumard, 1857), UC 8895, drift from the Hudson River Grp. (Katian) near Cincinnati, Ohio. **(1)** Lateral view of CD interray. **(2)** Lateral view of B ray. **(3)** *Protaxocrinus sideros* Ausich and Copper, 2010, GSC 126758, from the Jupiter Fm. (Telychian) of Anticosti Island, Québec (image courtesy of W.I. Ausich). Lateral view of CD interray. **(4)** *Clidochirus vaurealensis* Ausich and Copper, 2010, GSC 126669, from the Vauréal Fm. (Katian) of Anticosti Island, Québec (image courtesy of W.I. Ausich). Lateral view of crown. **(5)** *Kyphosocrinus tetreaulti*, BMS E26377, from the Wolcott Ls. (Telychian) of New York (reproduced from Eckert and Brett, 2001, with permission from the Paleontological Research Institution, Ithaca, NY). Lateral view of C ray. **(6)** *Tintinnabulicrinus estoniensis* Wright and Toom, 2017, GIT 563-3, from the Vasalemma Fm. (Katian) of Estonia. Lateral view of D ray and posterior plating, whitened with ammonium chloride. **(7)** *Paerticrinus arvosus* Wright and Toom, 2017, GIT 405-255, from the Varbola Fm. (Rhuddanian) of Estonia. Lateral view of A ray, photographed under alcohol. **(8)** *Anticosticrinus natiscotecensis* Cole, Wright, and Hopkins, 2025*,* AMNH-FI-139850, float likely from the Ellis Bay Fm. (Hirnantian) of Anticosti Island, Québec. Lateral view of A ray, photographed under alcohol. **(9)** *Scapanocrinus muricatus*, BMS E26386, from the Wolcott Ls. (Telychian) of New York (reproduced from Eckert and Brett, 2001, with permission from the Paleontological Research Institution, Ithaca, NY). **(10–11)** Sagenocrinid sp., OU 238400, from the Vauréal Fm. (Katian) of Carleton Point, Anticosti Island, Québec. **(10)** Lateral view of crown whitened with ammonium chloride. **(11)** Enlarged view of **(10)** showing details of interbrachial plating and nodose sculpture; brachial patelloid process marked with arrow. All scale bars = 5 mm unless otherwise noted.

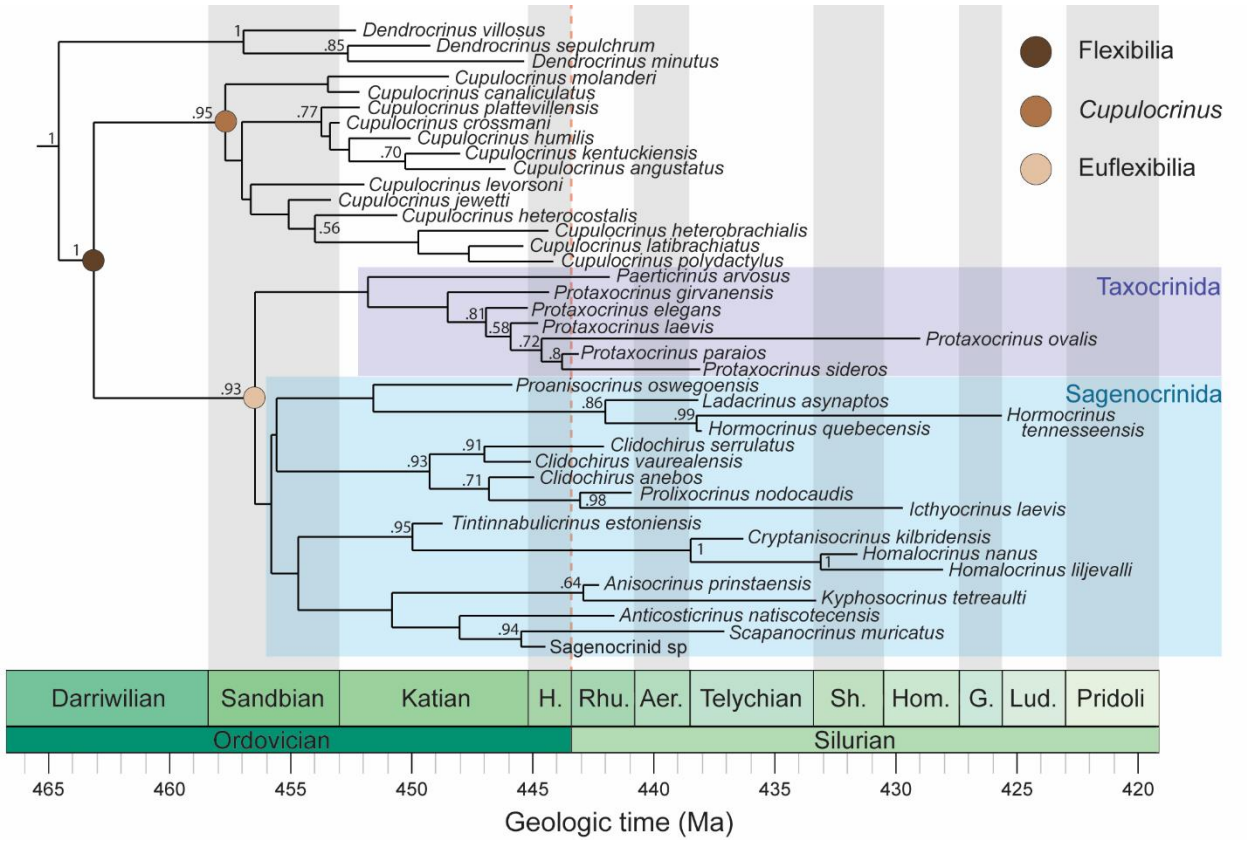

Figure 2. MCC tree from the tip-dated Bayesian phylogenetic analysis incorporating the FBD process. Nodes with posterior probabilities higher than 0.50 are labeled. Branch lengths are scaled to geologic time. Three nodes are labeled with colored circles to indicate those clades later analyzed in divergence dating estimates: all members of Superorder Flexibilia (dark brown); species within the genus *Cupulocrinus* (brown); and species within Euflexibilia (light brown). Within Euflexibilia, colored boxes encapsulate the two monophyletic groups that represent the orders Taxocrinida (purple) and Sagenocrinida (blue). H. = Hirnantian; Rhu. = Rhuddanian; Aer. = Aeronian; Sh. = Sheinwoodian; Hom. = Homerian; G. = Gorstian; Lud. = Ludfordian. Vertical red dashed line highlights the Ordovician–Silurian boundary.

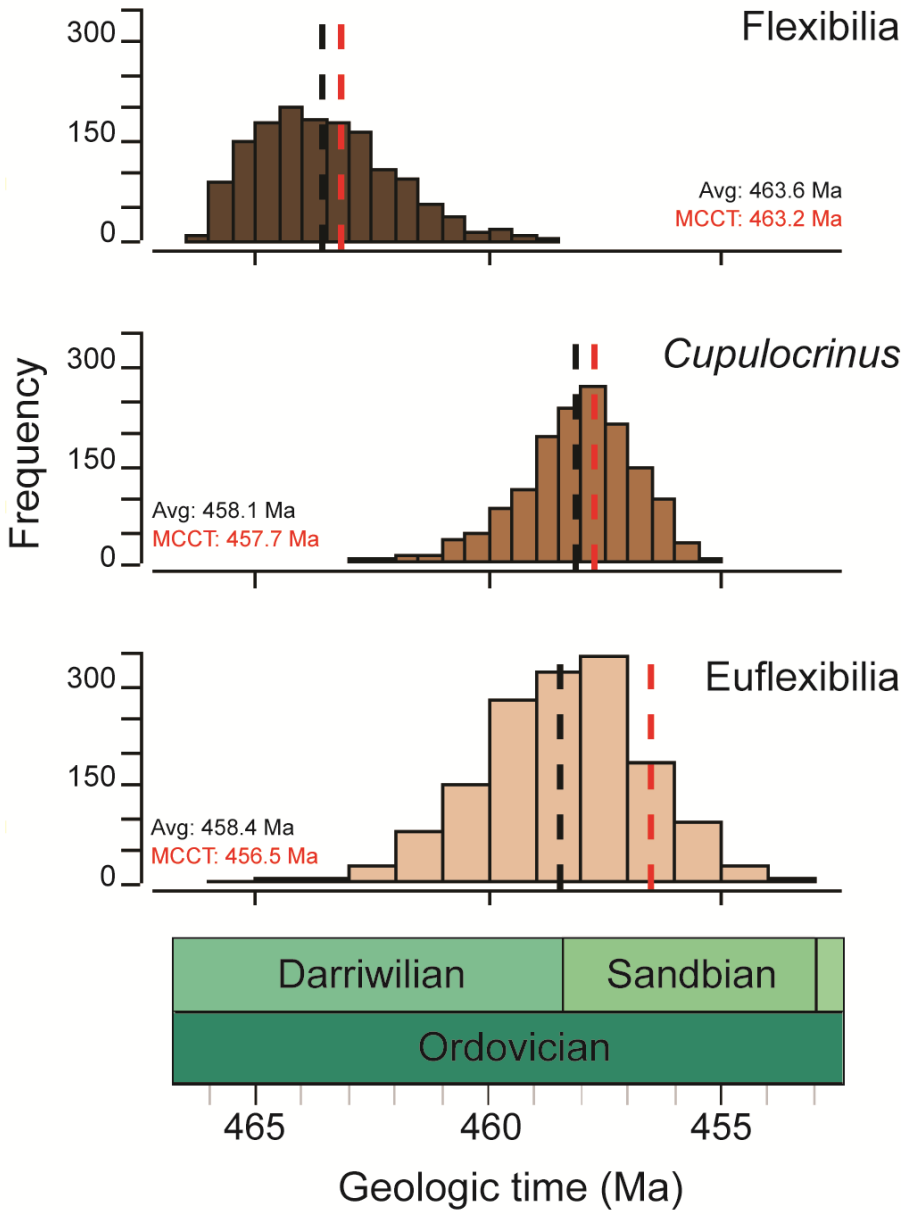

Figure 3. Frequency distribution of clade origination times across the subset of trees from the posterior distribution that supported a reciprocally monophyletic relationship between *Cupulocrinus* and Euflexibilia (92.4% of trees). Divergence estimates shown for three clades: **(1)** all Flexibilia (dark brown), **(2)** *Cupulocrinus* (brown), and **(3)** Euflexibilia (light brown). Black dashed line indicates the average origin time across the posterior subset of trees. Red dashed line indicates the recovered origin time on the MCC tree.

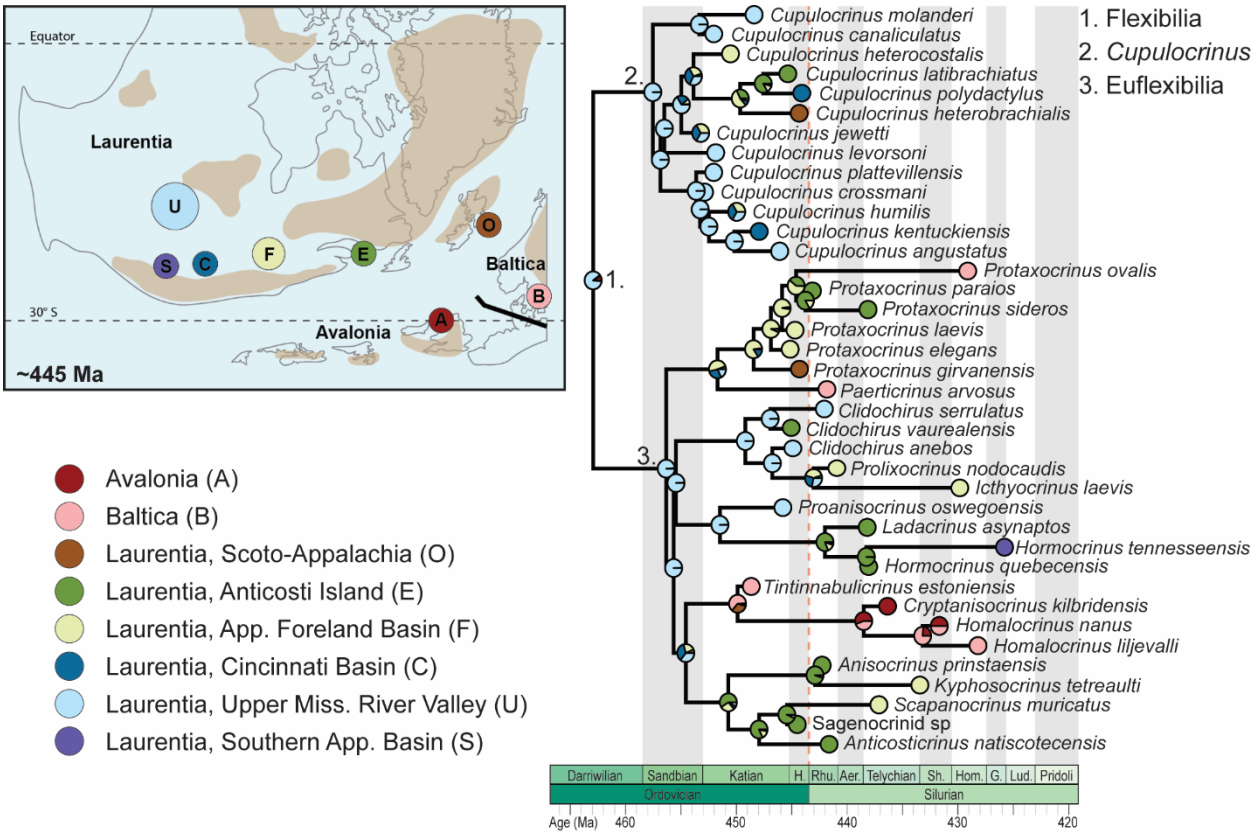

Figure 4. Biogeographic evolution across the MCC phylogeny for Ordovician and lower Silurian flexibles. Colored circles at terminal branch tips indicate the observed geographic basin(s) of occurrence(s) for each taxon. Species found in only a single region are represented by a filled circle of one color; species found in multiple basins possess a multi-colored circle with slices proportional to the number of regions they occupy. Pie charts at interior nodes represent the proportional likelihood of various geographic affinities for the unsampled ancestors at those nodes. Map inset shows paleogeographic reconstruction for the latest Ordovician, ~445 Ma (after Cocks and Torsvik, 2011). Geographic basins of interest are indicated by colored circles with alphabetical codes as listed in the text. Light gray lines show the margin of modern continental landmasses for reference; beige coloring indicates landmasses at O–S time. The thick black line between Avalonia and Baltica marks the

approximate suture line between those two paleocontinents, which fused at the end of the Ordovician. H. = Hirnantian; Rhu = Rhuddanian; Aer. = Aeronian; Sh. = Sheinwoodian; Hom. = Homerian; G. = Gorstian; Lud. = Ludfordian. Vertical red dashed line highlights the Ordovician–Silurian boundary.

Chapter II: The ecological and developmental dimensions of a post-extinction radiation in Ordovician–Silurian crinoids (Superorder Flexibilia)

Abstract.—The use of tip-dated fossil phylogenies alongside paleontologically-motivated phylogenetic comparative methods permits novel modeling approaches for investigating the tempo and mode of phenotypic diversification across mass extinction events. Crinoids of Superorder Flexibilia originated during the late Middle Ordovician and, following the Late Ordovician mass extinction (LOME), radiated to comprise one of the major constituents in Paleozoic crinoid communities. However, the mechanistic underpinnings of this radiation and the role of the LOME in shaping post-extinction diversification trajectories remains unclear. Here, we use a Bayesian tip-dated phylogenetic framework incorporating the fossilized birth–death process to fit five process-based macroevolutionary models of trait diversification for Late Ordovician through middle Silurian (Wenlock) flexible crinoid species. We test alternative hypotheses involving shifts in tempo and/or mode of trait diversification across the LOME for three morphologic traits directly related to flexible crinoid ecology and development. Models involving an evolutionary regime shift across the LOME are supported for body size and calyx complexity, although the relative filtration fan area of the clade appears largely constrained across the event. At a finer taxonomic resolution within Flexibilia, differing ecomorphological dynamics suggest the possibility of extinction selectivity acting against certain flexible subclades. These findings highlight the nuanced manner in which biotic and abiotic drivers in the Late Ordovician impacted subsequent phenotypic trajectories in the clade.

Introduction

The intrigue of mass extinctions is nothing new to paleontologists. The complex interplay between species' ecological response to environmental stressors and their evolutionary outcomes is impacted by mass extinction events, which generate ecological opportunity for phenotypic diversification among survivors (Cole and Hopkins, 2021; Monarrez et al., 2021; Edie et al., 2025). The Late Ordovician mass extinction (LOME) was the first of the five largest episodes of catastrophic diversity decline observed in the Phanerozoic marine fossil record, with glacially induced eustatic sea level fall triggering the extinction of some 40% of marine genera and 80% of marine species and initiating a long-lasting restructuring of the marine biota (Ausich and Deline, 2012; Marshall, 2023; Harper, 2024). The biological impacts of the LOME are expressed in multiple, quasi-independent macroevolutionary currencies: taxonomic diversity, morphologic disparity, and functional ecology (Jablonski, 2022). To better understand the short- and long-term evolutionary consequences of mass extinction events, we need detailed analyses of phylogenetically-constrained and ecologically-understood fossil taxa, and contextual examples for hypothesis testing of particular patterns of selectivity and rebound in these macroevolutionary currencies throughout deep time (Jablonski and Edie, 2025).

The LOME has been a study system rich in both phylogeny-based and paleoecological analyses. Particularly in crinoids, which are an abundant and diverse taxonomic group in many Paleozoic fossil assemblages, numerous studies have worked towards quantifying the shift in taxonomic composition or ecological niche occupation in taxa on either side of the LOME (Ausich and Deline, 2012; Wright, 2017a; Cole et al., 2019; Cole and Wright, 2022). Crinoid communities experienced a major faunal transition during

this time, and the waning of the Early Paleozoic crinoid evolutionary fauna (CEF) gave way to the increased taxonomic richness of constituents of the Middle Paleozoic CEF, including the species-rich and morphologically diverse Superorder Flexibilia (Ausich and Deline, 2012; Wright and Toom, 2017; Cole and Wright, 2022). The differential extinction of various crinoid taxa over the course of the LOME leads to intriguing questions regarding what traits operate as extinction filters, and similarly, what traits are impacting rebound dynamics during wholesale restructuring of post-extinction communities. These questions are applicable to multiple hierarchical levels, as not only did the taxonomic and ecological trajectories of crinoid higher taxa shift (i.e., the turnover in CEFs), but the response of various lineages within these clades to the LOME also differed. In Flexibilia, the superorder as a whole achieved greater taxonomic richness, ecological diversity, and morphological disparity in the Silurian, but this was due to the success of the flexible subclade Euflexibilia, not the flexible genus *Cupulocrinus*, which went extinct during the LOME (Crowley and Wright, in prep.).

Taxonomic turnover in crinoids was accompanied by changes in morphological disparity, including for morphological traits that correlate with ecological functions ("ecomorphological traits"), such as those related to feeding ecology or life history. Crinoid body size, estimated by measure of the volume of the calyx, experienced a significant decrease across the LOME, referred to as the "Lilliput Effect" (Borths and Ausich, 2011; Salamon et al., 2021). This macroevolutionary trend is a phenomenon observed in myriad organismal groups during mass extinction events and their rebounds (Monarrez et al., 2021). In the case of crinoids, body size is a trait which shows niche retention in some species and may relate to differences in metabolic levels or fecundity between taxa (Cole et al., 2019;

Borths and Ausich, 2011). Multivariate and comparative analyses of Ordovician crinoid ecology have also demonstrated a phylogenetic signal in community-level niche differentiation based on ecomorphological traits related to the passive suspension feeding strategies of these organisms, measured via calculation of the size of the feeding apparatus, or filtration fan area (Cole et al., 2019; Cole and Wright, 2022). Given that different clades of crinoids appear to have occupied different niches in Ordovician communities, we might expect to see selectivity among those clades on the basis of their feeding ecology during an episode of variable resource availability. In such a case, the rise of Middle Paleozoic CEF constituents including Superorder Flexibilia may relate to their possession of a phenotypic adaptive benefit in feeding ecomorphology or their more successful exploitation of food resources than Early Paleozoic CEF taxa. Additionally, the developmental control on the number of sutured plates in the calyx is more rigidly fixed (i.e., invariable) in some clades of crinoids than others (Ausich, 1988; Peter, 2019). Predisposition for lability in calyx construction could feasibly enable certain groups of crinoids to more quickly adapt their body size or relative size of the feeding apparatus as changes to their environment selected for alternate ecological traits. Thus, during a major mass extinction event and/or the subsequent recovery interval, selection for or against certain of these ecological and developmental traits might impact the overall evolutionary history of the group (Cole and Hopkins, 2021).

Phylogenetic comparative methods that investigate rate variation in phenotypic evolution are a reasonable approach when attempting to explain changes in morphological disparity over geologic time, but models which account for variation in both tempo *and* mode of evolution are biologically plausible for certain scenarios such as mass extinction

events (Slater, 2013). Indeed, during an interval of abiotic and biotic upheaval such as the LOME and coincident Early- to Middle-Paleozoic CEF faunal turnover, it is intuitive to hypothesize that the true evolutionary process generating morphological disparity might have changed, not merely the pace of evolution. Pre-extinction constraints on diversification due to competition or other factors very well may have been released over the course of the mass extinction event, with surviving taxa quickly diversifying post-extinction to occupy newly vacant ecological niche space. Similar stories have been proffered for dramatic episodes of faunal turnover associated with mass extinctions. For example, the K-Pg mass extinction has long been implicated as a key driver of mammal diversification following the rapid demise of non-avian dinosaurs (Alroy, 1998; Slater, 2013; Benevento et al., 2023). The rise and fall of higher order crinoid clades surrounding the Late Ordovician mass extinction offers a similarly ideal system for testing macroevolutionary regime shifts in phenotypic diversification across a mass extinction interval.

To address this question in crinoids over the LOME, we apply a series of macroevolutionary models using phylogenetic comparative methods to examine multiple phenotypic traits. First, we use the Ordovician to middle Silurian (Wenlock) fossil record of flexible crinoids to construct a Bayesian tip-dated phylogenetic framework for species occurring immediately prior to and following the Late Ordovician mass extinction. We use this phylogenetic inference as a template for comparative methods that investigate five alternative macroevolutionary models of phenotypic change in three traits directly related to crinoid ecology and development. The five tested models assess relative support for shifts in tempo and/or mode of phenotypic evolution in flexible crinoid body size, relative filtration fan area, and calyx complexity during the mass extinction, and in so doing, determine the

degree to which phenotypic evolution in the clade was impacted by the LOME. Determining whether observed patterns of disparity in flexibles are the result of changes in evolutionary pace or, rather, release from constrained Ordovician adaptive zones is informative of the evolutionary process generating those phenotypic patterns in the early history of the clade. Additionally, analyzing the macroevolutionary response of multiple ecomorphological and developmental traits allows for a more nuanced interpretation of how evolutionary forces might be shaping certain traits during the Silurian radiation of Flexibilia, and whether response among those traits may have varied in a manner significant to the transition between dominant constituents in pre- and post-LOME crinoid communities. This work serves as an important case study for contextualizing the phenotypic dynamics of higher order crinoid faunal turnover during one of the largest mass extinction events of the Phanerozoic.

Materials and methods

Phylogenetic analysis.—Phylogenetic assessment of Late Ordovician through middle Silurian flexible crinoids was performed using a tip-dated Bayesian inference incorporating the fossilized birth–death (FBD) process (Heath et al., 2014), which jointly estimates evolutionary relationships and divergence times given the observed stratigraphic occurrence and morphological character data for included taxa (Wright, 2017a; Mulvey et al., 2025). We added the temporal stratigraphic information for 65 middle Silurian flexibles to the phylogenetic framework of a recent study (Crowley and Wright, in prep.; see Chapter I) that focused on evaluating the relationships between Late Ordovician through early Silurian

(Llandovery) flexible species. We used the character matrix and maximum clade credibility (MCC) tree from Crowley and Wright (in prep.) to inform our analysis over this broader set of focal taxa, sampling all flexible species (n = 103) known from the Late Ordovician through the middle Silurian (Wenlock). Since the total number of flexible species within this interval is well above the number of characters in the coded character matrix (n = 60), and the addition of many Wenlock species with only stratigraphic data (not character data) might lead to convergence issues in the phylogenetic inference, we used the MCC topology from Crowley and Wright (in prep.) to set clade constraints on the nodes in our tree that represented strongly supported (posterior probability > 0.5) relationships among early flexibles. This served to limit the regions of treespace explored with the larger taxon set in a way that more accurately reflected the early evolution of Flexibilia as inferred using more comprehensive (both temporal and morphological) data in the smaller-scale study. Wenlock species were placed into this topological framework in a "taxonomy tree" manner, using the assignment of flexible orders, families, and genera as outlined in Moore (1978). As an example, middle Silurian species belonging to the flexible order Taxocrinida were appended in an unresolved polytomy with the Ordovician and early Silurian representatives of that order, and then allowed to explore topologies within that subclade. The full backbone cladogram used to constrain our tree inference is provided in Appendix III.

Phylogenetic analysis was conducted in MrBayes v3.2.7 (Ronquist et al., 2012) using the sampled ancestor implementation of the FBD process (Gavryushkina et al., 2014). We placed broad priors on FBD parameters as in recent flexible crinoid phylogenetic analyses (Wright and Toom, 2017; Cole et al., 2025; Crowley and Wright, in prep.). The model of morphological character evolution was set to the variable rates Mk model of Lewis (2001)

with a ‘relaxed-clock’ inverse gamma prior distribution that accounted for heterogeneity in rates of character evolution across the tree, and we used a standard gamma distribution to model rate variation among characters (Ronquist et al., 2012; Heath and Moore, 2014; Wright and Hopkins, 2025). Three species of the cladid crinoid genus *Dendrocrinus* were set as the outgroup. Two Markov chain Monte Carlo runs with two chains were run for 20 million generations and reached an average deviation of split frequencies < 0.01. Chains were sampled every 10,000 generations, and the first 20% of samples were discarded as burn-in. Convergence was diagnosed through inspection in Tracer 1.7.2 and confirmation of effective sample sizes ≥ 200 for all parameters (Rambaut et al., 2018).

Trait measurements.—We collected data for three composite traits that have previously been shown to relate to crinoid ecological function and development. We used the existing framework for quantifying aspects of crinoid niche differentiation via measurements of calyx and arm morphology (Cole et al., 2019; Cole and Wright, 2022) and modified our approach to account for the apinnulate nature of flexible crinoid arms. This involved measurement of calyx height (from the base of the calyx to where the arms break free), calyx width (at its maximum point, at or below where the arms break free), and arm length (from where the arms become free of the calyx to their tips) (Fig. 1.1). These measurements were then used to compute the composite characters of calyx volume and filtration fan area, following the equations described in Cole et al. (2019) (Fig. 1.2). Filtration fan area (FFA) is an ecomorphological trait which rarely exhibits phylogenetic signal in crinoid communities (Cole et al., 2019; Cole and Wright, 2022), and species with relatively similar FFA values can possess vastly different calyx sizes and constructions. To standardize the calculated fan

areas to more accurately capture the size of the feeding apparatus in relation to the overall body size of the crinoid, we converted the FFA values to *relative* filtration fan areas by dividing FFA by the calyx volume for each species. Finally, calyx complexity scores were computed for each species by summing the total number of plates in the fused portion of the calyx below where the arms break free (Fig. 1.3). Values for calyx volume, relative filtration fan area, and calyx complexity were log-transformed prior to model-fitting (Benson et al., 2022). Species with incomplete calyx data (n = 2) and species lacking known arm morphology (n = 10) were omitted from the model-fitting analyses for the volume/complexity and relative FFA traits, respectively. Calculated trait values for measured specimens are provided in Appendix IV.

Modeling trait evolution.—Five process-based macroevolutionary models were fit to the calyx volume, relative fan area, and calyx complexity datasets in order to test various hypotheses regarding the tempo and mode of trait evolution in Ordovician through middle Silurian flexibles. Two of these models, the Brownian motion (BM) and Ornstein-Uhlenbeck (OU) models, were investigated using the *fitContinuous* function in the R package *geiger* (Harmon et al., 2008). These models are time-homogenous and imply a uniform tempo and mode of evolution across the entirety of the study interval. Brownian motion represents a null model of trait evolution, with no inherent net directionality to trait change. In this mode of evolution, the variance in quantitative trait X increases linearly as a function of time, with a constant tempo (step rate, σ):

$$dX(t) = \sigma dW(t) \quad [1]$$

In Equation [1], the *dW(t)* term is the "white noise" that characterizes non-directional Brownian motion, with erratic movement of mean = 0 and a constant variance *dt* (Butler and King, 2004). In contrast, the Ornstein-Uhlenbeck model represents a mode of evolution interpreted as stabilizing selection, with a Brownian motion process that is constrained by an elastic band parameter (α) which pulls traits back towards an optimum value (θ), or "adaptive zone" (*sensu* Simpson, 1944), when they deviate from that optimum:

$$dX(t) = \alpha[\theta - X(t)]dt + \sigma dW(t) \quad [2]$$

When the value of that elastic rebound is zero (i.e., if α = 0), and no force is acting to constrain trait values around an adaptive peak, then Equation [2] collapses down to the BM process described by Equation [1].

We also apply three paleontologically-motivated, time-heterogeneous models involving changes in either tempo, evolutionary mode, or both (Slater, 2013; 2014). These three models, O–S Shift, O–S Release, and O–S Release & Radiate, are time-varying combinations of the simpler time-homogeneous BM and/or OU models and involve a shift in tempo and/or mode across the Late Ordovician mass extinction (Slater, 2013; 2014) (Table 1). The O–S Shift model describes a uniform Brownian motion process of evolution with a shift in tempo (step rate) across the LOME; the O–S Release model describes a uniform tempo of evolution with a change from a constrained Ornstein-Uhlenbeck mode to an unconstrained Brownian motion mode across the LOME; and the O–S Release and Radiate model describes a shift in both tempo and mode, as a constrained Ornstein-Uhlenbeck regime transitions across the LOME into an unconstrained Brownian motion regime with a different step rate. For additional details regarding the five models see Butler and King (2004) and Slater (2013; 2014).

Model fits for each trait were computed on the MCC tree generated herein, and model support was assessed using Akaike weights calculated from small-sample-corrected AIC scores (Burnham and Anderson, 2002). In order to assess how uncertainty in tree topology impacted the model fitting results (Soul and Wright, 2021), we also fit the five macroevolutionary models to a random subset of 200 trees drawn from the posterior distribution of the FBD phylogenetic analysis.

Results

The MCC tree from our phylogenetic analysis is shown in Fig. 2. Within Superorder Flexibilia, the most rootward divergence separates the monophyletic grouping of species of *Cupulocrinus* d'Orbigny, 1850, from the clade representing Euflexibilia (*sensu* Crowley and Wright, in prep.). While *Cupulocrinus* went extinct during the LOME, the more disparate and geographically widespread euflexible clade survived the mass extinction and radiated in the Silurian, exhibiting a diverse array of calyx constructions by Wenlock time (see plate diagrams, Fig. 2). The body size and calyx complexity of flexibles increased over the course of our study interval, while their relative filtration fan area decreased (Figs. S2–S4). In the wake of the LOME, these trends represent evolutionary trajectories for Euflexibilia only, as *Cupulocrinus* was extinct by this time.

Model fitting.—The exact nature and timing of the LOME is debated in the literature, with various global biological and environmental proxies showing some evidence for a two-pulse extinction bracketing the Hirnantian stage (Harper, 2024). We ran two iterations of our

model-fitting analyses, using either an end-Katian or an end-Hirnantian shift point, to capture both possible waves of extinction. The results were largely the same between iterations, and we discuss only the results corresponding to the Ordovician–Silurian boundary here (i.e., end-Hirnantian shift). Model parameters for the end-Katian shift iteration are given in Table S1. Likewise, model-fitting to the random subset of trees (n = 200) from the posterior distribution was mostly congruent with model support on the MCC tree, and so we focus our discussion on the results for the latter.

For calyx volume, the O–S Release and Radiate model was the best supported, with an Akaike weight of 0.52 (Fig. 3). The next best model was the Ornstein-Uhlenbeck (OU) model, at a comparable Akaike weight of 0.47. The remaining models showed negligible support. Rate parameters suggest that flexible crinoid body size data are best fit by a Release and Radiate scenario with a high rate, high elastic-rebound-to-optimum regime in the Ordovician followed by release into a much slower but unconstrained Brownian motion mode in the Silurian (Table 2; Figs. S5, S6). Despite the decreased Silurian rate of evolution under the best-fitting model scenario, the variance in overall body size of flexibles would still be expected to increase due to the release from constraint (Slater, 2013).

The model with the greatest support for relative filtration fan area was the Ornstein-Uhlenbeck model (Akaike weight = 0.58), but the O–S Release and Radiate model also found substantial support (Akaike weight = 0.31). Parameters for the time-homogeneous OU model indicate a step rate half as large as that of the Ordovician rate in the Release and Radiate scenario, and recover an optimum trait value that is 70% as large (Table 2; Figs. S7, S8). The parameters for the Release and Radiate model characterize a faster tempo of

evolution with a stronger pull (250%) towards the optimum in the Ordovician, which releases into a Brownian motion process with a rate 38% as large in the Silurian.

Calyx complexity exhibited the widest spread of support among models, but was best fit by the time-heterogeneous models, specifically evolution under an O–S Release (Akaike weight = 0.33) or O–S Shift (Akaike weight = 0.32) scenario. The α parameter for the O–S Release model was larger than that of the OU components for other models fit to calyx complexity, but the release of this attraction parameter would have led to the large increase in observed disparity of calyx complexity in the Silurian (Table 2; Figs. S4, S9). In contrast, the rise in calyx complexity under the O–S Shift model is explained by a doubling of the rate of evolution following the LOME (Fig. S10).

Discussion

Our model fitting results indicate that there is no single model that overwhelmingly characterizes the diversification regime of all three traits. This suggests that different evolutionary processes were likely shaping the phenotypic trajectories for calyx volume, relative filtration fan area, and calyx complexity. Even assessing the results for each trait individually, model support is distributed such that no single model eclipses the rest, and none surpasses the $\Delta AICc > 4$ threshold that is standard for determining strong support for one model over others (Burnham and Anderson, 2002). Despite this, we do generally observe support for the more complex models that incorporate a shift in tempo or mode at the O–S boundary. While there exists an inherent bias towards recovering models with low phylogenetic signal, such as the Ornstein-Uhlenbeck model, if there is uncertainty in tree

topology or error in trait measurement (Slater, 2013; Soul and Wright, 2021), it is more difficult to explain the observed support for complex models if not due to there being a true signal in the trait data that is strong enough to support increased model complexity despite penalization for the additional parameters. Thus, while our results do not incontrovertibly identify specific evolutionary processes affecting each trait, they are not uninformative, and indeed the variation in outcomes between traits provides an ideal opportunity to explore the nuances in the biological response of Flexibilia within the broader context of crinoid faunal turnover and Late Ordovician environmental change.

As has been documented previously (Borths and Ausich, 2011) for several major crinoid groups including flexibles, we observe a brief decrease in body size in the Hirnantian stage, followed by a rapid return to pre-extinction calyx volume by the early Silurian (Fig. S2). Under the best supported Release and Radiate model, this Silurian change in body size not only captures the return to previous values, but also indicates a general increase in the variance of flexible body size through the middle Silurian. Biological interpretation for this shift in tempo and mode suggests that a process of ecological release served to generate a greater range of body sizes in the Silurian despite an overall slower tempo of evolution, and by the end of the study interval, mean flexible calyx volume had increased compared to earlier stages of time. The context for this ecological release is best framed by considering the contemporaneous biotic response of other major crinoid groups with respect to body size during the turnover in crinoid evolutionary faunas. If flexibles were released from a constrained Ordovician adaptive zone, and expanded in the Silurian into vacated niche space, it was perhaps facilitated by the decline in diversity and abundance of diplobathrid camerates, which possessed the largest body sizes of Ordovician crinoid groups (Cole, 2018;

Cole and Wright, 2022). Diplobathrids were a major constituent of the Early Paleozoic CEF, but decreased in taxonomic diversity and abundance in crinoid communities following the LOME. This may have cleared the way for flexibles to explore a wider and larger range of body sizes in Silurian crinoid communities that were previously occupied by diplobathrid taxa.

Ecologically, body size is a trait with complex relationships to organismal metabolism and reproduction, and complicated and sometimes conflicting implications for selectivity during background versus mass extinction intervals (Jablonski, 1996; Monarrez et al., 2021). Crinoid calyx volume reflects the metabolic cost of growth, but likely also fecundity and feeding capacity; a smaller crinoid with reduced feeding capacity and lower fecundity may be disadvantaged during background intervals, but adaptive during a mass extinction event when faced with unstable ecological conditions including decreased primary productivity and increased biotic stressors (Borths and Ausich, 2011). The Hirnantian drop in mean flexible body volume may signify that flexibles survived the LOME by employing life strategies associated with smaller body size, but later expanded after the extinction into larger body sizes when they had the ecological opportunity and it was no longer detrimental for them to do so. Indeed, for many groups of invertebrates, organismal traits related to ecology and physiology are under greater selection during mass extinction events (Monarrez et al., 2021).

We recover little variation in diversification regime for relative filtration fan area across our study interval, as the best supported Ornstein-Uhlenbeck model is time-homogenous and connotes constrained adaptive zone occupation for this trait spanning the LOME. This seems at first surprising, given that the morphology of the filtration fan has

been shown to be immensely important in governing extinction rates for higher taxonomic groups of Paleozoic crinoids, and might therefore be expected to shape macroevolutionary dynamics during a mass extinction event (Baumiller, 1993). There are a couple of reasons this may be, the first of which is that our metric of relative filtration fan area may not be capturing the same aspect of feeding ecology as these earlier studies which have found macroevolutionary significance in the *density* of the filtration fan, and analyzed not only the area of the fan but also the number of terminal appendages within it (Baumiller, 1993; Cole et al., 2019; Cole and Wright, 2022). Generally speaking, flexible crinoids have an open-mesh filtration fan, and comparatively lower fan densities than camerate crinoids because they lack specialized feeding structures called pinnules, which evolved independently in camerate and articuliform crinoids (Wright et al., 2017; Wright, 2017b). These differences in fan density are phylogenetically structured among higher order crinoid groups, with long-term implications for extinction and origination dynamics at large taxonomic scales (Baumiller, 1993). But there is still variation within clades, and our data may be failing to capture differences in the degree of arm branching within flexibles that are more informative of feeding capacity than simply measuring the area of the fan in relation to body size. Further testing is warranted to characterize potential shifts in flexible fan density across the LOME. Our measurements for relative filtration fan area exhibit a slight decline in mean value over the course of the study interval (Fig. S3). However if, for example, flexibles are simultaneously increasing their number of arm branchings during this time, a morphological shift associated with altered feeding opportunities due to the LOME might lead to support for a time-heterogenous model recovering changes in tempo and/or mode of flexible feeding ecology.

Conversely, if our measure of relative fan area is adequately depicting flexible feeding capacity through the study interval, the seeming lack of change in evolutionary regime for the trait may be due to the fact that flexibles were preadapted in their morphological feeding ecology to withstand the extinction pressures of the LOME, and at least within Superorder Flexibilia, the extinction was non-selective for feeding ecology and thus flexibles did not face long term macroevolutionary consequences due to the event. Multiple authors have noted that crinoids such as flexibles which have larger mesh filters tend to be ecological "generalists," possessing wider ambulacral grooves designed to capture a larger range of prey sizes, and able to live in a broader range of environments with varying water current velocities (Brett, 1984; Baumiller, 1993; Brower, 2013). Such crinoid taxa have longer stratigraphic durations and lower extinction rates over the course of the Paleozoic, demonstrating the long-term success of that feeding strategy (Baumiller, 1993). If prevailing tendencies for generalization versus specialization in crinoid feeding ecology are structured at higher taxonomic scales, we would expect feeding morphologies to generate differential responses between major classes of crinoids, such as between camerates and flexibles, but less so to impact diversification trajectories at finer taxonomic scales, such as between species within Superorder Flexibilia. Overall, crinoids that were constrained to shallow, high-energy environments in order to capture sufficient prey to meet the metabolic requirements of a dense filtration fan may have faced heightened extinction risk against a backdrop of rapid and significant sea level fall during Late Ordovician glaciation. However, groups like flexibles that could inhabit deeper, quieter water environments and subsist on a more diverse array of food resources simply may not have felt as significant of an impact from the LOME.

It may also be the case that observed changes in calyx complexity are surreptitiously linked to flexible feeding ecology as well. Calyx complexity lies at the nexus of crinoid ecology and development, because change in the number of sutured plates in the calyx is facilitated by underlying developmental mechanisms, but any such change in plating has direct ramifications for calyx volume and, by extension, the size of the filtration fan compared to that volume. Both the mean and variance of flexible calyx complexity increased significantly over our study window (Fig. S4), with model support suggesting that this arose from either a release from constraint or a doubling of the rate of evolution post-LOME. The evolutionary trend towards increased calyx complexity was accomplished in multiple ways, with some flexibles adding numerous interradial and interbrachial plates (as in the sagenocrinitids), and others tending towards fusion of brachial plates even to the distal portions of the arms (as in *Icthyocrinus*). It has been noted that such extremes in Silurian flexible morphology would have rendered the filtration fan inefficient at capturing food in the manner traditionally envisioned for suspension feeding crinoids (Brett, 1984). Instead, such taxa with larger bowl-shaped calyxes and arms in proximal contact may have had a capacity for rapid arm closure, thereby creating an external chamber within which their numerous tube feet could aid in the digestion of larger food particles (Brett, 1984). The morphological architecture required for such an exploration of non-traditional crinoid feeding ecology would include a paired increase in calyx volume and calyx complexity alongside a comparative decrease in proportional size of the filtration fan, which does seem to represent the trends observed in some Silurian flexibles.

Finally, while our study design is best suited to characterize diversification regimes within Flexibilia as a whole, the differential success of its two major subclades,

Cupulocrinus and Euflexibilia, implicates smaller-scale outcomes in likewise shaping the long-term history of the clade. The flexible genus *Cupulocrinus* contained a less disparate grouping of taxa that were larger, less complex, and had proportionally more sizable filtration fans than Ordovician members of Euflexibilia (Figs. S11, S12). Additionally, the geographic range of *Cupulocrinus* was comparatively small, and its species were limited to Laurentia at a time when euflexibles had dispersed to adjacent paleocontinents (Crowley and Wright, in prep.). The combination of larger body size and narrower geographic range, alongside limited experimentation with morphology (low calyx complexity) and higher inferred metabolic requirements (large relative filtration fan area), are all factors expected to lead to heightened extinction risk during a mass extinction event (Jablonski, 1986, 1996; Payne and Finnegan, 2007; Monarrez, 2021). Indeed, *Cupulocrinus* went extinct during the LOME, yet Euflexibilia persisted and radiated during the Silurian. The greater evolutionary innovation evident in euflexible ecomorphology, and their wider geographic dispersal, very well may have aided their survival across the LOME. And in the wake of the mass extinction, they formed the taxonomic foundation from which phenotypic diversification progressed and shaped Silurian flexible evolution.

This study yields novel insight into the evolutionary processes generating patterns of phenotypic diversification in a major crinoid clade, and does so in a way that accounts for the phylogenetic structure of species-level trait data. We provide the first attempt at examining how not just body size, but also two traits directly related to crinoid feeding ecology and development, served to shape morphological trajectories in Superorder Flexibilia at multiple hierarchical scales. Our choice in models aimed at testing whether the biotic and abiotic disturbances associated with the Late Ordovician mass extinction elicited a

phenotypic response in evolutionary tempo and mode for early flexibles. We find that several traits, including calyx volume and calyx complexity, do exhibit such a macroevolutionary regime shift during the LOME, but others, including relative filtration fan area, do not. These results illustrate the variable mechanisms influencing the ecological and developmental dimensions of the radiation of Superorder Flexibilia, and we have expounded upon the biological significance of this variation in trait response. Nonetheless, further model-fitting efforts may reveal that there exists a better model to describe flexible trait diversification within this time interval. A recent study has suggested that the transition in crinoid evolutionary faunas was underway by Katian time, even before the onset of the LOME (Cole and Wright, 2022). If biotic change rather than abiotic change was more instrumental in altering flexible diversification regimes, the temporal shift built into our models may be better placed at an earlier point in time. Alternatively, it may be the case that temporal shift points are less appropriate than one determined by some anatomical innovation or adaptation in the flexible body plan. Especially considering the noted differences between ecomorphological disparity in the two major flexible subclades, *Cupulocrinus* and Euflexibilia, models allowing for different diversification trajectories among these subclade divisions within the phylogeny may be more suitable for exploring the factors affecting the evolutionary history of the clade (Soul and Wright, 2021).

Acknowledgments

This research was supported in part by NSF EAR #2346400 to D.F.W., and through funding to K.D.C. from the N. Gary Lane Student Research Grant (Paleontological Society), the Bob

& Jay Gilson Educational Fellowship (Oklahoma Geological Foundation), and the School of Geosciences at the University of Oklahoma.

Tables

Model	Category	VCV	Notes
Brownian motion (BM)	Time-homogeneous	$V_{ij} = \sigma^2 C$	Random walk; step rate (σ) is constant and variance increases linearly as a function of time.
Ornstein-Uhlenbeck (OU)	Time-homogeneous	$V_{ij} = \sigma^2 (exp^{-\alpha t_{ij}})(1 - exp^{-2\alpha C_{ij}})$	BM process with elastic band parameter (α) indicating strength of the pull towards an optimum value.
O–S Shift	Time-heterogeneous	$V_{ij} = \sigma_0^2 \, min(C_{ij}, t_{shift}) + \sigma_1^2 \, max(0, C_{ij} - t_{shift})$	BM process with different rate (σ) values at different time intervals.
O–S Release	Time-heterogeneous	$V_{ij} = \frac{\sigma^2}{2\alpha} (exp^{-\alpha tOU_{ij}})(1 - exp^{-2\alpha COU_{ij}}) + \sigma_1^2 \, max(0, C_{ij} - t_{shift})$	OU process that reverts to BM (α = 0) after the time shift.
O–S Release and Radiate	Time-heterogeneous	$V_{ij} = \frac{\sigma_{OU}^2}{2\alpha} (exp^{-\alpha tOU_{ij}})(1 - exp^{-2\alpha COU_{ij}}) + \sigma_{BM}^2 \, max(0, C_{ij} - t_{shift})$	OU process that reverts to BM (α = 0) after the time shift. The step rate (σ) differs between time intervals.

Table 1: Five macroevolutionary models of trait diversification tested for calyx volume, relative filtration fan area, and calyx complexity in flexibles across the LOME. Elements of the variance-covariance (VCV) matrix are from Butler and King (2004) for time-homogeneous models, and Slater (2013; 2014) for time-heterogeneous models.

Trait	Model	LnL	AICc	AICcWt	θ	Rate	α	Rate 2
Calyx Volume	Brownian motion	-191.60	387.32	0.00	5.09	0.53	NA	NA
	Ornstein-Uhlenbeck	-184.32	374.89	0.47	5.95	0.81	0.12	NA
	Ordo–Sil Shift	-191.28	388.82	0.00	5.10	0.64	NA	0.48
	Ordo–Sil Release	-188.06	382.36	0.01	5.15	0.61	0.13	NA
	Ordo–Sil Release & Radiate	**-183.12**	**374.67**	**0.52**	**5.17**	**5.37**	**1.10**	**0.08**
Relative Filtration	Brownian motion	-141.90	287.94	0.05	2.65	0.26	NA	NA
Fan Area	**Ornstein-Uhlenbeck**	**-138.31**	**282.90**	**0.58**	**1.58**	**0.36**	**0.08**	**NA**
	Ordo–Sil Shift	-141.31	288.90	0.03	2.65	0.33	NA	0.23
	Ordo–Sil Release	-141.04	288.36	0.04	2.36	0.28	0.06	NA
	Ordo–Sil Release & Radiate	-137.84	284.16	0.31	2.22	0.77	0.22	0.29
Calyx Complexity	Brownian motion	-69.23	142.58	0.13	3.13	0.05	NA	NA
	Ornstein-Uhlenbeck	-69.03	144.31	0.06	3.27	0.05	0.01	NA
	Ordo–Sil Shift	-67.30	140.85	0.32	3.12	0.03	NA	0.06
	Ordo–Sil Release	**-67.26**	**140.77**	**0.33**	**3.30**	**0.05**	**0.09**	**NA**
	Ordo–Sil Release & Radiate	-66.94	142.30	0.15	3.26	0.04	0.05	1.55

Table 2. Model fitting results and parameter values for the three ecomorphological and developmental traits analyzed. The best supported model for each trait, i.e., the model with the lowest AICc value and highest weight (AICcWt), is indicated in bold. Alpha (α) is the 'rubber band' parameter for the time-homogeneous Ornstein-Uhlenbeck (OU) model and the time-heterogenous models with an Ordovician OU regime. The Silurian rate parameter (σ^2) is indicated as "Rate 2" for time-heterogeneous models incorporating a change in tempo after the LOME.

Figures

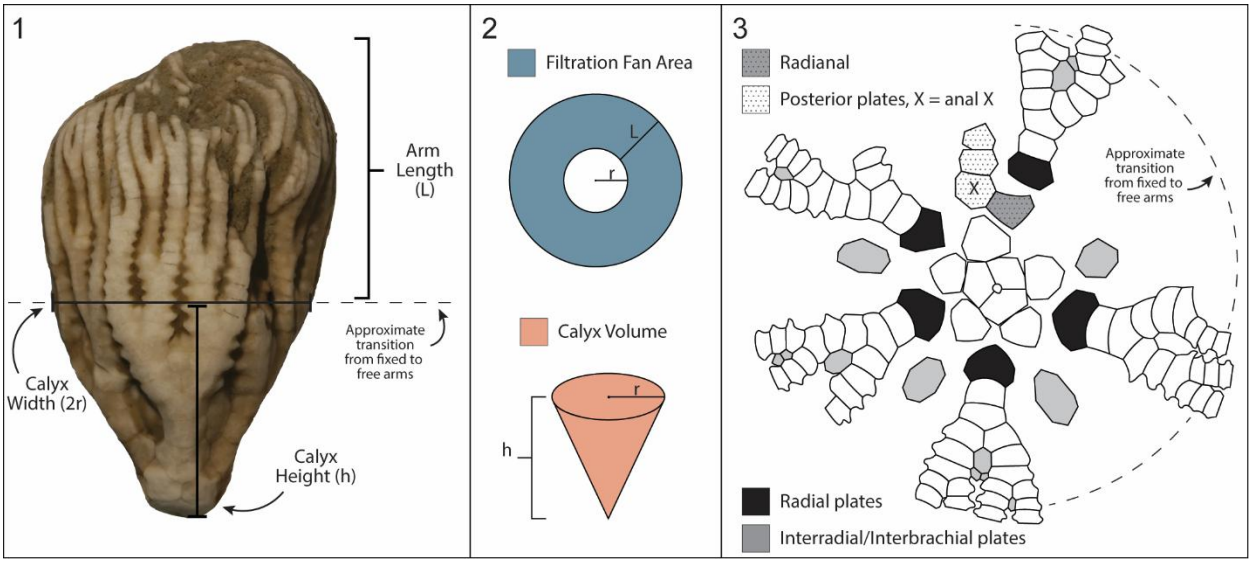

Figure 1. Measurements collected and the visual interpretation of calculated composite ecomorphological and developmental traits. **(1)** Example specimen showing measures for calyx height (calyx base to where the arms become free), calyx width (maximum width, at or below the point where the arms become free), and free arm length. **(2)** Calculated composite traits use the width, height, and length measurements to find the area of the filtration feeding apparatus (light blue), idealized as the area of the ring formed by the extended free arms, and to find the volume of the sutured calyx (light red), idealized as the volume of a cone. **(3)** Plate diagram indicating all plates in the fixed portion of the calyx for this example species. The summed number of sutured plates, including the infrabasals and basals (white, center), the radials (black), the posterior plates (white and gray stippled), the brachials (white, distal), and the interradials and interbrachials (light gray), describes the "complexity" of the calyx. Representative specimen shown is *Anticosticrinus natiscotecensis* (Hirnantian, American Museum of Natural History, AMNH-FI-139850; photo courtesy of S.R. Cole; plate diagram modified from Cole et al., 2025).

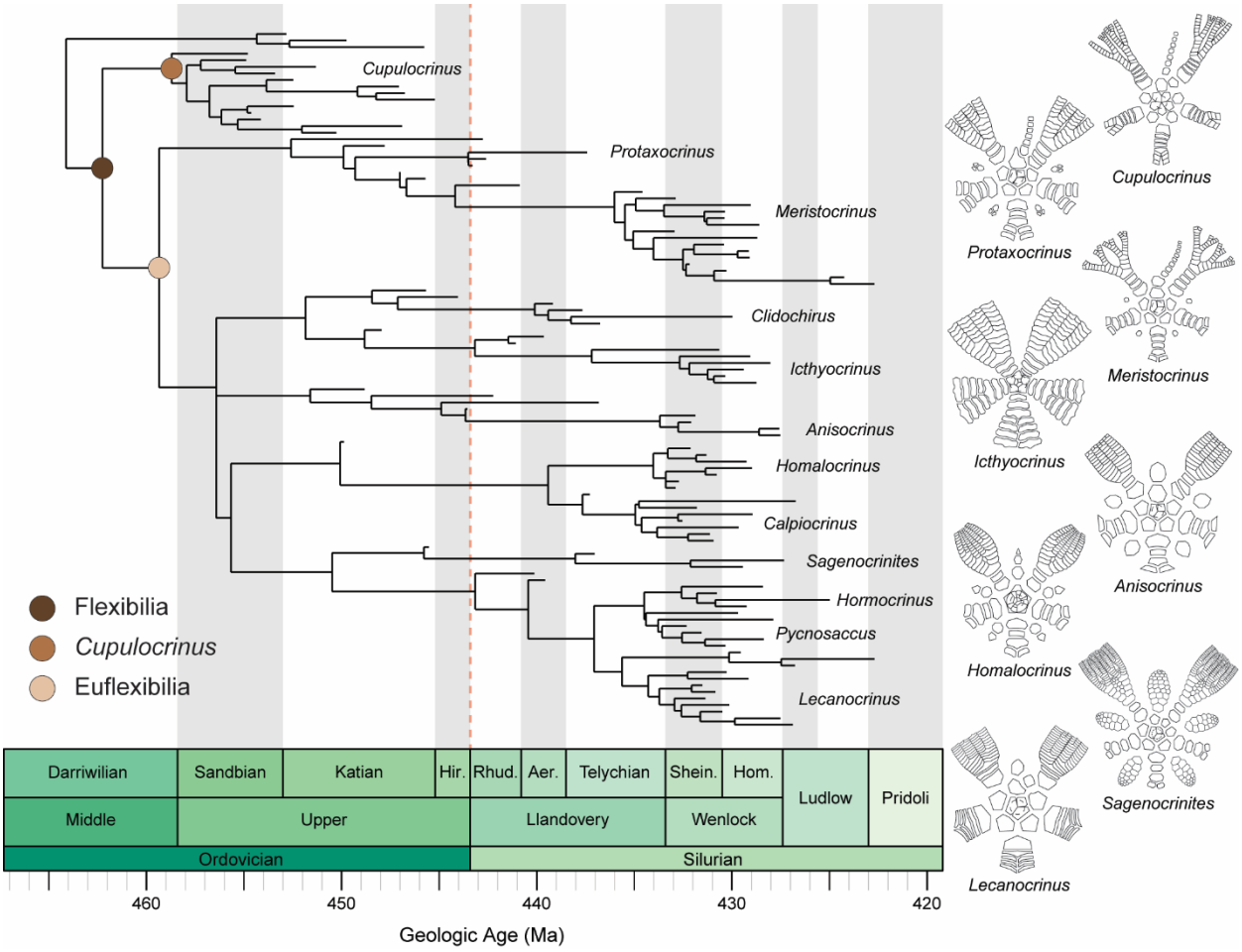

Figure 2. Maximum clade credibility (MCC) tree from the tip-dated Bayesian phylogenetic analysis incorporating the FBD process. Branch lengths are scaled to geologic time. Node labels (colored circles) indicate three major clades within the tree (*sensu* Crowley and Wright, in prep.): all members of Superorder Flexibilia (dark brown); species within the genus *Cupulocrinus* (brown); and species within Euflexibilia (light brown). Tip labels identify major genera, particularly during Wenlock time; Fig. S1 depicts the MCC tree with all species-level tips labeled. Plate diagrams of representative flexible genera are shown to the right of the tree and illuminate the range of morphological disparity in crown construction present in the group (redrawn from Springer, 1920). Hir. = Hirnantian; Rhud. =

Rhuddanian; Aer. = Aeronian; Shein. = Sheinwoodian; Hom. = Homerian. Vertical red dashed line highlights the Ordovician–Silurian boundary.

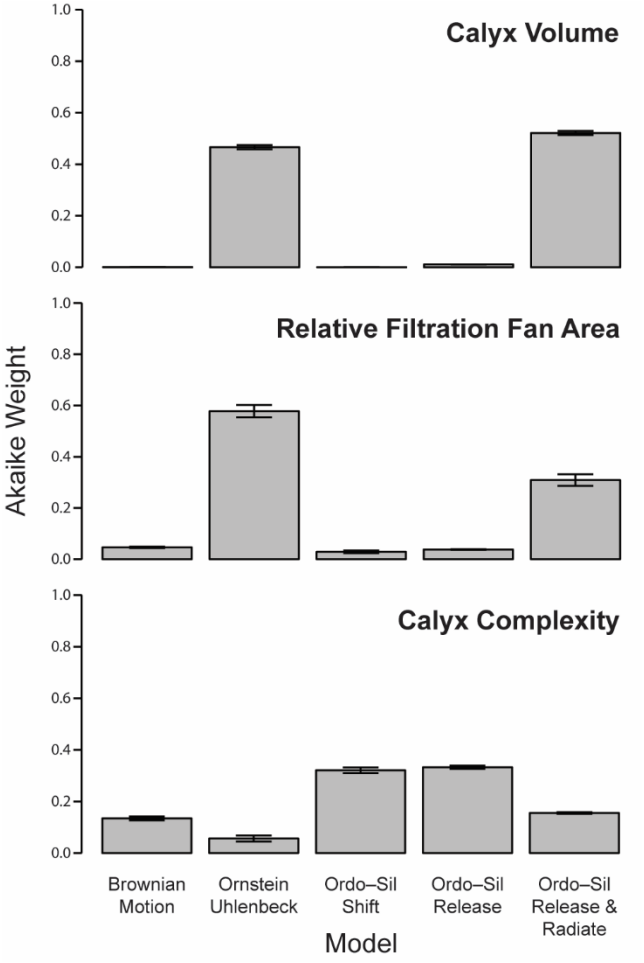

Figure 3. Akaike weights for the model-fitting analyses performed on the MCC tree for the three traits investigated: calyx volume, relative filtration fan area, and calyx complexity. Whiskers show standard errors for Akaike weights derived from model fits to a subset of 200 trees drawn randomly from the posterior distribution of trees.

Supplementary material for:

Chapter II: The ecological and developmental dimensions of a post-extinction radiation in Ordovician–Silurian crinoids (Superorder Flexibilia)

Trait	Model	LnL	AICc	AICcWt	θ	Rate	α	Rate 2
Calyx Volume	Brownian motion	-191.60	387.32	0.00	5.09	0.53	NA	NA
	Ornstein-Uhlenbeck	**-184.32**	**374.89**	**0.94**	**5.95**	**0.81**	**0.12**	**NA**
	end Katian Shift	-191.51	389.27	0.00	5.09	0.47	NA	0.55
	end Katian Release	-188.55	383.35	0.01	5.09	0.59	0.13	NA
	end Katian Release & Radiate	-186.23	380.87	0.05	5.16	11.36	2.46	0.04
Relative Filtration	Brownian motion	-141.90	287.94	0.06	2.65	0.26	NA	NA
Fan Area	**Ornstein-Uhlenbeck**	**-138.31**	**282.90**	**0.71**	**1.58**	**0.36**	**0.08**	**NA**
	end Katian Shift	-141.61	289.50	0.03	2.65	0.31	NA	0.24
	end Katian Release	-141.26	288.8	0.04	2.44	0.28	0.05	NA
	end Katian Release & Radiate	-138.65	285.76	0.17	2.34	0.94	0.28	0.24
Calyx Complexity	Brownian motion	-69.23	142.58	0.04	3.13	0.05	NA	NA
	Ornstein-Uhlenbeck	-69.03	144.31	0.02	3.27	0.05	0.01	NA
	end Katian Shift	**-65.93**	**138.10**	**0.39**	**3.1**	**0.02**	**NA**	**0.06**
	end Katian Release	-66.16	138.56	0.31	3.29	0.05	0.15	NA
	end Katian Release & Radiate	-65.30	139.03	0.24	3.20	0.03	0.07	2.22

Table S1. Model fitting results and parameter values for the three ecomorphological and developmental traits analyzed when the shift time for time-heterogeneous models was set to the Katian–Hirnantian boundary. The best supported model for each trait, i.e., the model with the lowest AICc value and highest weight (AICcWt), is indicated in bold. Alpha (α) is the 'rubber band' parameter for the time-homogeneous Ornstein-Uhlenbeck (OU) model and the time-heterogenous models with a partial OU regime. The post-shift rate parameter (σ^2) is indicated as "Rate 2" for time-heterogeneous models incorporating a change in tempo.

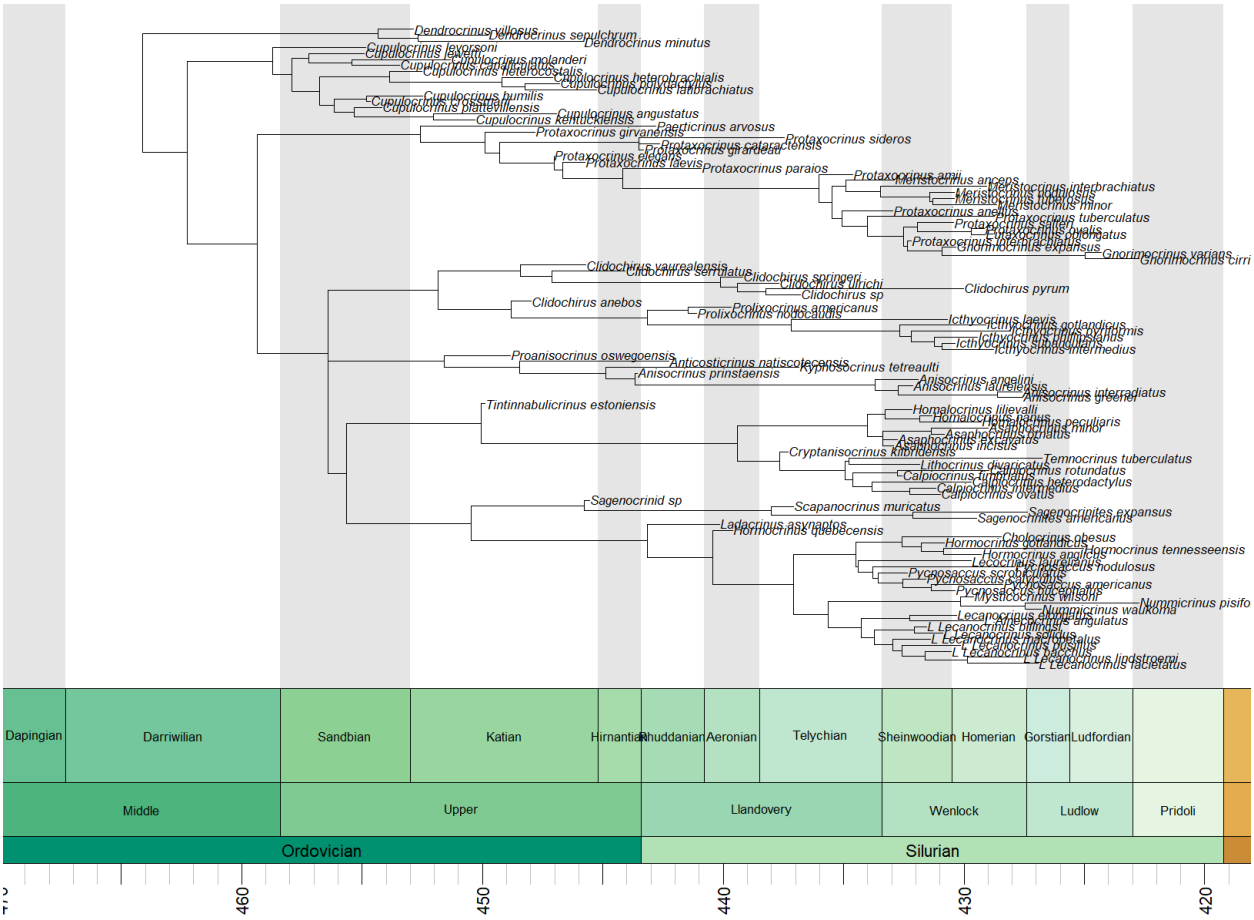

Figure S1. Maximum clade credibility (MCC) tree from the tip-dated Bayesian phylogenetic analysis incorporating the FBD process. Branch lengths are scaled to geologic time. Tips for all species included in the analysis are labeled (n = 106; 103 flexibles, 3 outgroup). Hir. = Hirnantian; Rhud. = Rhuddanian; Aer. = Aeronian; Shein. = Sheinwoodian; Hom. = Homerian.

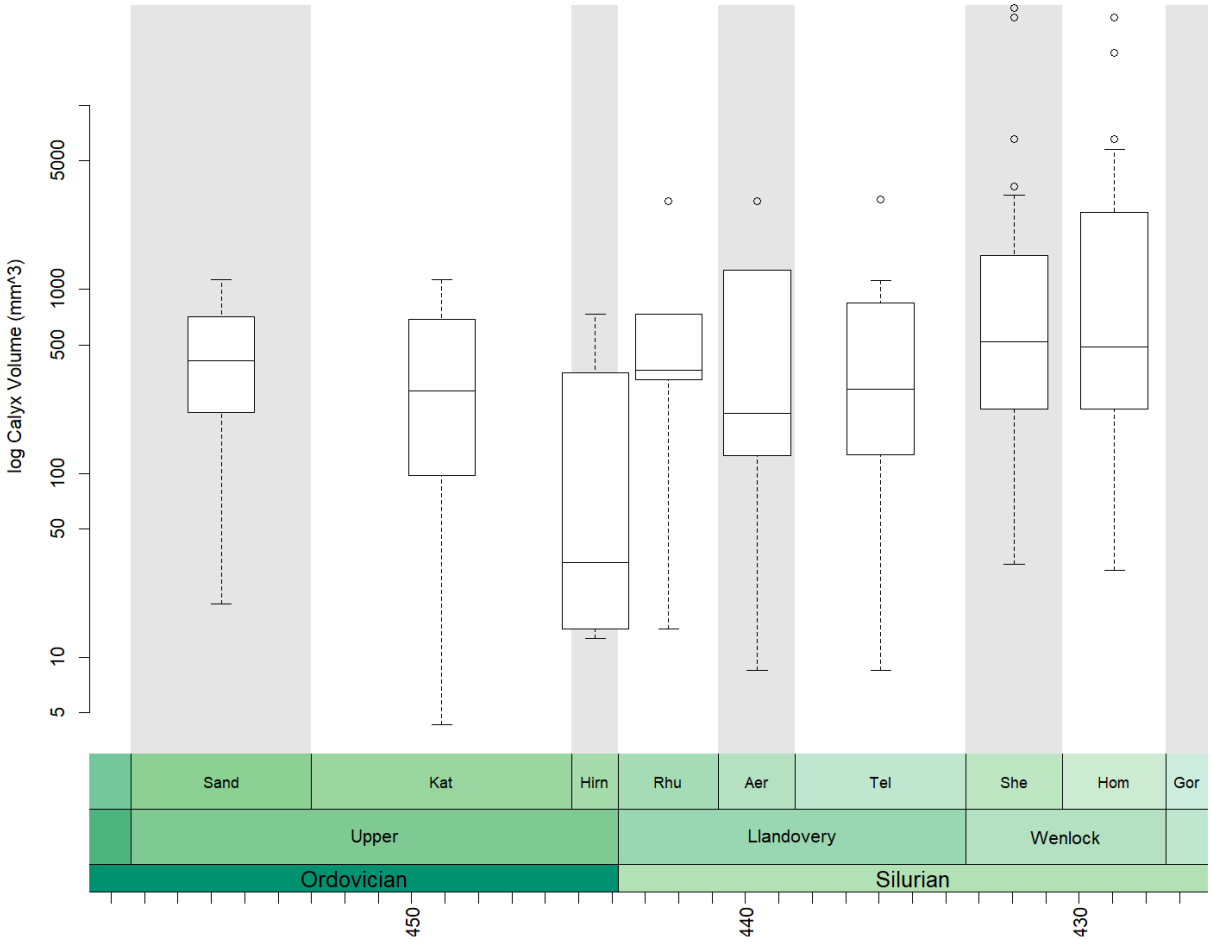

Figure S2. Log-transformed values of calyx volume through time for 101 flexible crinoid species spanning the Late Ordovician through the middle Silurian (Wenlock). Taxa were binned by stage, and plotted in geologic time at the midpoints for each bin.

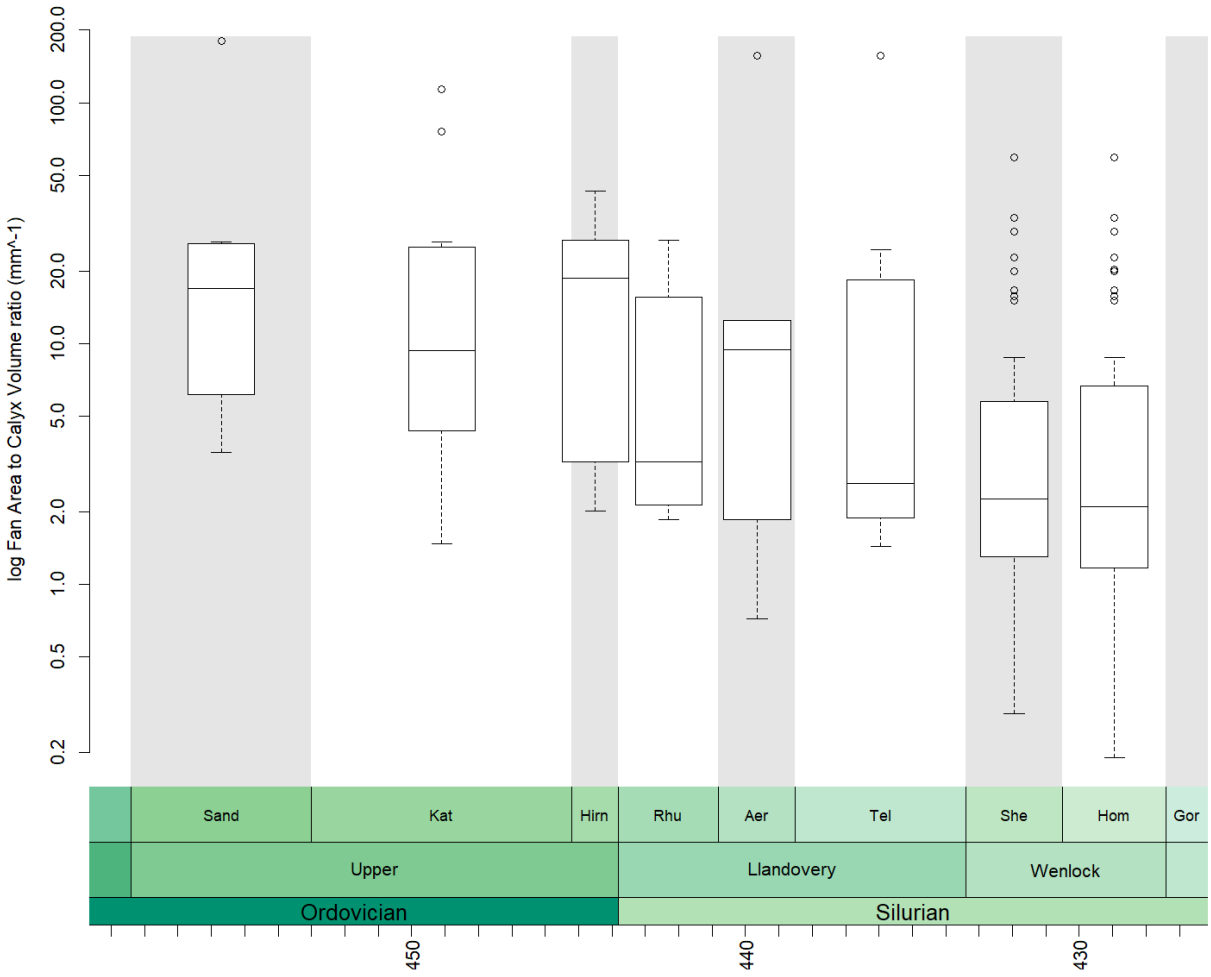

Figure S3. Log-transformed values of relative filtration fan area through time for 91 flexible crinoid species spanning the Late Ordovician through the middle Silurian (Wenlock). Taxa were binned by stage, and plotted in geologic time at the midpoints for each bin.

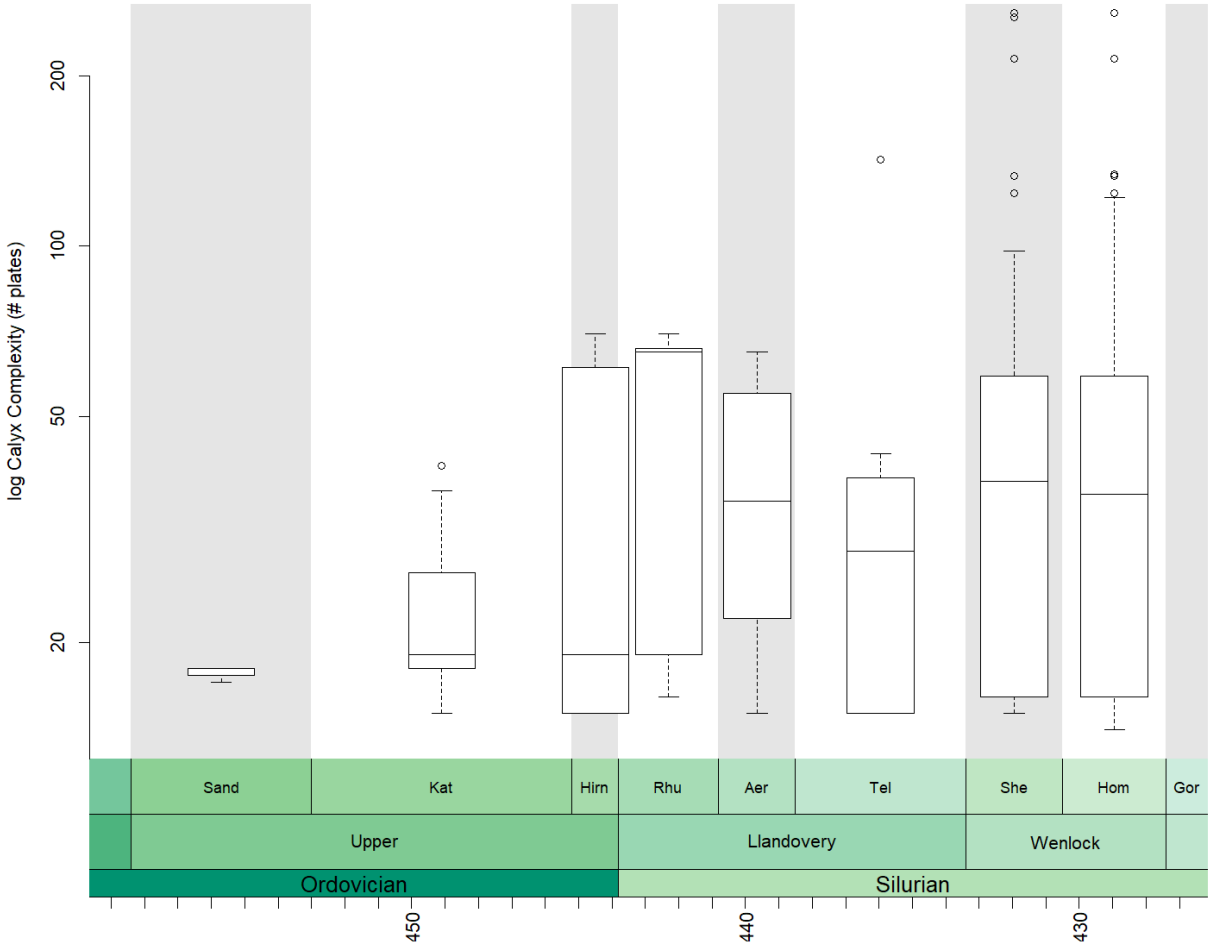

Figure S4. Log-transformed values of calyx complexity through time for 101 flexible crinoid species spanning the Late Ordovician through the middle Silurian (Wenlock). Taxa were binned by stage, and plotted in geologic time at the midpoints for each bin.

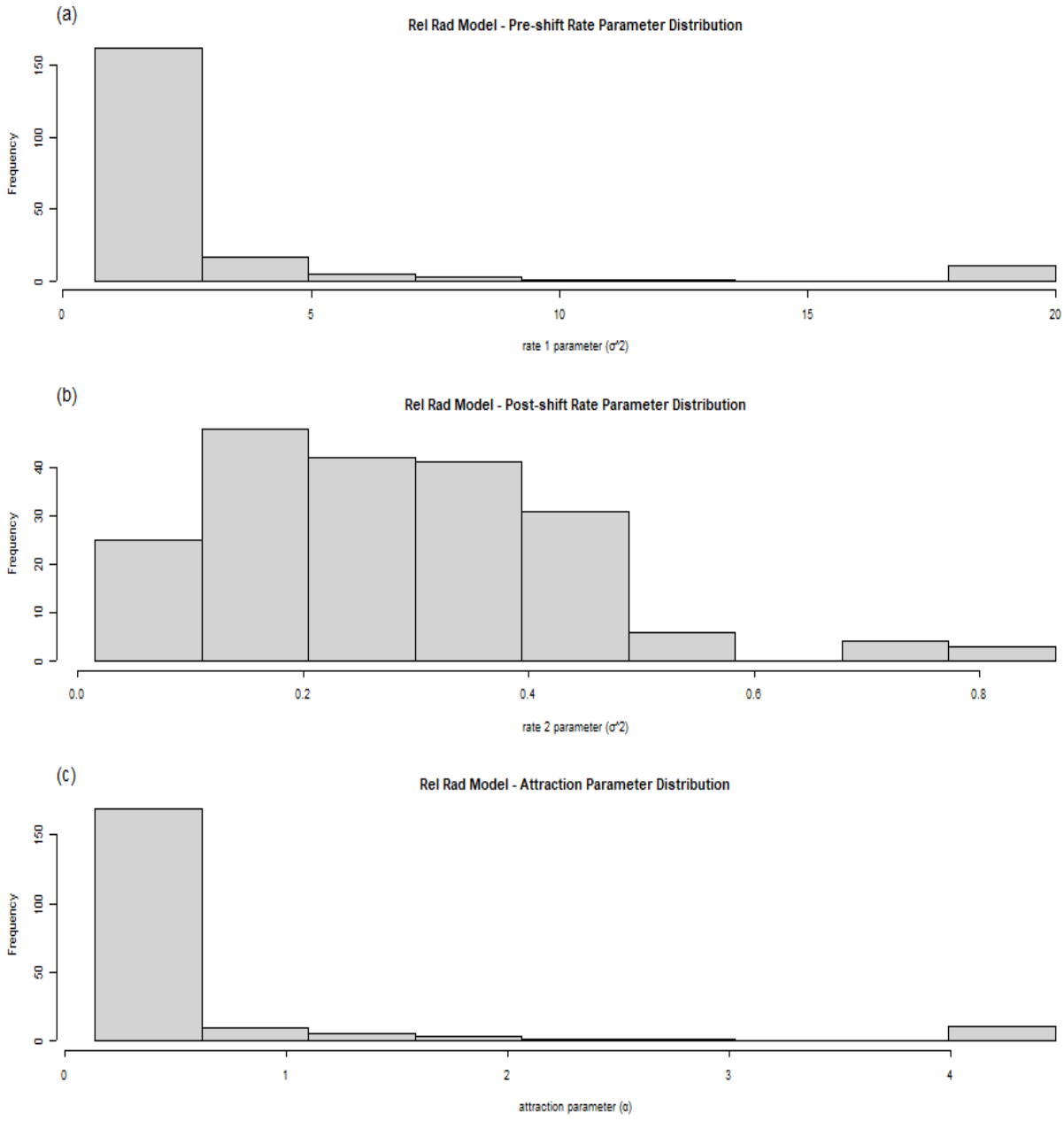

Figure S5. Parameter distribution for the Release and Radiate model when fitted to Calyx Volume data over 200 random trees from the posterior distribution of the FBD phylogenetic analysis.

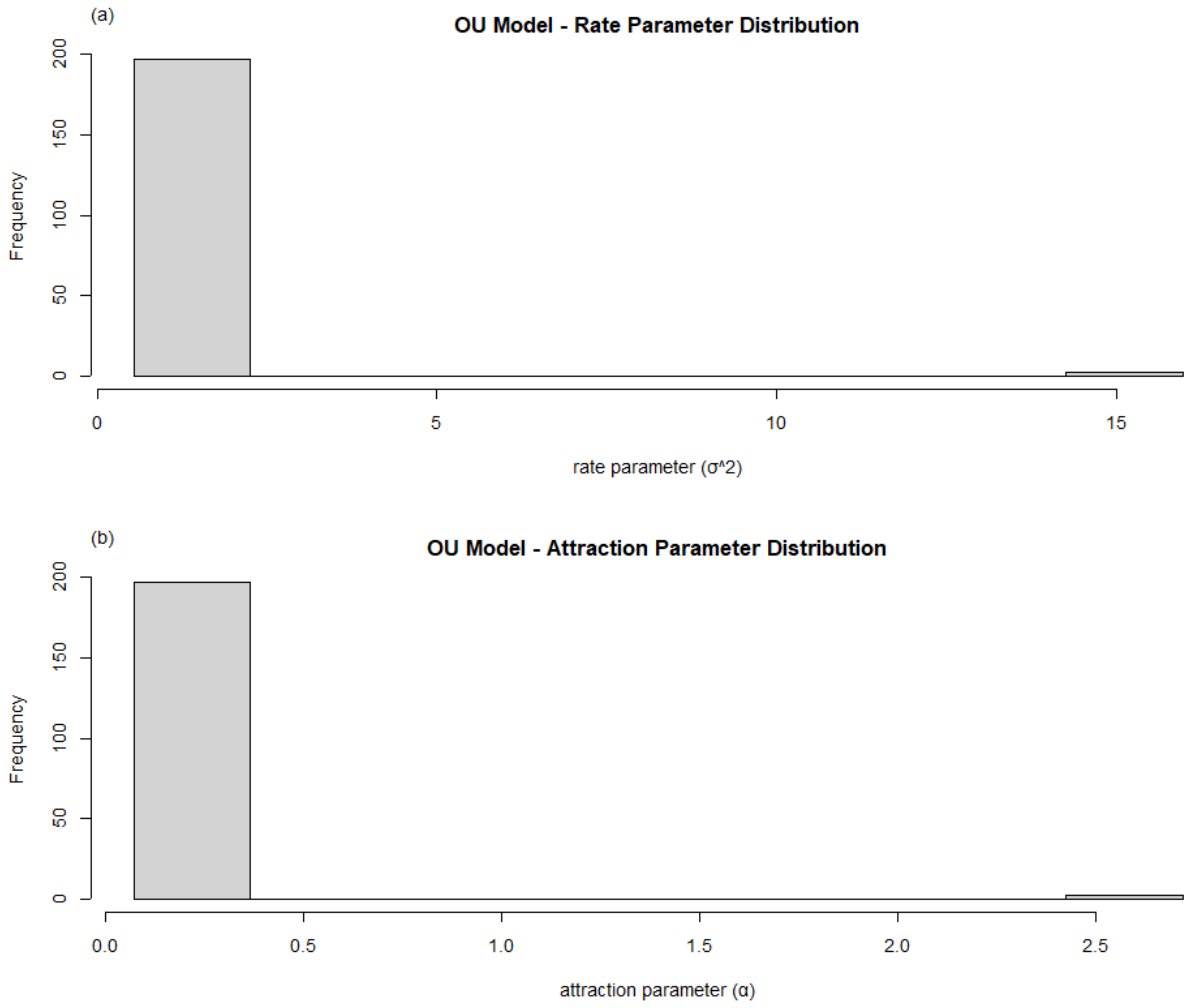

Figure S6. Parameter distribution for the Ornstein-Uhlenbeck model when fitted to Calyx Volume data over 200 random trees from the posterior distribution of the FBD phylogenetic analysis.

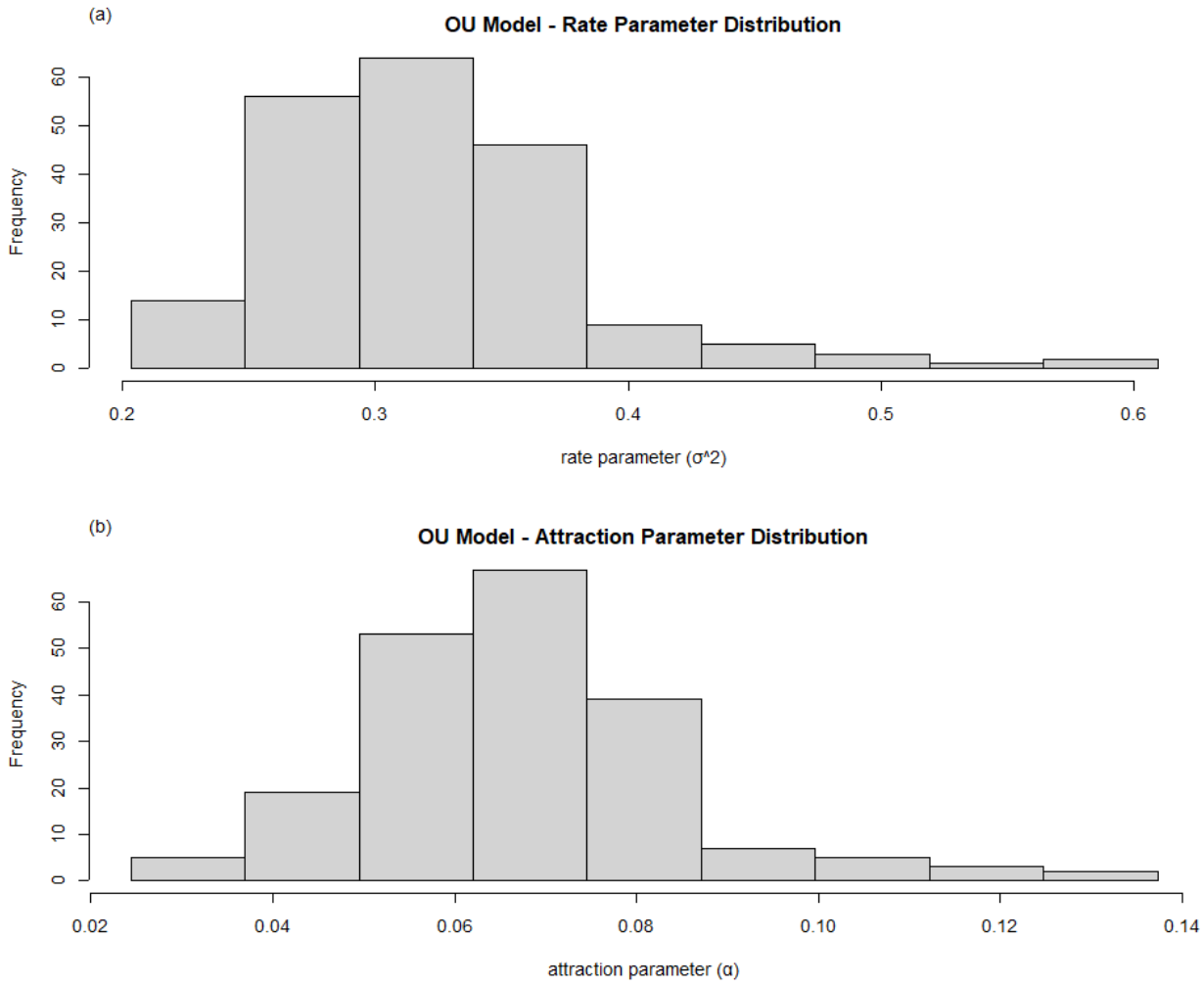

Figure S7. Parameter distribution for the Ornstein-Uhlenbeck model when fitted to Relative Filtration Fan Area data over 200 random trees from the posterior distribution of the FBD phylogenetic analysis.

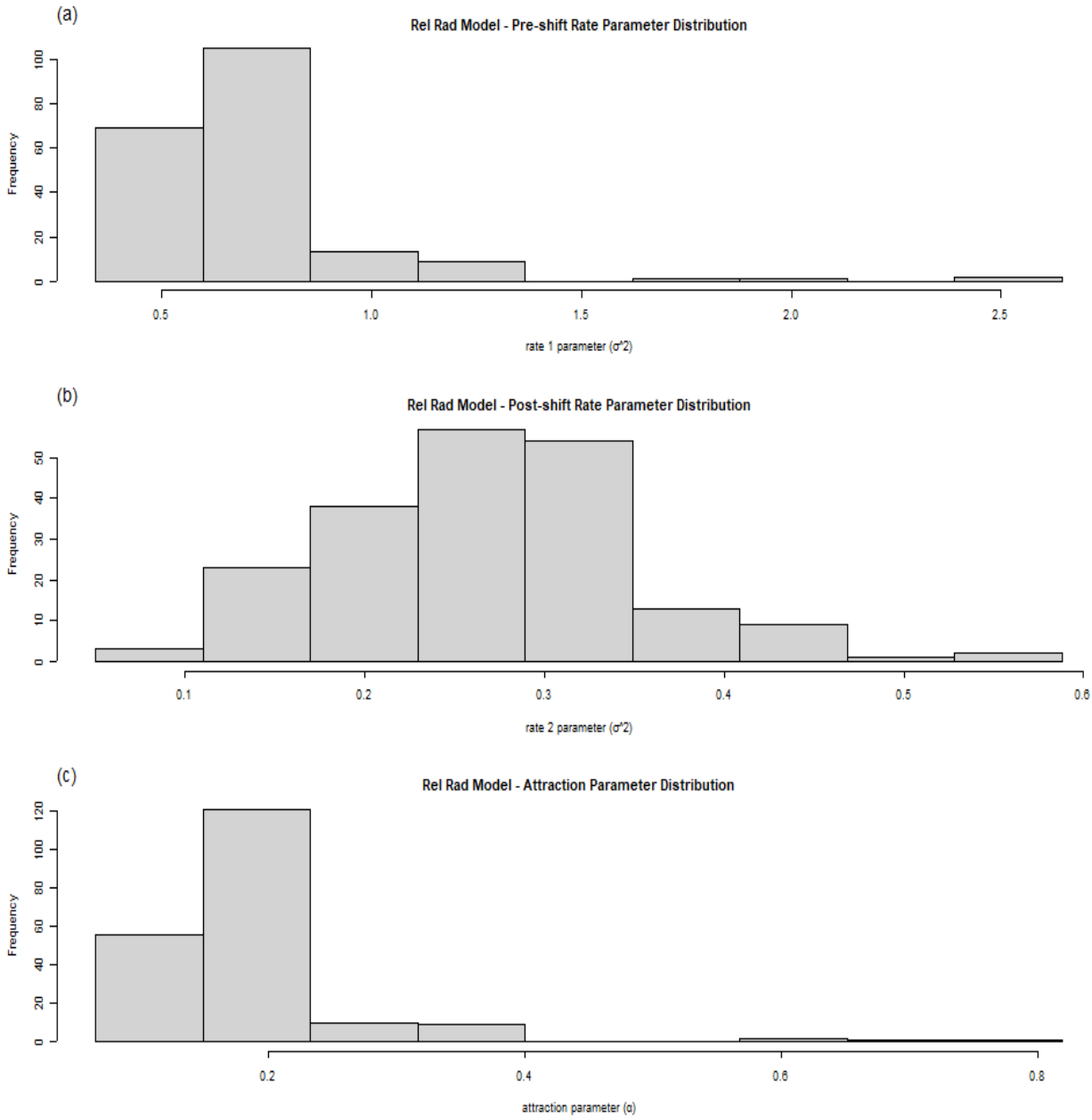

Figure S8. Parameter distribution for the Release and Radiate model when fitted to Relative Filtration Fan Area data over 200 random trees from the posterior distribution of the FBD phylogenetic analysis.

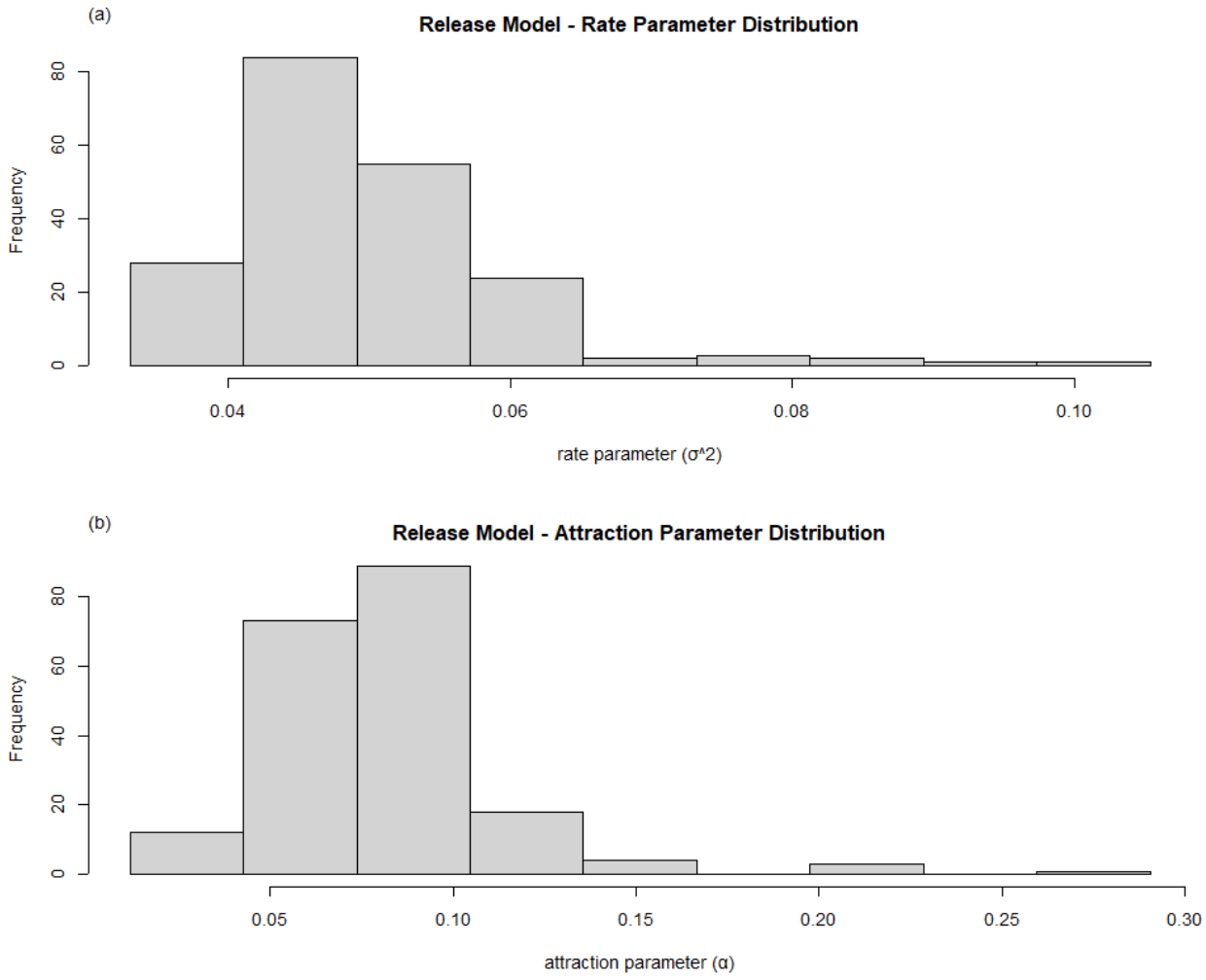

Figure S9. Parameter distribution for the Release model when fitted to Calyx Complexity data over 200 random trees from the posterior distribution of the FBD phylogenetic analysis.

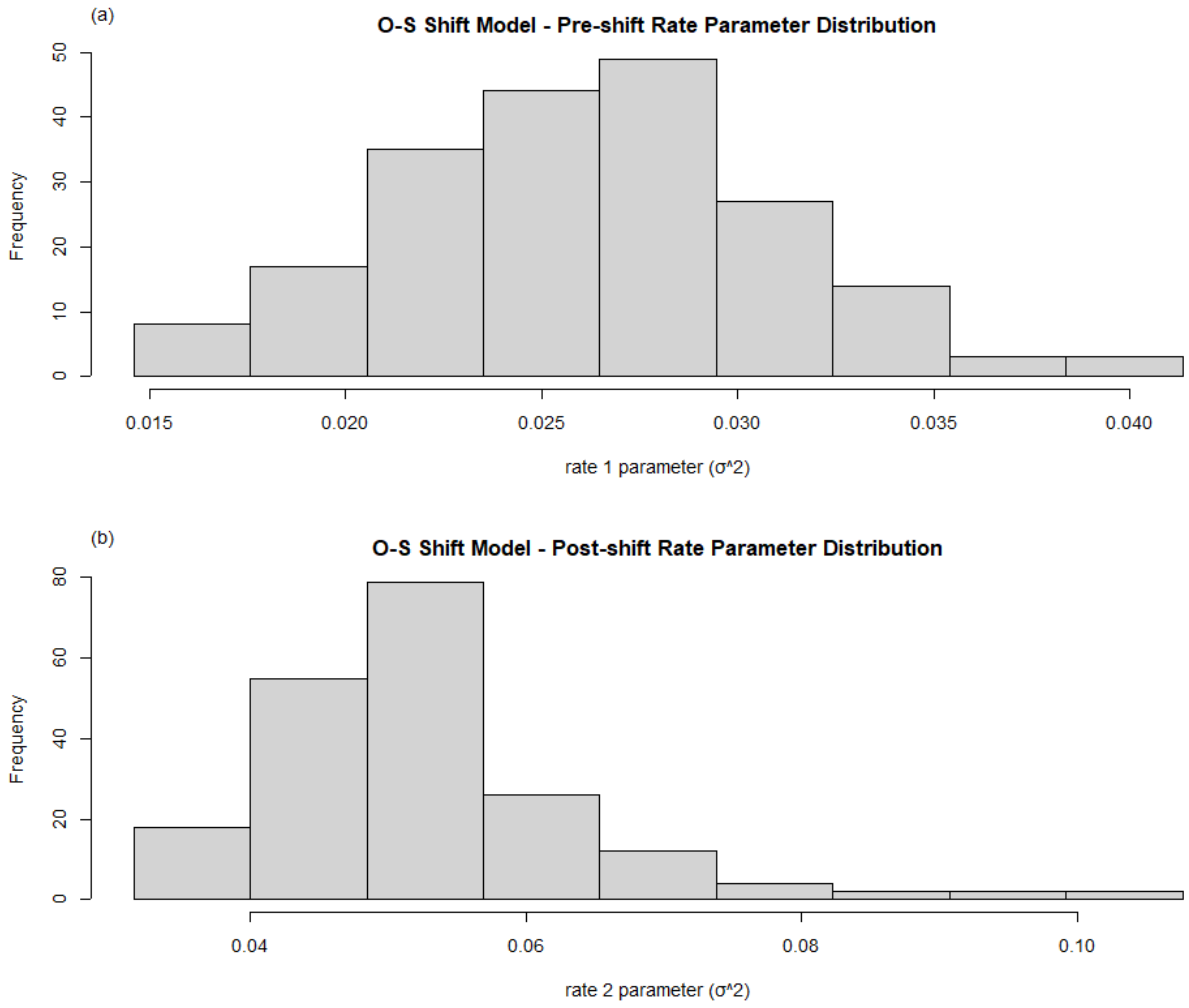

Figure S10. Parameter distribution for the Ordovician–Silurian Shift model when fitted to Calyx Complexity data over 200 random trees from the posterior distribution of the FBD phylogenetic analysis.

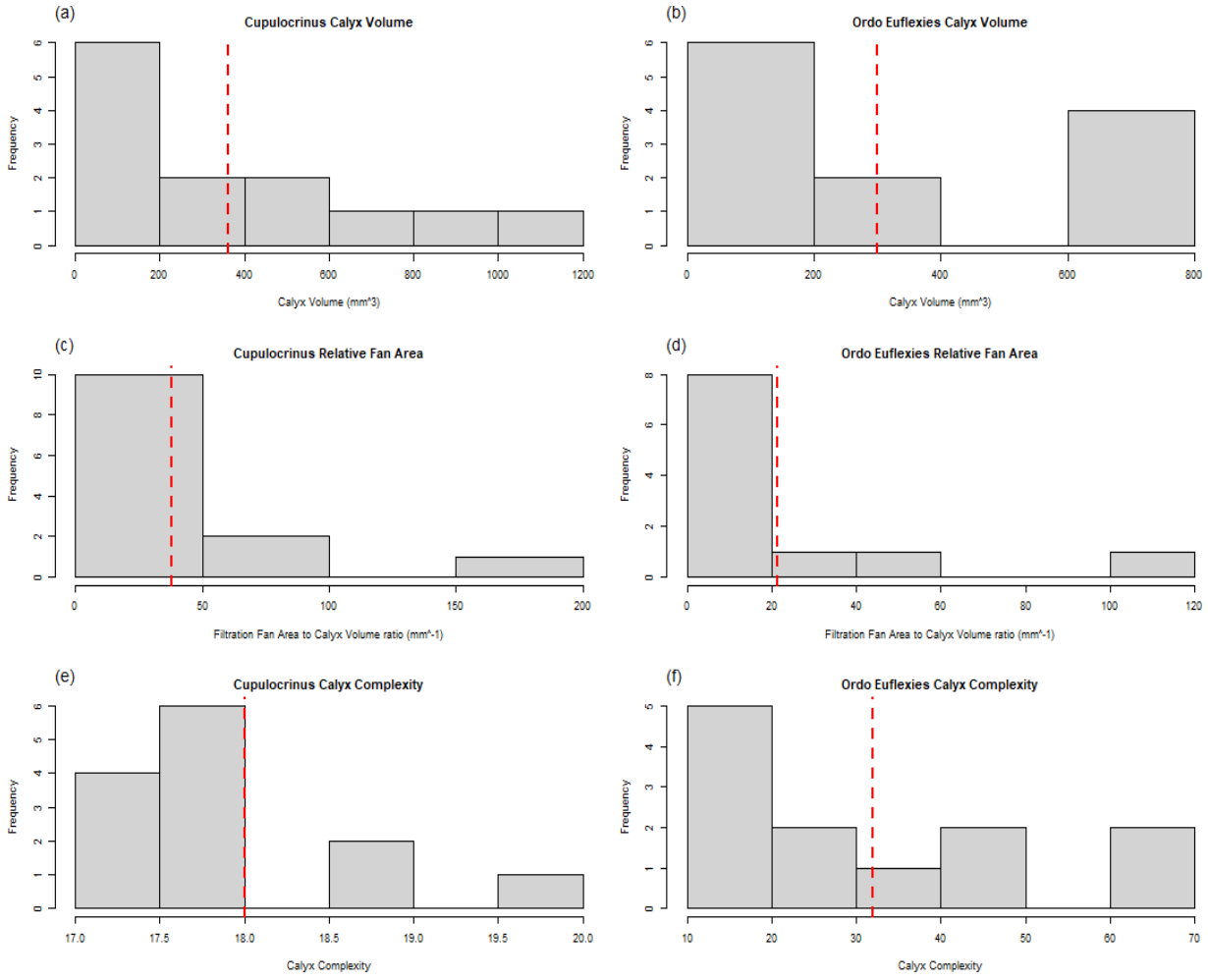

Figure S11. Frequency distribution of measured values of calyx volume, relative filtration fan area, and calyx complexity for Ordovician species of Superorder Flexibilia. Species of the genus *Cupulocrinus* are in the column on the left, and members of flexible subclade Euflexibilia are in the column on the right. Vertical red dashed line indicates the mean value for the taxa in each taxonomic/temporal subset.

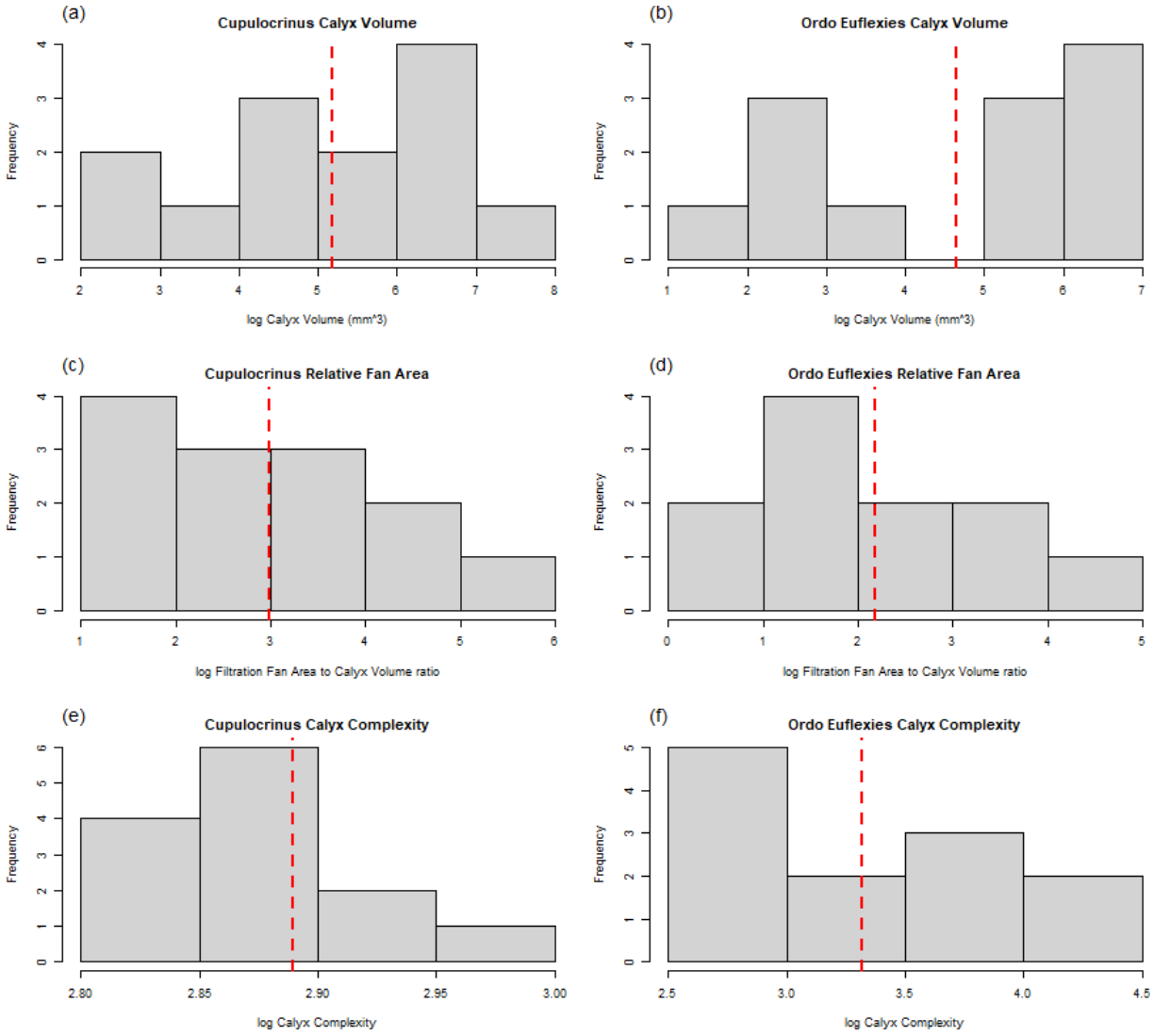

Figure S12. Frequency distribution of log-transformed values of calyx volume, relative filtration fan area, and calyx complexity for Ordovician species of Superorder Flexibilia. Species of the genus *Cupulocrinus* are in the column on the left, and members of flexible subclade Euflexibilia are in the column on the right. Vertical red dashed line indicates the mean value for the taxa in each taxonomic/temporal subset.

References

Alroy, J., 1998, Cope's rule and the dynamics of body mass evolution in North American fossil mammals: Science, v. 280, p. 731–734.

Angelin, N.P., 1878, Iconographia crinoideorum in stratis Suecia Siluricis fossilium: Sampson & Wallin, Holmiae, 32 p., 29 pls.

Ausich, W.I., 1988, Evolutionary convergence and parallelism in crinoid calyx design: Journal of Paleontology, v. 62, p. 906–916.

Ausich, W.I., and Copper, P., 2010, The Crinoidea of Anticosti Island, Québec (Late Ordovician to early Silurian): Canadian Society of Petroleum Geologists, Palaeontographica Canadiana 29, 157 p.

Ausich, W.I., and Deline, B., 2012, Macroevolutionary transition in crinoids following the Late Ordovician extinction event (Ordovician to Early Silurian): Palaeogeography, Palaeoclimatology, Palaeoecology, v. 361–362, p. 38–48.

Ausich, W.I., Kammer, T.W., and Baumiller, T.K., 1994, Demise of the Middle Paleozoic crinoid fauna: a single extinction event or rapid faunal turnover?: Paleobiology, v. 20, p. 345–361.

Ausich, W.I., Kammer, T.W., Rhenberg, E.C., and Wright, D.F., 2015, Early phylogeny of crinoids within the pelmatozoan clade: Palaeontology, v. 58, p. 937–952.

Ausich, W.I., Wright, D.F., Cole, S.R., and Sevastopulo, G.D., 2020, Homology of posterior interray plates in crinoids: a review and new perspectives from phylogenetics, the fossil record and development: Palaeontology, v. 63, p. 525–545.

Bapst, D.W., Bullock, P.C., Melchin, M.J., Sheets, H.D., and Mitchell, C.E., 2012, Graptoloid diversity and disparity became decoupled during the Ordovician mass extinction: Proceedings of the National Academy of Sciences, v. 109, p. 3428–3433.

Baumiller, T.K., 1993, Survivorship analysis of Paleozoic Crinoidea: effect of filter morphology on evolutionary rates: Paleobiology, v. 19, p. 304–321.

Beaulieu, J., O'Meara, B., Oliver, J., and Bokyo, J., 2022, corHMM: Hidden Markov models of character evolution: R package version 2.8.

Benevento, G.L., Benson, R.B.J., Close, R.A., and Butler, R.J., 2023, Early Cenozoic increases in mammal diversity cannot be explained solely by expansion into larger body sizes: Palaeontology, v. 66, p. e12653.

Bengtson, P., 1988, Open nomenclature: Palaeontology, v. 31, p. 223–227.

Benson, R.B.J., Godoy, P., Bronzati, M., Butler, R.J., and Gearty, W., 2022, Reconstructed evolutionary patterns for crocodile-line archosaurs demonstrate impact of failure to log-transform body size data: Communications Biology, v. 5, p. 171.

Billings, E., 1857, New species of fossils from Silurian rocks of Canada: Canada Geological Survey, Report of Progress 1853–1856, Report for the year 1856, p. 247–345.

Billings, E., 1859, On the Crinoideae of the Lower Silurian rocks of Canada. Canadian Organic Remains, Decade 4: Canada Geological Survey, 72 p.

Borths, M.R., and Ausich, W.I., 2011, Ordovician–Silurian Lilliput crinoids during the end-Ordovician biotic crisis: Swiss Journal of Paleontology, v. 130, p. 7–18.

Brett, C.E., 1984, Autecology of Silurian pelmatozoans: Special Papers in Palaeontology, v. 32, p. 87–120.

Brower, J.C., 1992, Cupulocrinid crinoids from the Middle Ordovician (Galena Group, Dunleith Formation) of northern Iowa and southern Minnesota: Journal of Paleontology, v. 66, p. 99–128.

Brower, J.C., 2001, Flexible crinoids from the Upper Ordovician Maquoketa Formation of the northern midcontinent and the evolution of early flexible crinoids: Journal of Paleontology, v. 75, p. 370–382.

Brower, J.C., 2013, Paleoecology of echinoderm assemblages from the Upper Ordovician (Katian) Dunleith Formation of northern Iowa and southern Minnesota: Journal of Paleontology, v. 87, p. 16–43.

Brower, J.C., and Veinus, J., 1978, Middle Ordovician crinoids from the Twin Cities area of Minnesota: Bulletins of American Paleontology, v. 74, p. 371–506.

Burnham, K.P., and Anderson, D.R., 2002, Model selection and multimodel inference: Springer, New York, 488 p.

Butler, M.A., and King, A.A., 2004, Phylogenetic comparative analysis: a modeling approach for adaptive evolution: The American Naturalist, v. 164, p. 683–695.

Cocks, L.R.M., and Torsvik, T.H., 2011, The Palaeozoic geography of Laurentia and western Laurussia: A stable craton with mobile margins: Earth-Science Reviews, v. 106, p. 1–51.

Cohen, K., Harper, D.A.T., Gibbard, P., and Car, N., 2024, ICS International Chronostratigraphic Chart 2024/12: International Commission on Stratigraphy, IUGS, www.stratigraphy.org.

Cole, S.R., 2018, Phylogeny and evolutionary history of diplobathrid crinoids (Echinodermata): Palaeontology, v. 62, p. 357–373.

Cole, S.R., and Hopkins, M.J., 2021, Selectivity and the effect of mass extinctions on disparity and functional ecology: Science Advances, v. 7, p. eabf4072.

Cole, S.R., and Wright, D.F., 2022, Niche evolution and phylogenetic community paleoecology of Late Ordovician crinoids: Elements of Paleontology, Cambridge University Press, Cambridge, 45 p.

Cole, S.R., Wright, D.F., and Ausich, W.I., 2019, Phylogenetic community paleoecology of one of the earliest complex crinoid faunas (Brechin Lagerstätte, Ordovician): Palaeogeography, Palaeoclimatology, Palaeoecology, v. 521, p. 82–98.

Cole, S.R., Wright, D.F., and Hopkins, M.J., 2025, Phylogenetic position and stratigraphic uncertainty of a new flexible crinoid from the Ordovician–Silurian boundary of Anticosti Island (Québec, Canada): Journal of Paleontology, v. 99, p. 358–368.

Crowley, K.D., and Wright, D.F., (*in prep*.), On the origin and evolution of Superorder Flexibilia (Echinodermata): a Bayesian tip-dated phylogenetic assessment of Ordovician–Silurian flexible crinoids: *Journal of Paleontology*.

Darroch, S.A.F., and Wagner, P.J., 2015, Response of beta diversity to pulses of Ordovician–Silurian mass extinction: Ecology, v. 96, p. 532–549.

Donovan, S.K., Doyle, E.N., and Harper, D.A.T., 1992, A flexible crinoid from the Llandovery (Silurian) of western Ireland: Journal of Paleontology, v. 66, p. 262–266.

Eckert, J.D., and Brett, C., 2001, Early Silurian (Llandovery) crinoids from the lower Clinton Group, western New York State: Bulletins of American Paleontology, no. 360, p. 1–88.

Edie, S.M., Collins, K.S., and Jablonski, D., 2025, The end-Cretaceous mass extinction restructured functional diversity but failed to configure the modern marine biota: Science Advances, v. 11, p. eadv1171.

Foote, M., 1999, Morphological diversity in the evolutionary radiation of Paleozoic andpost-Paleozoic crinoids: Paleobiology, v. 25(S2), p. 1–115.

Gavryushkina, A., Welch, D., Stadler, T., and Drummond, A.J., 2014, Bayesian inference of sampled ancestor trees for epidemiology and fossil calibration: PloS Computational Biology, v. 10, n. e1003919.

Goldman, D., Sadler, P.M., Leslie, S.A., Melchin, M.J., Agterberg, F.P., and Gradstein, F.M., 2020, The Ordovician Period, *in* Gradstein, F.M., Ogg, J.G., Schmitz, M.D., and Ogg, G.M., eds., Geologic Time Scale 2020: Amsterdam, Elsevier, p. 631–694.

Hall, J., 1847, Palaeontology of New York, v. 1, Containing descriptions of the organic remains of the lower division of the New-York system (equivalent of the Lower Silurian rocks of Europe): Natural History of New York: Albany, State of New York, v. 6, 338 p.

Hall, J., 1852, Palaeontology of New York, v. 2, Containing descriptions of the organic remains of the lower middle division of the New-York system: Natural History of New York: D. Appleton and Co., Wiley and Putnam, and Gould, Kendall, and Lincoln, New York and Boston, v. 6, 362 p.

Harmon, L.J., Weir, J.T., Brock, C.D., Glor, R.E., and Challenger, W., 2008, Geiger: investigating evolutionary radiations: Bioinformatics, v. 24, p. 129–131.

Harper, D.A.T., 2024, Late Ordovician mass extinction: Earth, fire and ice: National Science Review, v. 11, p. nwad319.

Heath, T.A., and Moore, B.R., 2014, Bayesian inference of species divergence times, *in* Chen, M-H., Kuo, L., and Lewis, P.O., eds., Bayesian Phylogenetics: Models, Algorithms, and Applications: CRC Press, Oxfordshire, p. 277–318.

Heath, T.A., Huelsenbeck, J.P., and Stadler, T., 2014, The fossilized birth–death process for coherent calibration of divergence-time estimates: Proceedings of the National Academy of Sciences, v. 111, p. E2957–E2966.

Jablonski, D., 1986, Background and mass extinctions: the alternation of macroevolutionary regimes: Science, v. 231, p. 129–133.

Jablonski, D., 1996, Body size and macroevolution, *in* Jablonski, D., Erwin, D.H., and Lipps, J.E., eds., Evolutionary Paleobiology: University of Chicago Press, Chicago, p. 256–289.

Jablonski, D., 2022, Evolvability and macroevolution: overview and synthesis: Evolutionary Biology, v. 49, p. 265–291.

Jablonski, D., and Edie, S.M., 2025, Mass extinctions and their rebounds: a macroevolutionary framework: Paleobiology, v. 51, p. 83–96.

Jaekel, O., 1918, Phylogenie und System der Pelmatozoen: Paläontologische Zeitschrift, v. 3, p. 1–128.

Jell, P.A., 1999, Silurian and Devonian crinoids from central Victoria: Memoirs of the Queensland Museum, v. 43, p. 1–114.

Kolata, D.R., 1975, Middle Ordovician echinoderms from northern Illinois and southern Wisconsin: Memoir 7, Paleontological Society Journal of Paleontology, Pt. II of II, Supplement to v. 49, 74 p.

Kolata, D.R., 1986, Crinoids of the Champlainian (Middle Ordovician) Guttenberg Formation—Upper Mississippi Valley region: Journal of Paleontology, v. 60, p. 711–718.

Lam, A.R., Stigall, A.L., and Matzke, N.J., 2018, Dispersal in the Ordovician: Speciation patterns and paleobiogeographic analyses of brachiopods and trilobites: Palaeogeography, Palaeoclimatology, Palaeoecology, v. 489, p. 147–165.

Lewis, P.O., 2001, A likelihood approach to estimating phylogeny from discrete morphological character data: Systematic Biology, v. 50, p. 913–925.

Marshall, C.R., 2023, Forty years later: The status of the “Big Five” mass extinctions: Cambridge Prisms: Extinction, v. e5, p. 1–13.

Meek, F.B., and Worthen, A.H., 1870, Descriptions of new species and genera of fossils from Paleozoic rocks of the western states: Proceedings of the Academy of Natural Sciences of Philadelphia, v. 22, p. 22–56.

Miller, J.S., 1821, A Natural History of the Crinoidea, or Lily-Shaped Animals; with Observations on the Genera, *Asteria*, *Euryale*, *Comatula* and *Marsupites*: Bristol, England, Bryan & Co., 150 p.

Monarrez, P.M., Heim, N.A., and Payne, J.L., 2021, Mass extinctions alter extinction and origination dynamics with respect to body size: Proceedings of the Royal Society, Biology, v. 288, p. 20211681.

Moore, R.C., 1978, Flexibilia, *in* Moore, R.C., and Teichert, C., eds., Treatise on Invertebrate Paleontology, Part T, Echinodermata 2: Lawrence, Kansas, Geological Society of America and University of Kansas Press, p. T759–T812.

Moore, R.C., and Laudon, L.R., 1943, Evolution and classification of Paleozoic crinoids: Geological Society of America Special Paper, v. 46, p. 1–154.

Mulvey, L.P.A., Nikolic, M.C., Allen, B.J., Heath, T.A., and Warnock, R.C.M., 2025, From fossils to phylogenies: exploring the integration of paleontological data into Bayesian phylogenetic inference: Paleobiology, v. 51, p. 214–236.

Nascimento, F.F., dos Reis, M., and Yang, Z., 2017, A biologist's guide to Bayesian phylogenetic analysis: Nature Ecology & Evolution, v. 1, p. 1446–1454.

Orbigny, A.D., d', 1849–1851, Cours élémentaire de paléontologie et géologie stratigraphiques: v. 1 (1849), p. 1–299; v. 2 (1851), p. 1–847. [Reprinted 1980, New York, Arno Press]

Pagel, M., 1999, The maximum likelihood approach to reconstructing ancestral character states of discrete characters on phylogenies: Systematic Biology, v. 48, p. 612–622.

Payne, J.L., and Finnegan, S., 2007, The effect of geographic range on extinction risk during background and mass extinction: Proceedings of the National Academy of Sciences, v. 104, p. 10506–10511.

Peter, M.E., 2019, Aberrations in the infrabasal circlet of the cladid crinoid genus *Cupulocrinus* (Echinodermata) and implications for the origin of flexible crinoids: Palaeogeography, Palaeoclimatology, Palaeoecology, v. 522, p. 52–61.

Rambaut, A., Drummond, A.J., Xie, D., Baele, G., and Suchard, M.A., 2018, Posterior summarization in Bayesian phylogenetics using Tracer 1.7: Systematic Biology, v. 67, p. 901–904.

Ramsbottom, W.H.C., 1961, A monograph on the British Ordovician Crinoidea: Palaeontographical Society, v. 114, 37 p., 8 pls.

Revell, L.J., and Harmon, L.J., 2022, Phylogenetic comparative methods in R: Princeton University Press, Princeton, New Jersey, 426 p.

Roemer, C.F., 1854–1855, Erste Periode, Kohlen-Gebirge, *in* Bronn, H.G., ed., Lethaea Geognostica, 3rd ed., v. 2: Stuttgart, E. Schweizerbart, 788 p.

Ronquist, F., Teslenko, M., van der Mark, P., Ayres, D.L., Darling, A., Höhna, S., Larget, B., Liu, L., Suchard, M.A., and Huelsenbeck, J.P., 2012, MRBAYES 3.2: Efficient Bayesian phylogenetic inference and model selection across a large model space: Systematic Biology, v. 61, p. 539–542.

Salamon, M.A., Brachaniec, T., Kolbuk, D., Saha, A., and Gorzelak, P., 2021, Shared patterns in body size declines among crinoids during the Palaeozoic extinction events: Scientific Reports, v. 11, p. 20351.

Sepkoski, J.J., Jr., 1981, A factor analytic description of the Phanerozoic marine fossil record: Paleobiology, v. 7, p. 36–53.

Shumard, B.F., 1858, Description of new fossil Crinoidea from the Palaeozoic rocks of the western and southern portions of the United States: Transactions of the St. Louis Academy of Science (1857), v. 1, p. 71–80, 1 pl.

Simpson, G.G., 1944, Tempo and mode in evolution: Columbia University Press, New York, NY, 237 p.

Slater, G.J., 2013, Phylogenetic evidence for a shift in the mode of mammalian body size evolution at the Cretaceous–Palaeogene boundary: Methods in Ecology and Evolution, v. 4, pg. 734–744.

Slater, G.J., 2014, Correction to ‘Phylogenetic evidence for a shift in the mode of mammalian body size evolution at the Cretaceous–Palaeogene boundary’, and a note on fitting macroevolutionary models to comparative paleontological datasets: Methods in Ecology and Evolution, v. 5, pg. 714–718.

Soul, L.C., and Wright, D.F., 2021, Phylogenetic comparative methods: a user's guide for paleontologists: Elements of Paleontology, Cambridge University Press, Cambridge, 64 p.

Springer, F., 1906, Discovery of the disk of *Onychocrinus* and further remarks on the Crinoidea Flexibilia: Journal of Geology, v. 14, p. 467–523.

Springer, F., 1911, On a Trenton echinoderm fauna: Canada Department Mines Memoir no. 15-P, 70 p.

Springer, F., 1913, Crinoidea, *in* Zittel, K.A. von, ed., Text-book of Paleontology, 2nd ed.: London, Macmillan & Co., p. 173–243.

Springer, F., 1920, The Crinoidea Flexibilia (with an Atlas of A., B., C., and 76 Plates): Washington, D.C., Smithsonian Institution, 504 p.

Stigall, A.L., 2023, A review of the Late Ordovician (Katian) Richmondian Invasion of eastern Laurentia: Palaeogeography, Palaeoclimatology, Palaeoecology, v. 618, p. 111520.

Stigall, A.L., Edwards, C.T., Freeman, R.L., and Rasmussen, C.M.Ø., 2019, Coordinated biotic and abiotic change during the Great Ordovician Biodiversification Event: Darriwilian assembly of early Paleozoic building blocks: Palaeogeography, Palaeoclimatology, Palaeoecology, v. 530, p. 249–270.

Stigall, A.L., Freeman, R.L., Edwards, C.T., and Rasmussen, C.M.Ø., 2020, A multidisciplinary perspective on the Great Ordovican Biodiversification Event and

the development of the early Paleozoic world: Palaeogeography, Palaeoclimatology, Palaeoecology, v. 543, p. 109521.

Stigall, A.L., Wright, D.F., and Censullo, S.M., 2026, Species-level diversity dynamics during the Great Ordovician Biodiversification Event: a phylodynamic case study of Laurentian brachiopod lineages: Palaeogeography, Palaeoclimatology, Palaeoecology.

Ubaghs, G., 1978, General morphology, *in* Moore, R.C., and Teichert, C., eds., Treatise on Invertebrate Paleontology. Pt. T. Echinodermata 2: Lawrence, Geological Society of America and University of Kansas Press, p. T58–T216.

Vilela-Andrade, M., and Stigall, A.L., 2025, Shifting speciation mode and biogeographic patterns during the Late Ordovician (Sandbian–Katian) in Laurentian brachiopods (Atrypida, Anazygidae): Palaeogeography, Palaeoclimatology, Palaeoecology, v. 675, p. 113037.

Wachsmuth, C., and Springer, F., 1885, Revision of the Palaeocrinoidea Pt. III, Sec. 1. Discussion of the Classification and Relations of the Brachiate Crinoids, and Conclusion of the Generic Descriptions: Proceedings of the Academy of Natural Sciences of Philadelphia, 225–364 p.

Webby, B.D., Paris, F., Droser, M.L., and Percival, I.G., 2004, The Great Ordovician Biodiversification Event: Columbia University Press, New York, 496 p.

Wright, A.M., Wagner, P.J., and Wright, D.F., 2021, Testing character evolution models in phylogenetic paleobiology: A case study with Cambrian echinoderms: Elements of Paleontology, Cambridge University Press, Cambridge, 34 p.

Wright, A.M., Bapst, D.W., Barido-Sottani, J., and Warnock, R.C.M., 2022, Integrating fossil observations into phylogenies using the Fossilized Birth–Death model: Annual Review of Ecology, Evolution, and Systematics, v. 53, p. 251–273.

Wright, D.F., 2015, Fossils, homology, and "Phylogenetic Paleo-ontogeny": a reassessment of primary posterior plate homologies among fossil and living crinoids with insights from developmental biology: Paleobiology, v. 41, p. 570–591.

Wright, D.F., 2017a, Bayesian estimation of fossil phylogenies and the evolution of early to middle Paleozoic crinoids (Echinodermata): Journal of Paleontology, v. 91, p. 799–814.

Wright, D.F., 2017b, Phenotypic innovation and adaptive constraints in the evolutionary radiation of Paleozoic crinoids: Scientific Reports, v. 7, p. 13745.

Wright, D.F., and Toom, U., 2017, New crinoids from the Baltic region (Estonia): Fossil tip-dating phylogenetics constrains the origin and Ordovician–Silurian diversification of the Flexibilia (Echinodermata): Palaeontology, v. 60, p. 893–910.

Wright, D.F., and Hopkins, M.J., 2025, Assessing the impact of character evolution models on phylogenetic and macroevolutionary inferences from fossil data: Palaeontology, v. 68, p. e70031.

Wright, D.F., Ausich, W.I., Cole, S.R., Peter, M.E., and Rhenberg, E.C., 2017, Phylogenetic taxonomy and classification of the Crinoidea (Echinodermata): Journal of Paleontology, v. 91, p. 829–846.

Wright, D.F., Cole, S.R., and Ausich, W.I., 2019, Biodiversity, systematics, and new taxa of cladid crinoids from the Brechin Lagerstätte: Journal of Paleontology, v. 94, p. 334–357.

Zittel, K. A. von, 1895, Grundzüge Der Paläontologie (Paläzoologie): München und Berlin, Druck und Verlag von R. Oldenbourg, 971 p.

Appendix I

[NEXUS file containing species list/authorities, character list and state descriptions, and commands to run a tip-dated Bayesian FBD phylogenetic analysis in MrBayes for Ordovician through Llandoverian flexible crinoids.]

****

SPECIES NAMES & AUTHORS

****

Dendrocrinus villosus Brower and Veinus, 1982

Dendrocrinus minutus Springer, 1928

Dendrocrinus sepulchrum (Ramsbottom, 1961)

Cupulocrinus angustatus (Meek and Worthen, 1870)

Cupulocrinus canaliculatus Brower and Veinus, 1978

Cupulocrinus crossmani Brower, 1992

Cupulocrinus heterobrachialis Ramsbottom, 1961

Cupulocrinus heterocostalis (Hall, 1847)

Cupulocrinus humilis (Billings, 1857)

Cupulocrinus jewetti (Billings, 1859)

Cupulocrinus kentuckiensis Springer, 1911

Cupulocrinus latibrachiatus (Billings, 1857)

Cupulocrinus levorsoni Kolata, 1986

Cupulocrinus molanderi Kolata, 1975

Cupulocrinus plattevillensis Kolata, 1975

Cupulocrinus polydactylus (Shumard, 1857)

Protaxocrinus elegans (Billings, 1857)

Protaxocrinus girvanensis Ramsbottom, 1961

Protaxocrinus laevis (Billings, 1857)

Protaxocrinus ovalis (Angelin, 1878)

Protaxocrinus paraios Ausich and Copper, 2010

Protaxocrinus sideros Ausich and Copper, 2010

Ladocrinus asynaptos Ausich and Copper, 2010

Paerticrinus arvosus Wright and Toom, 2017

Sagenocrinid sp. (this study)

Scapanocrinus muricatus Eckert and Brett, 2001

Tintinnabulicrinus estoniensis Wright and Toom, 2017

Homalocrinus liljevalli Springer, 1920

Homalocrinus nanus (Salter, 1873)

Hormocrinus quebecensis Ausich and Copper, 2010

Hormocrinus tennesseensis (Worthen, 1890)

Anisocrinus prinstaensis Ausich and Copper, 2010

Proanisocrinus oswegoensis (Miller and Gurley, 1894)

Cryptanisocrinus kilbridensis Donovan, Doyle, and Harper, 1992

Kyphosocrinus tetreaulti Eckert and Brett, 2001

Anticosticrinus natiscotecensis Cole, Wright, and Hopkins, 2025

Clidochirus anebos Brower, 2001

Clidochirus serrulatus Brower, 1973

Clidochirus vaurealensis Ausich and Copper, 2010

Prolixocrinus nodocaudis Eckert and Brett, 2001

Icthyocrinus laevis Conrad, 1842

****

CHARACTER LIST

****

Characters and character states associated with the matrix below:

1. Calyx shape ratio (height/width) measured at the top of the radials:

(0) very high, > 1.0; (1) intermediate, 1.0 - 0.5; (2) low, < 0.5

2. Calyx/aboral cup profile to the top of the radials:

(0) cone shaped (~straight sides); (1) bowl shaped (rounded base, vertical sides)

3. Arm height to cup height ratio:

(0) less than 2.95; (1) 2.95 to 6.3; (2) more than 6.3

4. Calyx plate sculpturing:

(0) absent (i.e., smooth); (1) present

5. Type of calyx plate sculpturing when present:

(0) non-stellate ridges; (1) stellate ridges; (2) spinose; (3) nodose; (4)granulose; (5) irregular nodose/pitting or "rugose"; (6) dorsal medial keel

6. Calyx basal invagination:

(0) absent; (2) present

7. Infrabasal circlet attitude:

(0) all plates visible in side view; (1) along flat base of calyx (neither entirely in basal concavity nor entirely visible in side view); (2) not visible in side view

8. Number of infrabasal plates:

(0) five; (1) four; (2) three

9. Infrabasal plate dimensions:

(0) wide, W>H; (1) H~W; (2) narrow, H>W

10. Infrabasal height percent of aboral cup:

(0) less than 20%; (1) 20% to 32%; (2) more than 32%

11. Basal circlet attitude:

(0) all plates visible in side view; (1) along flat base of calyx (neither entirely in basal concavity nor entirely visible in side view); (2) not visible in side view

12. Basal plate dimensions:

(0) W>H; (1) H~W; (2) H>W

13. Basal plates, relative sizes (including CD basal):

(0) subequal; (1) unequal

14. Basal circlet interruption:

(0) absent; (1) present

15. Radial plate dimensions:

(0) wide, W>H; (1) H~W; (2) narrow, H>W

16. Radial circlet interruption:

(0) absent; (1) present in CD interray

17. Radial plate largest plate in calyx:

(0) no; (1) yes

18. C radial plate much smaller than other radial plates:

(0) no; (1) yes

19. Number of posterior plates partially or completely in cup, at or below height of radials:
(0) one; (1) two; (2) three; (3) four or more

20. Radianal plate shape:

(0) pentagonal; (1) tetragonal; (2) hexagonal/septagonal

21. Proximal position of radianal plate:

(0) full width beneath C radial plate; (1) centered beneath C radial but not full width;
(2) to left and below C radial plate; (3) within radial circlet above the CD basal

22. Radianal and Anal X plates in contact:

(0) no; (1) yes

23. Radianal plate size compared to C-ray radial:

(0) smaller; (1) subequal; (2) larger

24. Anal X presence:

(0) absent; (1) present

25. Anal X shape:

(0) pentagonal; (1) hexagonal; (2) 7 or more sides

26. Anal X position within the calyx:

(0) entirely within cup; (1) partially in cup; (2) entirely above cup

27. Position of Anal X relative to plates below:

(0) above and to left of radianal and in contact with the CD basal; (1) directly above CD basal and in contact with both C and D radials

28. Anal X plate size compared to C-ray radial:

(0) smaller; (1) subequal; (2) larger

29. Right tube plate presence:

(0) absent; (1) present

30. Right tube plate shape:

(0) pentagonal; (1) tetragonal; (2) hexagonal

31. Right tube plate position within the calyx:

(0) entirely within cup; (1) partially in cup; (2) entirely above cup

32. Position of the right tube plate relative to plates below:

(0) above and to right of Anal X and in contact with C radial; (1) above and to right of Anal X and in contact with C primibrach(s); (2) directly above Anal X and in contact with only the C ray (not D ray); (3) directly above Anal X and in contact with both the C & D rays

33. Presence of an anal sac:

(0) absent; (1) present

34. Dominant medial column supporting sac:

(0) absent; (1) present

35. Tube-like anal series:

(0) absent; (1) present

36. Nature of interrays at level of primibrachials:

(0) not joined; (1) flexible; (2) rigid/fused

37. Nature of interrays at level of secundibrachials:

(0) not joined; (1) flexible; (2) rigid/fused

38. Fixed/interlocking rays:

(0) absent; (1) present

39. Interradial plates [plating between the rays]:

(0) absent; (1) sometimes present; (2) present

40. Number of ranges of interradials:

(0) none; (1) single range; (2) two ranges; (3) three or more ranges

41. Nature of proximal interradial:

(0) none; (1) small plate; (2) large plate; (3) very large plate

42. Nature of distal interradial(s):

(0) none; (1) small plate(s); (2) large plate(s)

43. Patelloid process:

(0) absent; (1) present

44. Highest position of axillary on primibrachials located in B-E rays:

(0) IPr1; (1) IPr2; (2) ≥ IPr3

45. Greatest number of axillaries per ray:

(0) two; (1) three; (2) four; (3) five or more

46. Overall outline pattern of arm bifurcations after first isotomous split:

(0) isotomous; (1) heterotomous; (2) endotomous

47. Height differential of splits at higher brachitaxes:

(0) all splits in a ray occur at the same height; (1) rays are internally symmetric with inner arm branches splitting at a different brachial position than outer arm branches

48. Equality of division during arm bifurcations:

(0) all splits yield equal-width divisions; (1) some splits above the primibrachitaxis yield one branch narrower than the other

49. Interbrachial plating [plating between branches in a ray]:

(0) absent; (1) sometimes present; (2) present

50. Number of ranges of interbrachials:

(0) none; (1) single range; (2) two ranges; (3) three or more ranges

51. Width of radial facets:

(0) narrower than radial width; (1) subequal to radial width; (2) wider than radial width

52. Overall area of the primibrachials:

(0) smaller than radials; (1) subequal to radials; (2) larger than radials

53. Primibrachial width to height ratio:

(0) less than 1.53; (1) 1.53 to 3.36; (2) more than 3.36

54. Maximum number of secundibrachials:

(0) two; (1) three; (2) four; (3) five; (4) six or more

55. Brachial plate sculpturing:

(0) absent; (1) present

56: Type of brachial plate ornamentation, when present:

(0) non-stellate ridges; (1) stellate ridges; (2) spinose; (3) nodose; (4)granulose; (5) irregular nodose/pitted/rugose; (6) dorsal medial keel; (7)expanded lateral medial projections; (8) lateral cornices

57. Nature of arm tips:

(0) straight and not curled; (1) distal-most tips curled inward; (2) significant portions of distal arms curled inward

58. Proximal cross-sectional shape of the stalk:

(0) circular; (1) pentagonal; (2) pentastellate

59. Proximal columnals enlarged (strongly tapering):

(0) absent; (1) present

60. Column aspect:

(0) isomorphic; (1) heteromorphic

****

BAYESIAN FOSSIL TIP-DATING ANALYSIS IN MRBAYES

****

[Runs a Bayesian fossil tip-dating analysis using both character and stratigraphic data to estimate divergence times. The sampled ancestor implementation of the fossilized birth-death process (SA-FBD) == prior on trees and branch lengths. Independent gamma rates model used to 'relax' the morphological clock. All SA-FBD and morphological clock priors intentionally set to be flat and/or vague. Note that outgroups in tip-dated analyses must be specified using topological constraints on ingroup; simply specifying outgroup is ignored.]

#NEXUS

BEGIN DATA;

DIMENSIONS NTAX = 41 NCHAR = 60;

FORMAT DATATYPE = STANDARD GAP = - MISSING = ? SYMBOLS = " 0 1 2 3 4 5 6 7 8"; [characters in parens are multistate]

MATRIX

Dendrocrinus_villosus

10215 00011 00100 10010 00011 0001? ??100 00000 0002? ???00 0?0?1 50110

Dendrocrinus_minutus

1020- 00001 01102 10010 0?011 00?1? ??100 00000 00020 00000 00010 -0001

Dendrocrinus_sepulchrum

0020- 00022 02102 10010 01011 00?11 ??100 00000 00023 00100 11040 -0100

Cupulocrinus_angustatus

100(0 1)3 00(0 1)22 02000 10020 01111 00112 10111 10011 10023 10100 10240 -0010

Cupulocrinus_canaliculatus

0010- 00011 01100 20010 01111 0011? ??111 00000 00123 1?100 1024(0 1) 800?0

Cupulocrinus_crossmani

1010- 00021 02000 10020 01111 00112 12111 00011 10123 11000 10141 80011

Cupulocrinus_heterobrachialis

1010- 00022 02000 10010 01111 00212 22111 00000 00023 10100 10141 80201

Cupulocrinus_heterocostalis

1010- 01021 02001 10020 01111 00112 12111 00000 00020 0?000 10140 -00?1

Cupulocrinus_humilis

1010- 00(0 1)01 02001 10020 01111 00112 12111 00011 10122 1?000 10240 -0001

Cupulocrinus_jewetti

1001(1 3) 00(0 1)22 02000 10020 01111 00112 12111 00000 00123 01100 1024(0 1) (3 8)0011

Cupulocrinus_kentuckiensis

1000- 00(0 1)12 01000 10020 01111 00112 12111 10011 10122 01100 10240 -0001

Cupulocrinus_latibrachiatus

1010- 00001 02000 10020 01111 00112 12111 10000 00021 10100 10240 -0001

Cupulocrinus_levorsoni

1020- 00021 02100 10020 01?11 00212 12111 00000 00123 00111 0003(0 1) 80001

Cupulocrinus_molanderi

1020- 00012 01000 10010 01111 00?12 ??111 00000 00121 00100 10031 80010

Cupulocrinus_plattevillensis

0000- 00(0 1)21 02100 10020 01111 00112 12111 00011 10023 10000 10140 -0010

Cupulocrinus_polydactylus

1010- 00(0 1)22 02000 10020 01111 00110 12111 00000 00022 10000 10240 -0010

Protaxocrinus_elegans

1010- 00201 01100 11020 01110 00010 121?1 20022 11012 01000 10041 81010

Protaxocrinus_girvanensis

1020- 00201 01000 10020 01211 00012 121?? 20022 11122 ??000 100?1 71010

Protaxocrinus_laevis

1010- 00201 01100 11020 01110 00010 12111 20022 11011 11000 10140 -1010

Protaxocrinus_ovalis

2120- 11200 00100 11120 01010 00010 12111 10022 11011 00000 00140 -1???

Protaxocrinus_paraios

1010- 00201 01100 11020 01010 00010 12111 00021 11021 00000 10130 -10?1

Protaxocrinus_sideros

1020- 00200 01100 11020 01010 0001? 1?1?1 00000 00021 10000 11030 -(0 1)011

Ladacrinus_asynaptos

1010- 00201 01110 11011 20011 10110 211?1 20022 21012 01000 10120 -0001

Paerticrinus_arvosus

2110- 12??0 01100 11020 01111 00112 111?1 20023 21020 00100 00030 -????

Sagenocrinid_sp

?1?12 ????? ????? ????? ????? ????? ??000 22013 ?11?2 01123 ????1 22???

Scapanocrinus_muricatus

21116 00201 02000 11020 01012 00112 11000 22023 21?13 11123 10111 (6 7)2011

Tintinnabulicrinus_estoniensis

21114 12??0 12110 1101? ?0012 1000- --000 21021 30111 00100 10210 -????

Homalocrinus_liljevalli

2120- 11202 2?010 1101? 10011 10012 23000 22023 31012 20121 00210 -2???

Homalocrinus_nanus

21210 11201 10010 1101? 10011 10012 23000 22022 32012 20121 10111 02011

Hormocrinus_quebecensis

20111 00201 00100 1100- -0-12 1101? 21?00 20022 21021 01021 10220 -0001

Hormocrinus_tennesseensis

21111 00201 00000 1100- -0-11 11010 21000 20022 31011 00021 00101 12001

Anisocrinus_prinstaensis

2110- 00202 01000 11020 01111 00011 13000 22021 20011 01000 00110 -1001

Proanisocrinus_oswegoensis

11015 00200 01100 10010 01011 00012 22000 21022 1101? 00000 10121 510?1

Cryptanisocrinus_kilbridensis

2100- 11201 10010 ?101? 1001? 10??? ??000 21022 31011 ?0000 00110 -1001

Kyphosocrinus_tetreaulti

110(0 1)3 00201 01000 11010 01112 1020- --000 20021 10012 10000 10110 -1001

Anticosticrinus_natiscotecensis

10115 01200 00000 11020 01112 00112 12?00 21021 30012 01022 00011 (5 7)1???

Clidochirus_anebos

1010- 00200 01100 11020 01111 00012 12?00 21000 00121 10000 22120 -1010

Clidochirus_serrulatus

1000- 00200 01100 11010 01?10 000?? ???00 11000 00000 00000 10121 72011

Clidochirus_vaurealensis

10?0- 00200 01?00 ?101? 0??11 100?? 2??00 11000 00110 00000 11120 -?0?0

Prolixocrinus_nodocaudis

1010- 00200 02100 11110 01111 0010- --000 22100 00012 01000 22120 -1010

Icthyocrinus_laevis

2020- 12200 12000 01000 1-00- ---0- --000 22100 00112 01000 22120 -(1 2)010

;

END;

BEGIN MRBAYES;

charset all = 1 - 60;

ctype ordered: 8 39 49;

[set up likelihood model of character evolution]

lset applyto=(all) rates=gamma coding=variable; [relaxed clock model]

[set up clade constraints]

constraint flexie partial = 4-41 : 1-3; [sets Dendrocrinus as the outgroup; leaves remaining species unconstrained]

[calibrate priors on stratigraphic ranges; numerical ages based on ICS (Cohen et al. 2024) and regional stages on Goldman et al. (2020)]

calibrate Dendrocrinus_villosus = uniform(452.8, 458.2);
[Sandbian]

calibrate Dendrocrinus_minutus = uniform(445.2, 446.5);
[Katian - upper]

calibrate Dendrocrinus_sepulchrum = uniform(449.1, 452.8);
[Katian - Caradocian]

calibrate Cupulocrinus_angustatus = uniform(445.2, 449.1);
[Katian - Ashgillian/Richmondian]

calibrate Cupulocrinus_canaliculatus = uniform(452.8, 455);
[Sandbian - Mohawkian/Chatfieldian]

calibrate Cupulocrinus_crossmani = uniform(452.8, 455);
[Sandbian - Mohawkian/Chatfieldian]

calibrate Cupulocrinus_heterobrachialis = uniform(445.2, 449.1);
[Katian - Ashgillian]

calibrate Cupulocrinus_heterocostalis = uniform(445.2, 452.8);
[Katian]

calibrate Cupulocrinus_humilis = uniform(449.1, 455);
[Sandbian-Katian (Chatfieldian)]

calibrate Cupulocrinus_jewetti = uniform(449.1, 455);
[Sandbian-Katian (Mohawkian/Chatfieldian)]

calibrate Cupulocrinus_kentuckiensis = uniform(449.1, 455);
[Sandbian-Katian (Chatfieldian)]

calibrate Cupulocrinus_latibrachiatus = uniform(445.2, 446.5);
[Katian - Rawtheyan]

calibrate Cupulocrinus_levorsoni = uniform(452.8, 455);
[Sandbian - Mohawkian/Chatfieldian]

calibrate Cupulocrinus_molanderi = uniform(449.1, 452.8);
[Sandbian-Katian (Champlainian)]

calibrate Cupulocrinus_plattevillensis = uniform(452.8, 458.2);
[Sandbian]

calibrate Cupulocrinus_polydactylus = uniform(445.2, 449.1);
[Katian - Richmondian]

calibrate Protaxocrinus_elegans = uniform(445.2, 452.8);
[Katian]

calibrate Protaxocrinus_girvanensis = uniform(445.2, 449.1);
[Katian - Ashgillian]

calibrate Protaxocrinus_laevis = uniform(445.2, 452.8);
[Katian]

calibrate Protaxocrinus_ovalis = uniform(426.7, 432.9);
[Wenlock]

calibrate Protaxocrinus_paraios = uniform(440.5, 445.2);
[Hirnantian to Rhuddanian]

calibrate Protaxocrinus_sideros = uniform(435, 439.5);
[upper Aeronian to lower Telychian]

calibrate Ladacrinus_asynaptos = uniform(438.6, 440.5);
[Aeronian]

calibrate Paerticrinus_arvosus = uniform(440.5, 443.1);
[Rhuddanian]

calibrate Sagenocrinid_sp = uniform(445.2, 446.5);
[Katian - Rawtheyan]

calibrate Scapanocrinus_muricatus = uniform(432.9, 438.6);
[Telychian]

calibrate Tintinnabulicrinus_estoniensis = uniform(449.1, 455.7);
[Keila regional stage, lower Katian]

calibrate Homalocrinus_liljevalli = uniform(426.7, 432.9);
[Wenlock]

calibrate Homalocrinus_nanus = uniform(426.7, 432.9);
[Wenlock]

calibrate Hormocrinus_quebecensis = uniform(438.6, 440.5);
[Aeronian]

calibrate Hormocrinus_tennesseensis = fixed(426.7);
[Ludlow; youngest taxon in dataset]

calibrate Anisocrinus_prinstaensis = uniform(443.1, 445.2);
[Hirnantian]

calibrate Proanisocrinus_oswegoensis = uniform(445.2, 449.1);
[Katian - Ashgillian/Richmondian]

calibrate Cryptanisocrinus_kilbridensis = uniform(432.9, 438.6);
[Telychian]

calibrate Kyphosocrinus_tetreaulti = uniform(432.9, 438.6);
[Telychian]

calibrate Anticosticrinus_natiscotecensis = uniform(440.5, 445.2);
[Hirnantian-Rhuddanian]

calibrate Clidochirus_anebos = uniform(445.2, 449.1);
[Katian - Ashgillian/Richmondian]

calibrate Clidochirus_serrulatus = uniform(443.1, 445.2);
[Hirnantian]

calibrate Clidochirus_vaurealensis = uniform(445.2, 446.5);
[Katian - Rawtheyan]

calibrate Prolixocrinus_nodocaudis = uniform(438.6, 443.1);
[lower Llandovery]

```
        calibrate Icthyocrinus_laevis = uniform(430.6, 432.9);
        [Sheinwoodian]


[set prior distributions on tree shape, node ages, and blens]

        prset treeagepr = uniform(458.4, 467.3); [Darriwilian]

        prset nodeagepr = calibrated; [set node age priors]

        prset brlenspr = clock : fossilization;

        prset topologypr = constraints(flexie);

[SA-FBD and relaxed morpho-clock settings]

        prset speciationpr = uniform(0,10);

        prset extinctionpr = beta(1,1);

        prset fossilizationpr = beta(1,1);

        prset samplestrat = random;

        prset sampleprob = 1;

        prset clockvarpr = Igr;

        prset clockratepr = normal(0.0025,0.1);   [truncated normal, mean=0.08, but very
flat; see Supp Table 2 of Matzke & A. Wright 2016]

        prset Igrvarpr = exp(1);


[mcmc settings]

        mcmcp ngen=20000000 samplefreq=10000 printfreq=5000 nruns=2 nchains=4
relburnin=yes burninfrac=0.25 temp = 0.1 savebrlens=yes;

        mcmc; sump; sumt;

        end;
```

Appendix II

[Biogeographic regional assignments for Ordovician through Llandoverian flexible crinoids, for use in marginal ancestral state reconstruction.]

A: Avalonia. Includes UK, Southern Ireland

B: Baltica. Includes Sweden, Estonia

O: Laurentia, Scoto-Appalachian. Includes southern Scotland

E: Laurentia, eastern Canada. Includes Quebec (Anticosti Island)

F: Laurentia, Appalachian Foreland Basin. Includes New York, southern Ontario, southern Quebec

C: Laurentia, Cincinnati Basin. Includes Ohio, northern Kentucky

U: Laurentia, Upper Mississippi Valley. Includes Minnesota, Iowa, Wisconsin, Illinois, Missouri

S: Laurentia, southern Appalachian Basin. Includes Tennessee

	A B O E F C U S
Cupulocrinus_angustatus	0 0 0 0 0 0 1 0
Cupulocrinus_canaliculatus	0 0 0 0 0 0 1 0
Cupulocrinus_crossmani	0 0 0 0 0 0 1 0
Cupulocrinus_heterobrachialis	0 0 1 0 0 0 0 0
Cupulocrinus_heterocostalis	0 0 0 0 1 0 0 0
Cupulocrinus_humilis	0 0 0 0 1 1 1 0
Cupulocrinus_jewetti	0 0 0 0 1 1 1 0
Cupulocrinus_kentuckiensis	0 0 0 0 0 1 0 0
Cupulocrinus_latibrachiatus	0 0 0 1 0 0 0 0
Cupulocrinus_levorsoni	0 0 0 0 0 0 1 0
Cupulocrinus_molanderi	0 0 0 0 0 0 1 0
Cupulocrinus_plattevillensis	0 0 0 0 0 0 1 0
Cupulocrinus_polydactylus	0 0 0 0 0 1 0 0

Protaxocrinus_elegans	0 0 0 0 1 0 0 0
Protaxocrinus_girardeau	0 0 0 0 0 0 1 0
Protaxocrinus_girvanensis	0 0 1 0 0 0 0 0
Protaxocrinus_laevis	0 0 0 0 1 0 0 0
Protaxocrinus_ovalis	0 1 0 0 0 0 0 0
Protaxocrinus_paraios	0 0 0 1 0 0 0 0
Protaxocrinus_sideros	0 0 0 1 0 0 0 0
Ladacrinus_asynaptos	0 0 0 1 0 0 0 0
Paerticrinus_arvosus	0 1 0 0 0 0 0 0
Sagenocrinid_sp	0 0 0 1 0 0 0 0
Scapanocrinus_muricatus	0 0 0 0 1 0 0 0
Tintinnabulicrinus_estoniensis	0 1 0 0 0 0 0 0
Homalocrinus_liljevalli	0 1 0 0 0 0 0 0
Homalocrinus_nanus	1 1 0 0 0 0 0 0
Hormocrinus_quebecensis	0 0 0 1 0 0 0 0
Hormocrinus_tennesseensis	0 0 0 0 0 0 0 1
Anisocrinus_prinstaensis	0 0 0 1 0 0 0 0
Proanisocrinus_oswegoensis	0 0 0 0 0 0 1 0
Cryptanisocrinus_kilbridensis	1 0 0 0 0 0 0 0
Kyphosocrinus_tetreaulti	0 0 0 0 1 0 0 0
Anticosticrinus_natiscotecensis	0 0 0 1 0 0 0 0
Clidochirus_anebos	0 0 0 0 0 0 1 0
Clidochirus_serrulatus	0 0 0 0 0 0 1 0
Clidochirus_vaurealensis	0 0 0 1 0 0 0 0
Prolixocrinus_nodocaudis	0 0 0 0 1 0 0 0
Icthyocrinus_laevis	0 0 0 0 1 0 0 0

Appendix III

[NEXUS file containing species list/authorities and commands to run a tip-dated Bayesian FBD phylogenetic analysis in MrBayes for Ordovician through Wenlock flexible crinoids. Backbone topology constraints are based on well supported relationships from the maximum clade credibility tree of Crowley and Wright (in prep.) for Ordovician through Llandoverian species. Character list and state descriptions are the same as in Appendix I, and are not reiterated here.]

****

SPECIES NAMES & AUTHORS

****

Dendrocrinus villosus Brower and Veinus, 1982

Dendrocrinus minutus Springer, 1928

Dendrocrinus sepulchrum (Ramsbottom, 1961)

Cupulocrinus angustatus (Meek and Worthen, 1870)

Cupulocrinus canaliculatus Brower and Veinus, 1978

Cupulocrinus crossmani Brower, 1992

Cupulocrinus heterobrachialis Ramsbottom, 1961

Cupulocrinus heterocostalis (Hall, 1847)

Cupulocrinus humilis (Billings, 1857)

Cupulocrinus jewetti (Billings, 1859)

Cupulocrinus kentuckiensis Springer, 1911

Cupulocrinus latibrachiatus (Billings, 1857)

Cupulocrinus levorsoni Kolata, 1986

Cupulocrinus molanderi Kolata, 1975

Cupulocrinus plattevillensis Kolata, 1975

Cupulocrinus polydactylus (Shumard, 1857)

Protaxocrinus elegans (Billings, 1857)

Protaxocrinus girardeau Springer, 1920

Protaxocrinus girvanensis Ramsbottom, 1961

Protaxocrinus laevis (Billings, 1857)

Protaxocrinus ovalis (Angelin, 1878)

Protaxocrinus paraios Ausich and Copper, 2010

Protaxocrinus sideros Ausich and Copper, 2010

Protaxocrinus amii Bolton, T.E., 1970

Protaxocrinus anellus Eckert and Brett, 2001

Protaxocrinus cataractensis Eckert, 1984

Protaxocrinus interbrachiatus (Angelin, 1878)

Protaxocrinus salteri (Angelin, 1878)

Protaxocrinus tuberculatus (Miller, 1821)

Eutaxocrinus oblongatus (Angelin, 1878)

Gnorimocrinus cirrifer Bassler, 1915

Gnorimocrinus expansus (Angelin, 1878)

Gnorimocrinus varians Bassler, 1915

Meristocrinus anceps Springer, 1920

Meristocrinus interbrachiatus (Angelin, 1878)

Meristocrinus minor Springer, 1920

Meristocrinus nodulosus Salter, 1873

Meristocrinus tuberosus Springer, 1920

Paerticrinus arvosus Wright and Toom, 2017

Sagenocrinid sp. (Crowley & Wright, in prep.)

Scapanocrinus muricatus Eckert and Brett, 2001

Sagenocrinites americanus (Springer, 1902)

Sagenocrinites expansus (Phillips in Murchinson, 1839)

Tintinnabulicrinus estoniensis Wright and Toom, 2017

Homalocrinus liljevalli Springer, 1920

Homalocrinus nanus (Salter, 1873)

Homalocrinus peculiaris Springer, 1920

Asaphocrinus excavatus (Ringueberg, 1886)

Asaphocrinus incisus (Ringueberg, 1886)

Asaphocrinus minor Springer, 1926

Asaphocrinus ornatus (Hall, 1852)

Calpiocrinus fimbriatus Angelin, 1878

Calpiocrinus heterodactylus Angelin, 1878

Calpiocrinus intermedius Springer, 1920

Calpiocrinus ovatus Angelin, 1878

Calpiocrinus rotundatus Springer, 1920

Lithocrinus divaricatus (Angelin, 1878)

Temnocrinus tuberculatus (Miller, 1821)

Ladacrinus asynaptos Ausich and Copper, 2010

Hormocrinus quebecensis Ausich and Copper, 2010

Hormocrinus tennesseensis (Worthen, 1890)

Hormocrinus anglicus Springer, 1920

Hormocrinus gotlandicus Springer, 1920

Cholocrinus obesus (Angelin, 1878)

Lecocrinus laurelianus (Springer, 1926)

Pycnosaccus americanus Weller, S., 1900

Pycnosaccus bucephalus (Bather, 1890)

Pycnosaccus calyculus (Hall, 1852)

Pycnosaccus nodulosus Angelin, 1878

Pycnosaccus scrobiculatus (Hisinger, 1840)

Lecanocrinus elongatus Springer, 1926

L. Alnecocrinus angulatus Springer, 1920

L. Lecanocrinus bacchus (Salter, 1873)

L. Lecanocrinus billingsi Angelin, 1878

L. Lecanocrinus facietatus (Angelin, 1878)

L. Lecanocrinus lindstroemi Springer, 1920

L. Lecanocrinus macropetalus Hall, 1852

L. Lecanocrinus pusillus (Hall, 1863)

L. Lecanocrinus solidus Ringueberg, 1886

Nummicrinus pisiformis (Roemer, 1860)

Nummicrinus waukoma (Hall, 1864)

Mysticocrinus wilsoni Springer, 1918

Anisocrinus prinstaensis Ausich and Copper, 2010

Anisocrinus angelini Wachsmuth and Springer, 1879

Anisocrinus greenei (Miller and Gurley, 1896)

Anisocrinus interradiatus Angelin, 1878

Anisocrinus laurelensis Frest and Strimple, 1978

Proanisocrinus oswegoensis (Miller and Gurley, 1894)

Cryptanisocrinus kilbridensis Donovan, Doyle, and Harper, 1992

Kyphosocrinus tetreaulti Eckert and Brett, 2001

Anticosticrinus natiscotecensis Cole, Wright, and Hopkins, 2025

Clidochirus anebos Brower, 2001

Clidochirus serrulatus Brower, 1973

Clidochirus vaurealensis Ausich and Copper, 2010

Clidochirus pyrum Angelin, 1878

Clidochirus springeri Ausich, 1984

Clidochirus ulrichi Foerste, 1919

Clidochirus sp. Donovan and Lewis, 2005

Prolixocrinus nodocaudis Eckert and Brett, 2001

Prolixocrinus americanus (Springer, 1920)

Icthyocrinus laevis Conrad, 1842

Icthyocrinus gotlandicus (Wachsmuth and Springer, 1880)

Icthyocrinus intermedius Angelin, 1878

Icthyocrinus phillipsianus Springer, 1920

Icthyocrinus pyriformis (Phillips, 1839)

Icthyocrinus subangularis (Hall, 1863)

****

BAYESIAN FOSSIL TIP-DATING ANALYSIS IN MRBAYES

****

[Runs a Bayesian fossil tip-dating analysis using both character and stratigraphic data to estimate divergence times. Uses results from previous analysis (Crowley & Wright, in prep.) to constrain tree topology for Ordovician through Llandoverian taxa. The sampled ancestor implementation of the fossilized birth-death process (SA-FBD) == prior on trees and branch lengths. Independent gamma rates model used to 'relax' the morphological clock. All SA-FBD and morphological clock priors intentionally set to be flat and/or vague.]

#NEXUS

BEGIN DATA;

DIMENSIONS NTAX = 106 NCHAR = 60;

FORMAT DATATYPE = STANDARD GAP = - MISSING = ? SYMBOLS = " 0 1 2 3 4 5 6 7 8"; [characters in parens are multistate]

MATRIX

[Same coded character matrix as Appendix I for all Ordovician through Llandoverian taxa. Wenlock species are added without morphological data, so they are coded as '?' for all traits.]

BEGIN MRBAYES;

charset all = 1 - 60;

ctype ordered: 8 39 49;

[set up likelihood model of character evolution]

lset applyto=(all) rates=gamma coding=variable; [relaxed clock model]

[set up clade constraints]

constraint flexibilia partial = 4-106 : 1-3; [sets Dendrocrinus as the outgroup]

[additional partial constraints according to backbone cladogram (see below)]

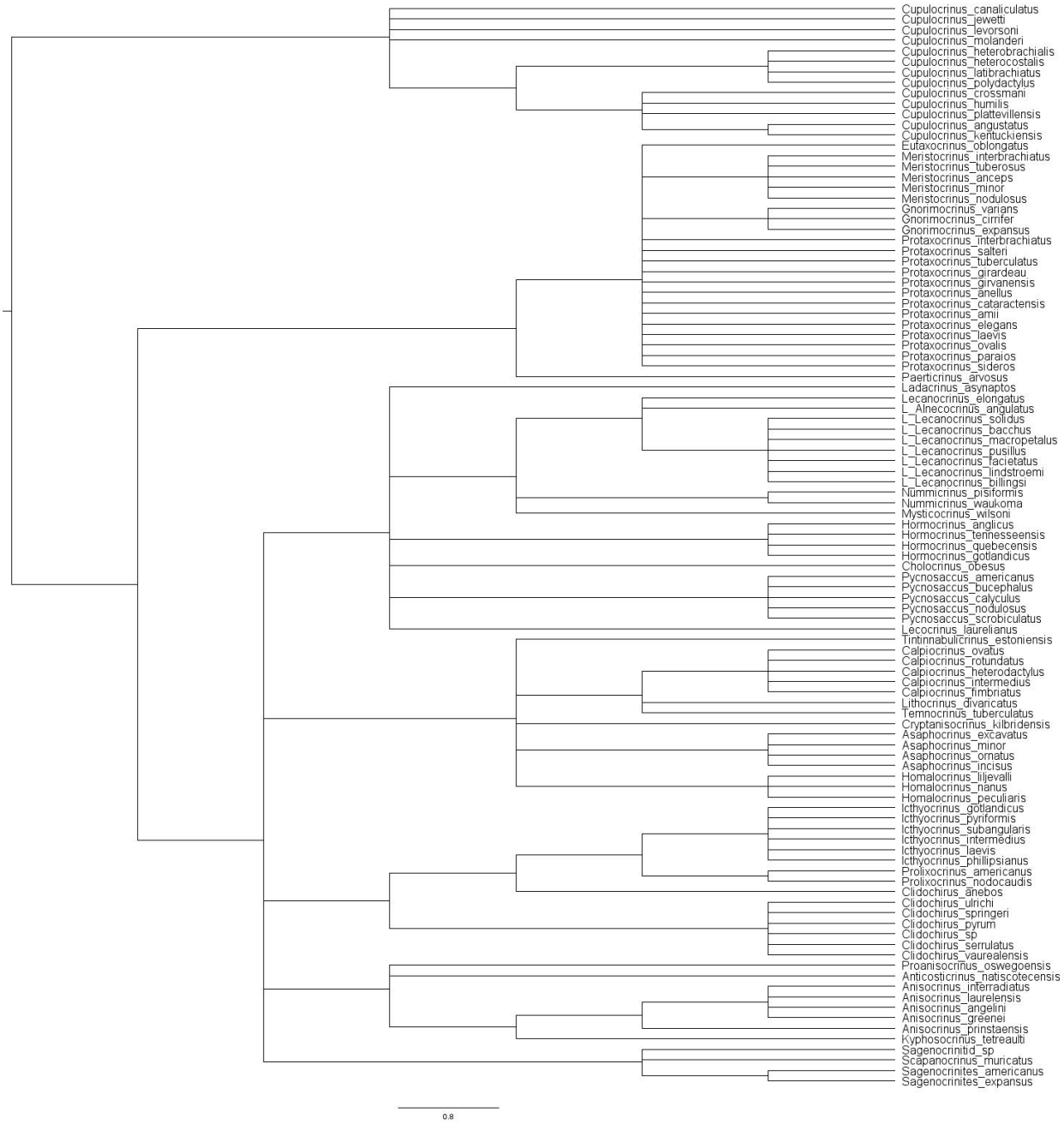

[calibrate priors on stratigraphic ranges; numerical ages based on ICS (Cohen et al. 2024) and regional stages on Goldman et al. (2020)]

calibrate Dendrocrinus_villosus = uniform(452.8, 458.2);
[Sandbian]

calibrate Dendrocrinus_minutus = uniform(445.2, 446.5);
[Katian - upper]

calibrate Dendrocrinus_sepulchrum = uniform(449.1, 452.8);
[Katian - Caradocian]

calibrate Cupulocrinus_angustatus = uniform(445.2, 449.1);
[Katian - Ashgillian/Richmondian]

calibrate Cupulocrinus_canaliculatus = uniform(452.8, 455);
[Sandbian - Mohawkian/Chatfieldian]

calibrate Cupulocrinus_crossmani = uniform(452.8, 455);
[Sandbian - Mohawkian/Chatfieldian]

calibrate Cupulocrinus_heterobrachialis = uniform(445.2, 449.1);
[Katian - Ashgillian]

calibrate Cupulocrinus_heterocostalis = uniform(445.2, 452.8);
[Katian]

calibrate Cupulocrinus_humilis = uniform(449.1, 455);
[Sandbian-Katian (Chatfieldian)]

calibrate Cupulocrinus_jewetti = uniform(449.1, 455);
[Sandbian-Katian (Mohawkian/Chatfieldian)]

calibrate Cupulocrinus_kentuckiensis = uniform(449.1, 455);
[Sandbian-Katian (Chatfieldian)]

calibrate Cupulocrinus_latibrachiatus = uniform(445.2, 446.5);
[Katian - Rawtheyan]

calibrate Cupulocrinus_levorsoni = uniform(452.8, 455);
[Sandbian - Mohawkian/Chatfieldian]

calibrate Cupulocrinus_molanderi = uniform(449.1, 452.8);
[Sandbian-Katian (Champlainian)]

calibrate Cupulocrinus_plattevillensis = uniform(452.8, 458.2);
[Sandbian]

calibrate Cupulocrinus_polydactylus = uniform(445.2, 449.1);
[Katian - Richmondian]

calibrate Protaxocrinus_elegans = uniform(445.2, 452.8);
[Katian]

calibrate Protaxocrinus_girvanensis = uniform(445.2, 449.1);
[Katian - Ashgillian]

calibrate Protaxocrinus_laevis = uniform(445.2, 452.8);
[Katian]

calibrate Protaxocrinus_ovalis = uniform(426.7, 432.9);
[Wenlock]

calibrate Protaxocrinus_paraios = uniform(440.5, 445.2);
[Hirnantian to Rhuddanian]

calibrate Protaxocrinus_sideros = uniform(435, 439.5);
[upper Aeronian to lower Telychian]

calibrate Protaxocrinus_amii = uniform(432.9, 438.6);
[Telychian]

calibrate Protaxocrinus_anellus = uniform(432.9, 438.6);
[Telychian]

calibrate Protaxocrinus_cataractensis = uniform(440.5, 443.1);
[Rhuddanian]

calibrate Protaxocrinus_girardeau = uniform(443.1, 445.2);
[Hirnantian]

calibrate Protaxocrinus_interbrachiatus = uniform(426.7, 432.9);
[Wenlock]

calibrate Protaxocrinus_salteri = uniform(426.7, 432.9);
[Wenlock]

calibrate Protaxocrinus_tuberculatus = uniform(426.7, 432.9);
[Wenlock]

calibrate Eutaxocrinus_oblongatus = uniform(426.7, 432.9);
[Wenlock]

calibrate Gnorimocrinus_cirrifer = uniform(422.7, 425.0);
[Ludfordian]

calibrate Gnorimocrinus_expansus = uniform(426.7, 432.9);
[Wenlock]

calibrate Gnorimocrinus_varians = uniform(422.7, 425.0);
[Ludfordian]

calibrate Meristocrinus_anceps = uniform(426.7, 432.9);
[Wenlock]

calibrate Meristocrinus_interbrachiatus = uniform(426.7, 432.9);
[Wenlock]

calibrate Meristocrinus_minor = uniform(426.7, 432.9);
[Wenlock]

calibrate Meristocrinus_nodulosus = uniform(426.7, 430.6);
[Homerian]

calibrate Meristocrinus_tuberosus = uniform(426.7, 432.9);
[Wenlock]

calibrate Paerticrinus_arvosus = uniform(440.5, 443.1);
[Rhuddanian]

calibrate Sagenocrinid_sp = uniform(445.2, 446.5);
[Katian - Rawtheyan]

calibrate Scapanocrinus_muricatus = uniform(432.9, 438.6);
[Telychian]

calibrate Sagenocrinites_americanus = uniform(426.7, 430.6);
[Homerian]

calibrate Sagenocrinites_expansus = uniform(426.7, 432.9);
[Wenlock]

calibrate Tintinnabulicrinus_estoniensis = uniform(449.1, 455.7);
[Keila regional stage, lower Katian]

calibrate Cryptanisocrinus_kilbridensis = uniform(432.9, 438.6);
[Telychian]

calibrate Homalocrinus_liljevalli = uniform(426.7, 432.9);
[Wenlock]

calibrate Homalocrinus_nanus = uniform(426.7, 432.9);
[Wenlock]

calibrate Homalocrinus_peculiaris = uniform(426.7, 432.9);
[Wenlock]

calibrate Asaphocrinus_excavatus = uniform(430.6, 432.9);
[Sheinwoodian]

calibrate Asaphocrinus_incisus = uniform(430.6, 432.9);
[Sheinwoodian]

calibrate Asaphocrinus_minor = uniform(426.7, 430.6);
[Homerian]

calibrate Asaphocrinus_ornatus = uniform(430.6, 432.9);
[Sheinwoodian]

calibrate Calpiocrinus_fimbriatus = uniform(426.7, 432.9);
[Wenlock]

calibrate Calpiocrinus_heterodactylus = uniform(426.7, 432.9);
[Wenlock]

calibrate Calpiocrinus_intermedius = uniform(426.7, 432.9);
[Wenlock]

calibrate Calpiocrinus_ovatus = uniform(426.7, 432.9);
[Wenlock]

calibrate Calpiocrinus_rotundatus = uniform(426.7, 432.9); [Wenlock]

calibrate Lithocrinus_divaricatus = uniform(426.7, 432.9); [Wenlock]

calibrate Temnocrinus_tuberculatus = uniform(426.7, 430.6); [Homerian]

calibrate Ladacrinus_asynaptos = uniform(438.6, 440.5); [Aeronian]

calibrate Hormocrinus_quebecensis = uniform(438.6, 440.5); [Aeronian]

calibrate Hormocrinus_tennesseensis = uniform(422.7, 425.0); [Ludfordian]

calibrate Hormocrinus_anglicus = uniform(426.7, 430.6); [Homerian]

calibrate Hormocrinus_gotlandicus = uniform(426.7, 432.9); [Wenlock]

calibrate Cholocrinus_obesus = uniform(426.7, 432.9); [Wenlock]

calibrate Lecocrinus_laurelianus = uniform(426.7, 430.6); [Homerian]

calibrate Pycnosaccus_americanus = uniform(426.7, 430.6); [Homerian]

calibrate Pycnosaccus_bucephalus = uniform(426.7, 430.6); [Homerian]

calibrate Pycnosaccus_calyculus = uniform(430.6, 432.9); [Sheinwoodian]

calibrate Pycnosaccus_nodulosus = uniform(426.7, 432.9); [Wenlock]

calibrate Pycnosaccus_scrobiculatus = uniform(426.7, 432.9); [Wenlock]

calibrate Lecanocrinus_elongatus = uniform(426.7, 430.6); [Homerian]

calibrate L_Alnecocrinus_angulatus = uniform(426.7, 432.9); [Wenlock]

calibrate L_Lecanocrinus_bacchus = uniform(426.7, 430.6); [Homerian]

calibrate L_Lecanocrinus_billingsi = uniform(430.6, 432.9);
[Sheinwoodian]

calibrate L_Lecanocrinus_facietatus = uniform(426.7, 432.9);
[Wenlock]

calibrate L_Lecanocrinus_lindstroemi = uniform(426.7, 432.9);
[Wenlock]

calibrate L_Lecanocrinus_macropetalus = uniform(426.7, 432.9);
[Wenlock]

calibrate L_Lecanocrinus_pusillus = uniform(426.7, 430.6);
[Homerian]

calibrate L_Lecanocrinus_solidus = uniform(430.6, 432.9);
[Sheinwoodian]

calibrate Nummicrinus_pisiformis = fixed(422.7);
[Pridoli; taxon with youngest strat range in dataset]

calibrate Nummicrinus_waukoma = uniform(426.7, 430.6);
[Homerian]

calibrate Mysticocrinus_wilsoni = uniform(426.7, 430.6);
[Homerian]

calibrate Anisocrinus_prinstaensis = uniform(443.1, 445.2);
[Hirnantian]

calibrate Anisocrinus_angelini = uniform(426.7, 432.9);
[Wenlock]

calibrate Anisocrinus_greenei = uniform(425, 428);
[Homerian to lower Ludlow]

calibrate Anisocrinus_interradiatus = uniform(426.7, 432.9);
[Wenlock]

calibrate Anisocrinus_laurelensis = uniform(430, 435);
[Telychian to lower Wenlock]

calibrate Proanisocrinus_oswegoensis = uniform(445.2, 449.1);
[Katian - Ashgillian/Richmondian]

calibrate Kyphosocrinus_tetreaulti = uniform(432.9, 438.6);
[Telychian]

calibrate Anticosticrinus_natiscotecensis = uniform(440.5, 445.2);
[Hirnantian-Rhuddanian]

calibrate Clidochirus_anebos = uniform(445.2, 449.1);
[Katian - Ashgillian/Richmondian]

calibrate Clidochirus_serrulatus = uniform(443.1, 445.2);
[Hirnantian]

calibrate Clidochirus_vaurealensis = uniform(445.2, 446.5);
[Katian - Rawtheyan]

calibrate Clidochirus_pyrum = uniform(426.7, 432.9);
[Wenlock]

calibrate Clidochirus_springeri = uniform(438.6, 440.5);
[Aeronian]

calibrate Clidochirus_ulrichi = uniform(432.9, 438.6);
[Telychian]

calibrate Clidochirus_sp = uniform(432.9, 438.6);
[Telychian]

calibrate Prolixocrinus_nodocaudis = uniform(438.6, 443.1);
[lower Llandovery]

calibrate Prolixocrinus_americanus = uniform(438.6, 440.5);
[Aeronian]

calibrate Icthyocrinus_laevis = uniform(430.6, 432.9);
[Sheinwoodian]

calibrate Icthyocrinus_gotlandicus = uniform(426.7, 432.9);
[Wenlock]

calibrate Icthyocrinus_intermedius = uniform(426.7, 432.9);
[Wenlock]

calibrate Icthyocrinus_phillipsianus = uniform(426.7, 430.6);
[Homerian]

calibrate Icthyocrinus_pyriformis = uniform(426.7, 432.9);
[Wenlock]

calibrate Icthyocrinus_subangularis = uniform(426.7, 430.6);
[Homerian]

[set prior distributions on tree shape, node ages, and blens]

prset treeagepr = uniform(458.4, 467.3); [Darriwilian]

prset nodeagepr = calibrated; [set node age priors]

prset brlenspr = clock : fossilization;

prset topologypr =
constraints(flexibilia,cupulocrinus,cupulo1,cupulo2,cupulo3,cupulo4,euflexibilia,taxocrinida,tax

ocrinidae,meristocrinus,gnorimocrinus,sagenocrinida,lecanocrinacea,lecanocrinidae,lecanocrinus,lecanocrinusss,nummicrinus,hormocrinus,pycnosaccus,node20,dactylocrinidae,calpiocrinus,asaphocrinus,homalocrinus,icthyocrinidae,node26,node27,icthyocrinus,prolixocrinus,clidochirus,anisocrinidae,node32,anisocrinus,wenanisocrinus,sagenocrinitidae,sagenocrinites);

[SA-FBD and relaxed morpho-clock settings]

prset speciationpr = uniform(0,10);

prset extinctionpr = beta(1,1);

prset fossilizationpr = beta(1,1);

prset samplestrat = random;

prset sampleprob = 1;

prset clockvarpr = Igr;

prset clockratepr = normal(0.0025,0.1); [truncated normal, mean=0.08, but very flat; see Supp Table 2 of Matzke & A. Wright 2016]

prset Igrvarpr = exp(1);

[mcmc settings]

mcmcp ngen=20000000 samplefreq=10000 printfreq=5000 nruns=2 nchains=4 relburnin=yes burninfrac=0.25 temp = 0.1 savebrlens=yes;

mcmc; sump; sumt;

end;

Appendix IV

[Measures of three ecomorphological/developmental traits (calyx volume, filtration fan area, and calyx complexity) used in macroevolutionary model-fitting. Measurements in cubic mm, square mm, and number of plates for calyx volume, fan area, and calyx complexity, respectively.]

Species	calyx_volume	ff_area	calyx_complexity
Anisocrinus_angelini	37.60	49.34	39
Anisocrinus_greenei	1343.13	1077.16	39
Anisocrinus_interradiatus	286.20	307.94	49
Anisocrinus_laurelensis	393.15	0	39
Anisocrinus_prinstaensis	352.88	712.42	61
Anticosticrinus_natiscotecensis	735.40	2359.26	70
Asaphocrinus_excavatus	526.08	2418.90	15
Asaphocrinus_incisus	575.78	905.43	15
Asaphocrinus_minor	0	819.16	0
Asaphocrinus_ornatus	916.24	3857.27	15
Calpiocrinus_fimbriatus	1466.67	3314.95	59
Calpiocrinus_heterodactylus	458.30	2627.61	39
Calpiocrinus_intermedius	1803.71	3340.92	57
Calpiocrinus_ovatus	872.04	2174.42	90
Calpiocrinus_rotundatus	512.29	2204.49	94
Cholocrinus_obesus	843.01	4754.58	15
Clidochirus_anebos	4.28	484.79	16
Clidochirus_pyrum	6559.82	3435.06	56
Clidochirus_serrulatus	12.60	235.07	15
Clidochirus_springeri	228.57	2667.05	22
Clidochirus_ulrichi	842.49	1212.42	36

Clidochirus_vaurealensis	19.32	83.83	25
Clidochirus_sp	259.82	682.79	25
Cryptanisocrinus_kilbridensis	1122.32	0	43
Cupulocrinus_angustatus	759.60	4455.28	19
Cupulocrinus_canaliculatus	467.25	7913.18	17
Cupulocrinus_crossmani	146.33	3725.63	17
Cupulocrinus_heterobrachialis	37.12	2818.77	17
Cupulocrinus_heterocostalis	129.89	2129.26	19
Cupulocrinus_humilis	281.41	7442.10	18
Cupulocrinus_jewetti	960.83	5066.06	18
Cupulocrinus_kentuckiensis	1134.22	4012.25	18
Cupulocrinus_latibrachiatus	65.74	1657.97	20
Cupulocrinus_levorsoni	19.42	3498.25	18
Cupulocrinus_molanderi	15.90	1402.72	17
Cupulocrinus_plattevillensis	411.51	2890.80	18
Cupulocrinus_polydactylus	263.66	4454.75	18
Eutaxocrinus_oblongatus	141.79	8425.84	20
Gnorimocrinus_cirrifer	124.22	2265.03	15
Gnorimocrinus_expansus	113.95	1796.08	16
Gnorimocrinus_varians	146.88	1545.82	15
Homalocrinus_liljevalli	786.09	2244.85	95
Homalocrinus_nanus	429.35	274.16	45
Homalocrinus_peculiaris	180.43	528.29	35
Hormocrinus_anglicus	1120.81	2207.16	32
Hormocrinus_gotlandicus	534.37	2641.21	18
Hormocrinus_quebecensis	124.59	888.04	31
Hormocrinus_tennesseensis	519.51	1360.13	41
Icthyocrinus_gotlandicus	1248.97	1058.28	133
Icthyocrinus_intermedius	1524.50	2594.78	124
Icthyocrinus_laevis	33929.59	9903.18	254

Icthyocrinus_phillipsianus	5033.24	5799.70	134
Icthyocrinus_pyriformis	3635.54	3079.58	214
Icthyocrinus_subangularis	19358.39	3633.51	134
Kyphosocrinus_tetreaulti	286.34	574.57	29
Ladacrinus_asynaptos	193.33	2412.66	40
Lecanocrinus_elongatus	434.35	0	45
L_Alnecocrinus_angulatus	3003.73	0	59
L_Lecanocrinus_bacchus	290.58	130.51	45
L_Lecanocrinus_billingsi	545.47	329.87	55
L_Lecanocrinus_facietatus	315.23	0	25
L_Lecanocrinus_lindstroemi	212.38	309.28	20
L_Lecanocrinus_macropetalus	3262.94	4248.72	35
L_Lecanocrinus_pusillus	434.24	1897.24	20
L_Lecanocrinus_solidus	2773.34	2094.70	55
Lecocrinus_laurelianus	187.27	1424.54	15
Lithocrinus_divaricatus	2644.61	4226.15	98
Meristocrinus_anceps	222.72	0	16
Meristocrinus_interbrachiatus	266.00	2328.93	24
Meristocrinus_minor	34.74	579.13	15
Meristocrinus_nodulosus	337.00	6805.81	14
Meristocrinus_tuberosus	172.19	3445.04	16
Mysticocrinus_wilsoni	29.57	59.30	15
Nummicrinus_pisiformis	261.02	548.15	25
Nummicrinus_waukoma	2647.12	0	25
Paerticrinus_arvosus	364.99	780.65	66
Proanisocrinus_oswegoensis	165.93	0	41
Prolixocrinus_americanus	1271.78	917.90	55
Prolixocrinus_nodocaudis	3030.05	5618.71	65
Protaxocrinus_amii	126.67	3098.88	15
Protaxocrinus_anellus	34.54	426.19	15

Protaxocrinus_cataractensis	322.58	5037.44	16
Protaxocrinus_elegans	601.71	2847.06	41
Protaxocrinus_girardeau	32.75	1412.04	15
Protaxocrinus_girvanensis	754.02	9635.38	15
Protaxocrinus_interbrachiatus	204.32	5975.60	38
Protaxocrinus_laevis	279.19	1162.06	37
Protaxocrinus_ovalis	103.91	1562.44	25
Protaxocrinus_paraios	14.21	380.55	19
Protaxocrinus_salteri	307.65	7009.94	41
Protaxocrinus_sideros	8.52	1338.15	15
Protaxocrinus_tuberculatus	31.86	1058.59	15
Pycnosaccus_americanus	1200.96	0	15
Pycnosaccus_bucephalus	5766.74	6850.91	15
Pycnosaccus_calyculus	223.98	504.56	15
Pycnosaccus_nodulosus	457.30	898.14	15
Pycnosaccus_scrobiculatus	2613.75	0	15
Sagenocrinid_sp	0	1978.66	0
Sagenocrinites_americanus	3497.05	2567.91	122
Sagenocrinites_expansus	30189.83	15583.71	258
Scapanocrinus_muricatus	3072.25	5374.64	142
Temnocrinus_tuberculatus	2651.20	6447.82	45
Tintinnabulicrinus_estoniensis	627.79	922.97	28